Trajectories of a Ball Moving Inside a Spherical Cavity Using First Integrals of The Governing Nonlinear System

Jiri Naprstek (naprstek@itam.cas.cz)
Institute of Theoretical and Applied Mechanics of the Czech Academy of Sciences
https://orcid.org/0000-0002-2323-8439

Cyril Fischer
Institute of Theoretical and Applied Mechanics Czech Academy of Sciences: Ustav teoreticke a aplikovane mechaniky Akademie ved Ceske republiky

---

Research Article

Keywords: Non-holonomic systems, Movement potentials, First integrals, Dynamic stability, Limit trajectories.

Posted Date: March 22nd, 2021

DOI: https://doi.org/10.21203/rs.3.rs-315428/v1

Version of Record: A version of this preprint was published at Nonlinear Dynamics on September 23rd, 2021. See the published version at https://doi.org/10.1007/s11071-021-06709-4.

Nonlinear Dynamics manuscript No.
(will be inserted by the editor)

TRAJECTORIES OF A BALL MOVING INSIDE A SPHERICAL CAVITY USING FIRST INTEGRALS OF THE GOVERNING NONLINEAR SYSTEM

Jiří Náprstek · Cyril Fischer

Received: date / Accepted: date

Abstract Analytical study of ball vibration absorber behavior is presented in the paper. The dynamics of trajectories of a heavy ball moving without slipping inside a spherical cavity are analyzed. Following our previous work, where a similar system was investigated through various numerical simulations, research of the dynamic properties of a sphere moving in a spherical cavity was carried out by methods of analytical dynamics. The strategy of analytical investigation enabled definition of a set of special and limit cases which designate individual domains of regular trajectories. In order to avoid any mutual interaction between the domains along a particular trajectory movement, energy dissipation at the contact of the ball and the cavity has been ignored, as has any kinematic excitation due to cavity movement. A governing system was derived using the Lagrangian formalism and complemented by appropriate non-holonomic constraints of the Pfaff type. The three first integrals are defined, enabling the evaluation of trajectory types with respect to system parameters, the initial amount of total energy, the angular momentum of the ball and its initial spin velocity. The neighborhoods of the limit trajectories and their dynamic stability are assessed. Limit and transition special cases are investigated along with their individual elements. The analytical means of investigation enabled the performance of broad parametric studies. Good agreement was found when comparing the results achieved by the analytical procedures in this paper with those obtained by means of numerical simulations, as they followed from the Lagrangian approach and the Appell-Gibbs function presented in previous papers.

Keywords Non-holonomic systems, · Movement potentials · First integrals · Dynamic stability · Limit trajectories.

Mathematics Subject Classification (2010) 34A05 · 34C25 · 37C20 · 37M05

J. Náprstek* · C. Fischer
Institute of Theoretical and Applied Mechanics of the CAS, Prosecká 76, 190 00 Prague 9, The Czech Republic
Tel.: +420 225 443 221
*Corresponding author, E-mail: naprstek@itam.cas.cz

1 INTRODUCTION

Passive vibration absorbers of various types are widely used in civil and other types of engineering when vibration should be suppressed. TV towers, masts and other slender structures exposed to wind, earthquake and environmental types of excitation are usually equipped with such devices. Conventional passive absorbers are of the pendulum type; see a number of papers and monographs by J.P. den Hartog, B.G. Korenev, A.H. Nayfeh, S. Krenk and others. These absorbers can be based also on the auto-parametric principle; see for instance [15,29,30,49]. Although they are very effective and reliable, they have several disadvantages limiting their application. First of all, they have certain spatial requirements, particularly in the vertical direction. It is not possible to satisfy these requirements when the absorber is to be installed as supplementary equipment. Horizontal constructions, like foot bridges, cannot incorporate absorbers of the pendulum type either. Another disadvantage is the need for regular maintenance; this is a topic which is gaining increasing popularity, [10].

All the above shortcomings can be avoided using an absorber of the ball type. The basic principle comes from the rolling movement of a metallic ball of radius r inside a metallic spherical cavity of radius $R > r$, Fig. 1 with a rubber lining. This system is closed in an airtight case. Such a device is practically maintenance free. Its vertical dimension can be relatively small, and it can be also used in such cases where a pendulum absorber is inapplicable due to lack of vertical space or difficult maintenance. Not surprisingly this type of absorber is growing in popularity in connection with wind turbines, e.g., [8].

The first papers dealing with the theory and practical aspects of ball absorbers were published during the past decades, see [45] and [46], and are based on engineering approaches. However, to the best of the authors' knowledge, the first papers that dealt with this issue from the perspective of rational (analytical) dynamics were published only some years ago; see [43] and [42]. These papers are probably the first attempt to present a basic mathematical model in 2D together with its numerical evaluation, and a report on its practical application, including some results of long-term in-situ measurements. The 2D approach is satisfactory when the absorber is limited to acting in a specific direction, e.g. in bridges, systems of multiple one-directionally acting elements, etc. However, structures like masts or towers require equipment which works simultaneously in both horizontal directions, and hence a 3D model must be considered.

Modeling of a homogeneous sphere rolling on a perfectly rough surface has a long tradition in classical mechanics. Several 3D approaches are available which respect the strongly nonlinear and spatial character of the system. The system is non-holonomic with linear constraints in the first derivatives with respect to time. The classical setting of several particular cases, including the one that this paper is concerned with, are considered by Routh in [47]. He and other authors of popular monographs use the general Lagrangian methodology, [31,44,4], which is by far the most popular approach in classical mechanics; it offers many advantages which are actively applied in practice and research, including the rolling sphere problems, [16]. For example, a study regarding the rolling of a ball over a spherical surface based on homogeneous Lagrange equations has recently been published, [17]. There the author analyzes the free and undamped movement of a ball in the vertical plane using phase portraits for different initial conditions together with generalizations regarding vibro-impact dynamics.

The approach based on the Appell-Gibbs function, even though not frequently used, has proven very effective in subsequent numerical simulations. For details and

some specific attributes of this approach; see, e.g., papers [50,13,52,25,11,27]. Recently, the rolling of a ball over a curved surface was dealt with on an abstract basis using the Lie group theoretical methods, e.g., [18]. Borisov et al [7] use a similar abstract methodology and present a more complete analysis of the Routh solution for the solid of revolution. They derived new integrals for the ball rolling on non-symmetrical surfaces of the second order. Jurdjevic and Zimmerman [19] extended the problem to a hyperbolic analogue in which the spheres are replaced by the hyperboloids, and rolling is taken in an isometric sense in either Euclidean or Riemann geometry. A numerical analysis of the ball rolling in a spherical recess, also based on the Appell-Gibbs function, was studied numerically by Legeza, [23].

Another derived topic with high publication activity regards the rolling of a so-called Chaplygin sphere—a dynamically non-symmetric non-homogeneous sphere—which represents one of the best known integrable systems of classical nonholonomic mechanics, [5], either with or without considering a spin [21]. There is no doubt that devices based on similar effects find their use in absorbing unwanted vibrations. The usage of non-homogeneous spheres, hemishperes or semielliptic spheres would allow the absorber to be fine-tuned for a precisely-limited nonlinear damping effect or multidirectional damping [27,26]. These topics are already popular in the engineering literature, however, still only partially treated analytically. For example, a prospective tuned vibration absorber based on the nested ball principle has been vaguely described in a patent proposal [32]. The theoretical analysis of this set-up is partially addressed in an abstract way by Borisov, [6], and a case with a semielliptic cavity was described by Legeza, [24].

The above-mentioned abstract solutions offer valuable tools of investigation. From the engineering perspective, however, the actual trajectories that can be encountered in a particular vibration absorbing device are interesting because they determine its efficiency. The authors addressed two possible strategies for this purpose: (i) the Lagrangian formalism in 2D, [42,38], and (ii) the Appell-Gibbs function in 3D; see [39, 41,40]. In each case, a governing differential system was composed, and the solution itself was conducted numerically with subsequent analysis of the extensive data set. These two variants of the differential system are significantly different from one another, each having its strengths and shortcomings, and being suitable for a different

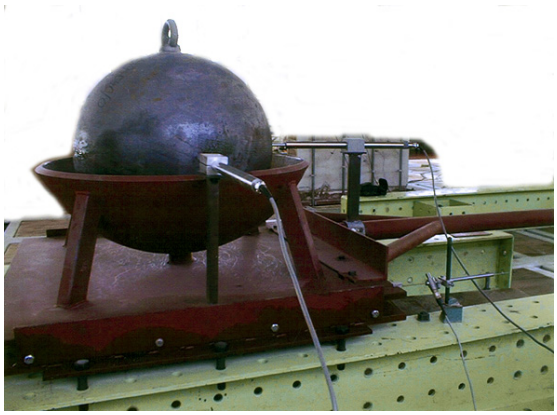

Fig. 1 Ball vibration absorber in a dynamic testing laboratory

type of analysis. Important physical properties of the "ball - spherical cavity" system were discovered in these papers, and many particular trajectory types were identified numerically, however, without proper analytical explanation. This indicates that the problem should also be investigated at an analytical level using energy, momentum and angular momentum balance principles related to relevant first integrals. This strategy makes a qualitative investigation of the system behavior possible at least in the setting of the homogeneous problem. A similar technique was also adopted for investigating a nonlinear spherical pendulum; see, e.g., [37]. In general, such an approach can significantly improve insight into the internal character of the system and increase the possibilities for practical applications. It enables a systematic identification of limit trajectories and the definition of relevant categories. The existence of limit trajectories depends on the system parameters and the initial conditions setting. The possibility of delimiting the domains of parameters can significantly contribute to an analysis of a system's reliability and its lifetime period. Moreover, the obtained results can serve in constructing effective forms of the Lyapunov function intended for particular cases; see [9, 22, 34–36] and other resources in the domain of dynamic stability.

Finally, it is worth mentioning that many of the algebraic manipulations required to derive or verify formulas in this paper were done using the Wolfram Mathematica Package [51].

The paper is organized as follows. First, after this introduction, the governing system and three of the first integrals based on the Lagrangian approach are derived. A particular characteristic function is then introduced as a basic tool for further classification of the response trajectories. Next, the particular "separation circle" trajectory is introduced, which separates two main trajectory groups. Sections 4 and 5 describe settings with and without consideration of the initial spin of the ball. A particular type of an almost planar rocking is then analyzed in detail in Section 6. Finally, the last section concludes.

2 GOVERNING SYSTEM AND FIRST INTEGRALS

2.1 Lagrangian system and first integrals

The rolling without slipping of a ball on a surface is a non-holonomic problem because constraints relating to the mutual movement of a ball and a surface include velocity components. When putting together an expression for the kinetic and potential energies T, V, and external forces $\mathbf{Q} = [Q_1, ..., Q_n]$, the relevant Lagrangian equations should be written as follows:

$$\frac{\mathrm{d}}{\mathrm{d}t}\left(\frac{\partial T}{\partial \dot{q}_j}\right) - \frac{\partial T}{\partial q_j} + \frac{\partial V}{\partial q_j} = Q_j + \sum_{m=1}^{l} \lambda_m \cdot B_{mj}\,, \tag{1}$$

$j = 1, ..., n$, and with non-holonomic constraints:

$$\sum_{j=1}^{n} B_{mj} \cdot \dot{q}_j + B_m = 0. \qquad m = 1, ..., l\,, \tag{2}$$

where q_j $(j = 1, ..., n)$ are generalized coordinates. Symbols B_{mj} and B_m are generally functions of q_j. Explicit time can be usually omitted as constraints are considered scleronomous as a rule if external kinematic excitation is absent and only initial conditions

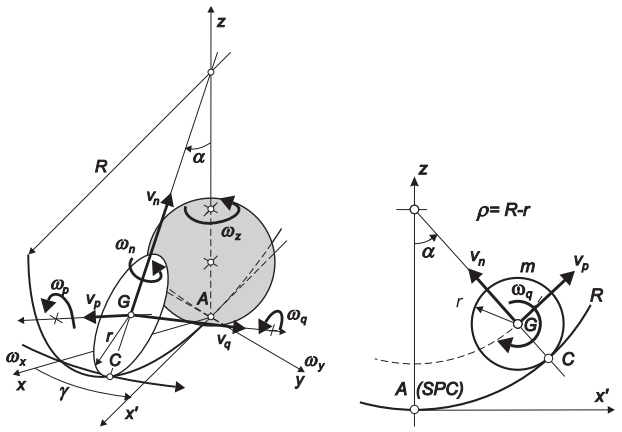

Fig. 2 Outline of coordinate systems; left: axonometric view; right: plane ξz view — along γ orientation.

provide energy to the system. Provided that kinematic excitation works, the respective parameters $B_m \neq 0$, and should then be considered as functions of time. Symbols λ_m $(m = 1, ..., l)$ are Lagrangian multipliers which are used to add non-holonomic conditions to the basic Hamiltonian functional. Therefore the system Eqs (1), (2) includes $n + l$ unknowns q_j, λ_m; see for instance the popular monographs [2, 14, 12, 3]. The non-holonomic constraints Eq. (2) are formulated as linear functions of velocities $\dot{q}_j$; this has been shown to be satisfactory concerning the problems considered. For more details and generalization; see [4] or [48].

In order to arithmetize the mathematical model, we need to introduce three adequate coordinate systems. In accordance with Fig. 2, the fixed Cartesian coordinates (x, y, z) are obvious. Their origin is in the "Southern Pole of the Cavity" (SPC) denoted A. The position of the ball center is described in standard spherical coordinates with their origin being in the center of the cavity and α, γ denoting the polar and azimuthal angles, respectively. The origin of the moving coordinates is located in the center of the moving ball, so that it lies on the concentric sphere with radius $\varrho = R - r$. Moving axis p follows a tangent of the concentric sphere meridian in the vertical plane (x', z), axis q is always horizontal, and axis n has the direction of the upward directed normal at the contact of both bodies; see Fig. 2. Rotation of the ball with respect to the moving coordinates is represented by the Euler angles φ, θ, ψ. Components of the angular velocity vector $\boldsymbol{\omega} = [\omega_p, \omega_q, \omega_n]^T$ in moving coordinates are positive as corresponds to the usual convention. The velocities of the ball center with respect to global coordinates are $\mathbf{v} = [v_p, v_q, v_n]^T$.

In further text, only the components of vectors $\mathbf{v}, \boldsymbol{\omega}$ will be used. Nevertheless, their relation to the velocity components $\dot{q}_j$ used in Eqs (1), (2) is obvious.

The basic formulae for kinetic and potential energies with respect to moving coordinates read

$$T = \frac{1}{2} m \left(v_p^2 + v_q^2 + v_n^2 + \frac{2}{5} r^2 \left(\omega_p^2 + \omega_q^2 + \omega_n^2 \right) \right), \tag{3a}$$

$$V = mg\varrho(1 - \cos\alpha), \qquad (\varrho = R - r), \tag{3b}$$

where m, g represent the mass of the ball and gravitational acceleration, respectively. In order to relate the angular velocity vector $\boldsymbol{\omega}$ and the velocity components expressed in Euler angles φ, θ, ψ, we write

$$\omega_p = -\dot{\varphi}\sin\theta\cos\psi + \dot{\theta}\sin\psi, \tag{4a}$$
$$\omega_q = \dot{\varphi}\sin\theta\sin\psi + \dot{\theta}\cos\psi, \tag{4b}$$
$$\omega_n = \dot{\varphi}\cos\theta + \dot{\psi}. \tag{4c}$$

Because the spherical cavity has a constant curvature $1/\varrho$ at every point regardless of direction, the relation between angles α, γ and velocities v_p, v_q can be expressed simply, see Fig. 2,

$$v_p = \varrho\dot{\alpha}, \quad v_q = \varrho\dot{\gamma}\sin\alpha, \quad v_n = 0, \tag{5}$$

where the expression $v_n = 0$ represents one of the three contact constraints. For the same reasons, the Pfaff contact conditions of perfect rolling without slipping can be easily expressed. They specify the relations between angular velocities $\omega_p, \omega_q, \omega_n$ and angles α, γ or displacements v_p, v_q. With respect to Eq. (5), the contact conditions can be reformulated as follows:

$$\begin{aligned} v_p - r\omega_q &= 0, & r\omega_q - \varrho\dot{\alpha} &= 0, \\ v_q + r\omega_p &= 0, \quad \Longrightarrow & r\omega_p + \varrho\dot{\gamma}\sin\alpha &= 0, \\ v_n &= 0, & v_n &= 0. \end{aligned} \tag{6}$$

Taking into account Eqs (5) and (6), the expressions for energies from Eq. (3) can be rewritten in the form

$$T = \frac{1}{2}m\left(\frac{7}{5}\varrho^2(\dot{\alpha}^2 + \dot{\gamma}^2\sin^2\alpha) + \frac{2}{5}r^2(\dot{\psi} + \dot{\gamma}\cos\alpha)^2\right), \tag{7a}$$
$$V = mg\varrho(1 - \cos\alpha). \tag{7b}$$

With reference to the problem definition, no external excitation or energy dissipation are assumed. Hence, the internal energy introduced to the system by non-homogeneous initial conditions has the form:

$$\begin{aligned} E_0 = T + V = &\frac{1}{2}m\left(\frac{7}{5}\varrho^2(\dot{\alpha}^2 + \dot{\gamma}^2\sin^2\alpha) + \frac{2}{5}r^2\omega_n^2\right) \\ &+ mg\varrho(1 - \cos\alpha). \end{aligned} \tag{8}$$

Here the spin of the moving sphere is given in the form $\omega_n = \dot{\psi} + \dot{\gamma}\cos\alpha$ with respect to Eq. (4c) and the geometric properties of the cavity.

Every conservative Lagrangian system (in the sense of energy balance) possesses at least one first integral, which can be considered a multiple of the total energy of the system. Therefore, with respect to Eq. (8), it can be formulated as follows:

$$\dot{\alpha}^2 + \dot{\gamma}^2\sin^2\alpha + \mu\omega_n^2 + 2\omega_0^2(1 - \cos\alpha) = E, \tag{9}$$

where the following notations were adopted:

$$\mu = \frac{2r^2}{7\varrho^2}, \quad \omega_0^2 = \frac{5g}{7\varrho}, \quad E = \frac{10E_0}{7m\varrho^2}. \tag{10}$$

Due to the transparent structure of the problem, although it is non-holonomic, it can be rewritten in three degrees of freedom only, and no procedure via Lagrangian multipliers has to be applied. Moreover, since no explicit external excitation is present, both terms on the right hand side of Eq. (1) identically vanish. Therefore, after some modifications, we obtain three Lagrangian equations for the three unknowns α, γ, ω_n:

$$\alpha: \ \ddot{\alpha} - (\dot{\gamma}^2 \cos\alpha - \mu\omega_n\dot{\gamma} - \omega_0^2)\sin\alpha = 0, \tag{11a}$$

$$\gamma: \quad \frac{\mathrm{d}}{\mathrm{d}t}\left(\dot{\gamma}\sin^2\alpha + \mu\omega_n\cos\alpha\right) = 0, \tag{11b}$$

$$\psi: \quad \frac{\mathrm{d}}{\mathrm{d}t}(\omega_n) = 0. \tag{11c}$$

It is obvious that Eqs (11b,c) are the first integrals, because γ and ω_n are cyclic coordinates. Therefore, we can write

$$\gamma: \ \dot{\gamma}\sin^2\alpha + \mu\omega_n\cos\alpha = H, \quad H = \frac{5H_0}{7m\varrho^2}, \tag{12a}$$

$$\omega_n: \quad \omega_n = S. \tag{12b}$$

Parameters E_0 and H_0 represent the energy and angular momentum of the system, respectively; they are given by Eqs (8,12a) or (9, 12a), where the initial conditions $\alpha, \dot{\alpha}, \dot{\gamma}, \omega_n$ are substituted.

Equations (12) are the second and third first integrals of the system. The first one represents the conservation of the system's angular momentum with respect to axis z at the constant level H, while Eq. (12b) shows the spin velocity (proportional to S) of the ball with respect to the normal n. We can see that the spin velocity is constant throughout the whole period of the system movement, although it interacts with the other angular velocity components of the ball through relations Eq. (4). Note that this very special character of the spin is a direct consequence of the spherical shape of both the cavity and the ball. Any other combination of two bodies in contact would lead to a variable spin velocity. The general form of Eq. (11c) would encompass an additional term dependent on differences in the principal curvatures of the two bodies. This difference is zero for spherical surfaces.

2.2 Characteristic Equation

The three first integrals Eqs (9,12) represent certain invariants and an alternative description of the system behavior; they provide a possibility for a transparent introduction of energy and movement through initial parameters. Thus, they enable the investigation of particular states of the system, an analytical formulation of various characteristics of trajectories, and, consequently, much greater insight into the nature of system parameters than one based solely on a numerical integration of the original differential system.

Let δ denotes the height of the ball above the bottom of the cavity, i.e., the z coordinate of the center of the sphere:

$$\delta = 1 - \cos\alpha \quad \Rightarrow \quad \dot{\alpha} = \dot{\delta}/\sin\alpha, \tag{13}$$

If $\dot{\gamma}$ is eliminated from Eq. (9) using Eq. (12a), one obtains after some manipulation

$$\begin{aligned} \dot{\delta}^2 &= (E - \mu\omega_n^2 - 2\omega_0^2\delta)(2\delta - \delta^2) - (H - \mu\omega_n(1-\delta))^2 \\ &= f(\delta) \end{aligned} \tag{14a}$$

$$\dot{\gamma} = \frac{H - \mu\omega_n(1-\delta)}{2\delta - \delta^2}. \tag{14b}$$

In further text, we term $f(\delta)$ defined by Eq. (14) the "Characteristic Function" (CF), and $f(\delta) = 0$ the "Characteristic Equation" (CE). Symbols E and H in Eq. (14) represent the measure of energy introduced into the ball at the moment $t = 0$ by means of the initial conditions: δ—the initial height of the ball, $\dot{\gamma}$—"Initial Horizontal Velocity" (IHV), and ω_n—"Initial Spin Velocity" (ISV); see Eqs (9, 12a). Based on these initial conditions, the energy in the system may be quantified using the following relations:

$$\begin{aligned} E &= \dot{\gamma}_0^2\delta_c(2-\delta_c) + 2\omega_0^2\delta_c + \mu\omega_n^2\,, \\ H &= \dot{\gamma}_0\delta_c(2-\delta_c) + \mu\omega_n(1-\delta_c)\,. \end{aligned} \tag{15}$$

Function $f(\delta)$ is a cubic parabola which attains positive or negative values based on system parameters μ, ω_0, state variables $\alpha, \dot{\alpha}, \dot{\gamma}, \omega_n$ together with their initial values $\alpha_c, \dot{\alpha_c}, \dot{\gamma}_0, \omega_{n0}$ (hidden in E, H), and with respect to independent variable δ. The general form of the CF is obvious in Fig. 3. The interval $\delta \in (0, 2)$ spans the whole diameter $2R$ of the cavity from the SPC to the NPC (NPC — "Northern Pole of the Cavity").

Obviously it holds that

$$\begin{aligned} &f(-\infty) < 0, \\ &f(0) = -(H - \mu\omega_n)^2,\ f(2) = -(H + \mu\omega_n)^2, \\ &f(1) = E - H^2 - 2\omega_0^2 - \mu\omega_n^2, \\ &f(\infty) > 0. \end{aligned} \tag{16}$$

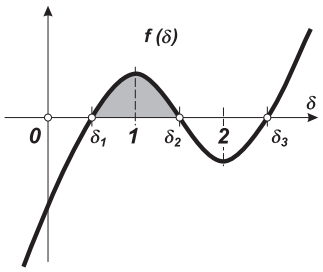

Fig. 3 General shape of Characteristic Function $f(\delta)$ and of the area delimiting the active spherical strip in the interval $\delta \in (\delta_1, \delta_2)$

The cubic polynomial Eq. (14a) is physically meaningful only for values where $f(\delta) > 0$, as $\dot{\delta}$ is considered to be real. The first derivative of $f(\delta)$ may be formally written as a general quadratic polynomial:

$$\begin{aligned} \frac{\mathrm{d}f(\delta)}{\mathrm{d}\delta} &= A\delta^2 - 2B\delta + C, \\ A &= 6\omega_0^2, \quad B = 4\omega_0^2 + E - \mu\omega_n^2(1-\mu), \\ C &= 2\left(E - H\mu\omega_n - \mu\omega_n^2(1-\mu)\right). \end{aligned} \tag{17}$$

Quadratic equation Eq. (17) has two real roots because its discriminant is always positive:

$$\begin{aligned} &B^2 - A \cdot C > 0 \;\Rightarrow \\ &\left(E - \mu\omega_n^2(1-\mu) - 2\omega_0^2\right)^2 + 12\omega_0^2\left(\omega_0^2 + \mu\omega_n H\right) > 0. \end{aligned} \tag{18}$$

The inequality Eq. (18) is fulfilled trivially for $\omega_n H > 0$. Otherwise, introduction of initial conditions $\delta_c, \dot{\gamma}_0$ and ω_n into E, H, defined by Eqs (9,12a), implies that Eq. (18) is valid for $0 \le \delta_c < 2$. Therefore, the cubic parabola Eq. (14a) has two extremes. The analogous procedure confirms that $C > 0$. Thus

$$B^2 > B^2 - AC, \tag{19}$$

and both the extremes are situated on the positive semi-axis: $0 \le \delta_{e1} \le \delta_{e2}$; the first one is positive and the second is negative:

$$f(\delta_{e1}) \ge 0, \quad f(\delta_{e2}) \le 0. \tag{20}$$

Summarizing the above contemplation, one can conclude that the CE Eq. (14a) has three real roots satisfying the following conditions:

$$0 \le \delta_1 \le \delta_2 < 2 < \delta_3. \tag{21}$$

The first two roots are physically meaningful, as they delimit an interval on axis δ where $\dot{\delta}^2 \ge 0$, which is a necessary condition for the energy accumulated in the system to be real. For geometrical reasons, the values $\delta > \delta_3 > 2$ do not represent a physically meaningful state, although $\dot{\delta}^2 \ge 0$ there as well. Note that zero and the coinciding roots can occur. As we will see later, they represent physically important cases.

3 THE SEPARATION CIRCLE AND ITS NEIGHBORHOOD

3.1 Definition and relevance of the Separation Circle

Previous studies by the authors [41,40] have shown that the most important separation limit between trajectory types (or groups) that start at a certain point is a trajectory running at constant angular velocity Γ along a parallel of the cavity. This trajectory will be called the "Separation Circle" (SC), because it separates qualitatively different trajectories. The SC can be characterized as follows: the ball is pulled up along a

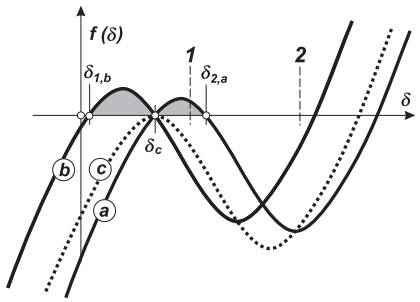

Fig. 4 Active area: solid curve (b) - trajectory below the SC: $\delta \in (\delta_{1,b}, \delta_{2,b} = \delta_c)$; solid curve ($a$) - trajectory above the SC: $\delta \in (\delta_{1,a} = \delta_c, \delta_{2,b})$; dashed curve ($c$) - transition case representing the SC - no active area due to coincidence $\delta_c = \delta_1 = \delta_2$.

meridian of the cavity to a certain level δ_c to the "Starting Point of the Trajectory" (SPT), and subsequently a horizontal impulse is applied to it. The intensity of the impulse is so high that it sets the ball onto a horizontal circular trajectory at the vertical level δ_c. This condition can be used reversely to determine the necessary IHV $\dot{\gamma}_c = \Gamma$ or v_{qc}, the values of which represent the constant angular or tangential velocities relevant to movement along the SC. The initial spin velocity ω_n is considered zero in the first step. The spin velocity can also be set such that it compensates for $\dot{\gamma}_c$ when different from Γ in order to maintain the SC trajectory.

Let us evaluate the notion of the SC from the viewpoint of the CE discussed above. Figure 4 shows parabola $f(\delta)$ for a given height δ_c and three different values of the IHV. Intervals where $f(\delta) \geq 0$ for $\delta \in \langle 0, 2\rangle$ represent possible heights at which the trajectory of the ball in the cavity can occur. In the case of the SC trajectory, i.e. for IHV $\dot{\gamma}_c = \Gamma$, one double root $\delta_1 = \delta_2 = \delta_c$ of $f(\delta) = 0$ occurs; this case provides an active area of zero width, see the dotted curve (c) in Fig. 4.

For $\dot{\gamma}_c < \Gamma$, the active area spans between δ_1 and δ_2 which coincide with δ_c. An initial velocity higher than Γ leads to a trajectory within the spherical strip above the $\delta_c = \delta_1$ boundary and goes up to δ_2. In such a case, it can occur that $\delta_2 > 1$, which means that the ball passes into the upper hemisphere of the cavity. The limit case is reached when the IHV approaches an infinite value. Then δ_1, δ_2 are symmetrically distributed with respect to $\delta = 1$. The upper boundary of the active strip is represented by the SC mirrored in the upper hemisphere. The trajectory becomes planar again although the plane is slanted passing the SPT and the center of the cavity.

The classification strategy based on the SC was intuitively adopted by the authors in their earlier studies, e.g. [38,41,40]. Actually it appears that this classification well describes all possible trajectories of a ball rolling inside a spherical cavity and starting from a certain point. Whatever the orientation and intensity of the initial impulse, the movement of the ball takes place within a uniquely defined spherical strip delimited by the two lower roots δ_1, δ_2 of the CE, Eq. (14), which are related to the energy contained in the system.

3.2 Position of the Separation Circle and its dynamic stability

Let us inspect Eq. (11a). Provided the ball follows the SC at a height given by initial condition $\alpha_c < \pi/2$, i.e., $\delta_c < 1$, its angular velocity is constant, $\dot{\gamma}_0 = \Gamma$, and vertical acceleration $\ddot{\alpha}$ vanishes, so that we can write

$$\Gamma^2 \cos\alpha_c - \mu\omega_n\Gamma - \omega_0^2 = 0, \quad 0 < \alpha_c < \pi/2\,. \tag{22}$$

This quadratic equation has two real roots:

$$\Gamma = \frac{\mu\omega_n \pm \sqrt{\mu^2\omega_n^2 + 4\omega_0^2\cos\alpha_c}}{2\cos\alpha_c} \;\Rightarrow$$

$$v_{qc} = \frac{1}{2}\varrho\cdot \mathrm{tg}\alpha_c\left(\mu\omega_n \pm \sqrt{\mu^2\omega_n^2 + 4\omega_0^2\cos\alpha_c}\right). \tag{23}$$

When zero spin velocity is assumed, these relations simplify greatly:

$$\Gamma_0 = \pm\frac{\omega_0}{\sqrt{\cos\alpha_c}} = \pm\frac{\omega_0}{\sqrt{1-\delta_c}}\,. \tag{24}$$

The IHV v_{qc} or angular velocity Γ satisfying Eq. (23) produces the SC for the given polar angle α_c. The roots represent two opposite directions with respect to the trajectory initial point. Their ratio depends on the sign of the spin velocity ω_n. For zero initial spin, the image is symmetrical in the horizontal plane with respect to the initial point of the trajectory. The schematic plots in Fig. 5 demonstrate the dependence of velocity v_{qc} on both the initial height (given by parameter α_c) and the ratio of the sphere to the cavity. Graph (a): fixed height $\alpha_c = \pi/4$, plot (b): fixed ratio r/R. In this latter case, the dependence starts from zero for the SPC ($\alpha_c = 0$) and tends to infinity for the "Equator of the Cavity" (EQC) ($\alpha_c = \pi/2$). The bold-black curves in plots (a) and (b) represent the spin-free state ($\omega_n = 0$), while the color curves show the influence of the initial spin. The relation between the velocity v_{qc} and the initial spin ω_n, which maintains the trajectory in the SC, may be deduced from Eq. (22), and is illustrated in picture (c). A decrease in horizontal velocity is compensated by a negative spin, whereas an increase in horizontal velocity implies a proportional increase in positive spin. One-sided limits of ω_n for $v_{qc} \to 0^+$ and $v_{qc} \to \infty$ exist and equal $\pm\infty$.

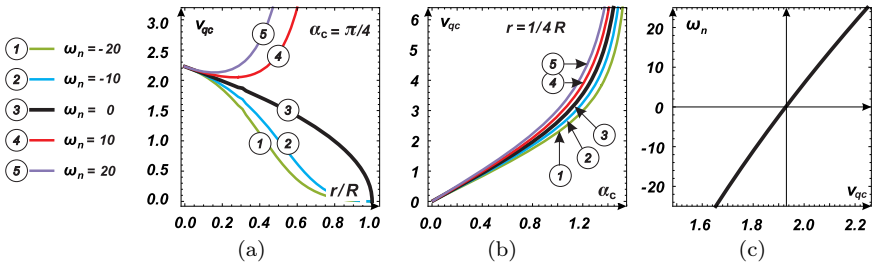

Fig. 5 Initial Horizontal Velocity producing the trajectory of the SC: (a) fixed initial height $\alpha_c = \pi/4$, varying ratios r/R, (b) fixed ratio r/R, various heights α_c; color curves in (a) and (b) correspond to various spin values, (c) compensation spin.

We now examine the neighborhood near the SC. We revisit Eq. (11a) and also the first integral Eq. (12a). The vertical position of the ball on the SC is given by the angle α_c, and the horizontal angular velocity Γ is determined by Eq. (23). These are the nominal values which are subjected to small perturbations generated by dispersion in the initial conditions setting. Thus, we reformulate the initial conditions as

$$\dot{\gamma}_0 \approx \Gamma + \eta, \quad \alpha \approx \alpha_c + \zeta, \tag{25}$$

where ζ and η are small values.

Substituting perturbed initial conditions Eq. (25) into Eq. (11a), a linearized equation for $\zeta(t)$ can be deduced. Disregarding the higher order terms $\zeta^2, \eta^2, \eta \cdot \zeta$, one obtains

$$\begin{aligned} &\ddot{\alpha}_c - \left(\Gamma^2 \cos\alpha_c - \mu\omega_n\Gamma - \omega_0^2\right)\sin\alpha_c + \\ &\ddot{\zeta} - \left(\left(\Gamma^2 \cos\alpha_c - \mu\omega_n\Gamma - \omega_0^2\right)\cos\alpha_c - \Gamma^2\sin^2\alpha_c + \right)\zeta \\ &\quad - (2\Gamma\cos\alpha_c - \mu\omega_n)\sin\alpha_c \cdot \eta = 0. \end{aligned} \tag{26}$$

The first line of Eq. (26) vanishes due to Eq. (11a), and the coefficient of the term with $\cos\alpha_c$ on the second line disappears because of Eq. (22). Hence, it holds that

$$\ddot{\zeta} + \Gamma^2 \sin^2\alpha_c \cdot \zeta + (\mu\omega_n - 2\Gamma\cos\alpha_c)\sin\alpha_c \cdot \eta = 0\,. \tag{27}$$

This equation is solvable for zero initial conditions in a closed form:

$$\zeta = \frac{2\eta\,(2\Gamma\cos\alpha_c - \mu\omega_n)}{\Gamma^2\sin\alpha_c}\sin^2\left(t \cdot \frac{1}{2}\Gamma\sin\alpha_c\right)\,. \tag{28}$$

At the level of the first approximation, supposing that a small increase of initial tangential velocity is considered, it is obvious that the trajectory lies above the SC within the narrow spherical strip $\delta \in (\delta_c = \delta_1, \delta_2)$, where $\delta_1 < \delta_2$. Similarly, decreasing the IHV, we get a trajectory below the SC within the limits $0 < \delta_1 < \delta_2 = \delta_c$. The width of the strip in both cases is $|\eta|/\Omega_v$.

The explicit form of perturbation Eq. (28) represents a harmonic function with period

$$T_{per} = \frac{4\pi}{\Gamma\sin\alpha_c}\,.$$

One loop around the SC takes $T_{loop} \approx 2\pi/(\Gamma + \eta)$. Therefore, the number of vertical periods during one loop is

$$N_{per} = \frac{2(\Gamma+\eta)}{\Gamma\sin\alpha_c} \approx \frac{2}{\sin\alpha_c}\,, \tag{29}$$

which, in general, is not a rational number, and the trajectory alternating above or below the SC does not pass the SPT.

We should be aware that the estimates Eq. (25) and also the results Eq. (28) are applicable if $0 < \alpha_c < \pi/2$. Indeed, for small α_c, the values α_c and ζ are commeasurable as are the values Γ, η, and classification according to the powers of a small parameter becomes invalid. Of course, the perturbations η, ζ should also remain small in order for linear approximation to be justified.

Finally, one can conclude that the SC (perhaps with the exception of the SPC neighborhood) is dynamically stable, and a small initial perturbation does not cause a receding of this trajectory from the original SC.

Let us show an example of a time history of the trajectory corresponding to the SC; see Fig. 6. The time history shows a harmonic process in both horizontal coordinates and a constant value in the vertical coordinate, plot (a).

4 TRAJECTORIES NOT INFLUENCED BY INITIAL SPIN OF THE BALL

4.1 Trajectories above the SC

Let us examine the case where $\delta_c = \delta_1 \le \delta_2$ and $\omega_n = 0$, i.e., the ball is rolling above the SC and no spin is assumed, $\dot\gamma_0 > \Gamma_0$; see also curve (a) in Fig. 4.

Setting the position for the SPT on a meridian of the cavity at a certain level characterized by polar angle $0 < \alpha_c < \pi/2$ or equivalently by height $\delta_1 \in (0,1)$ (in the lower hemisphere of the cavity) in fact means that the lowest root $\delta_1 = \delta_c$ of the CE is fixed. Considering that one root is known, we can rewrite Eq. (14a) in the form of a partial decomposition with respect to the root factors:

$$
\begin{aligned}
&f(\delta) = (\delta - \delta_c)(K\delta^2 + 2L\delta + M) = 0, \qquad (30)\\
&K = 2\omega_0^2, \quad L = -\left(2\omega_0^2 + \frac{1}{2}\dot\gamma_0^2\delta_c(2-\delta_c)\right),\\
&M = \dot\gamma_0^2\delta_c\,(2-\delta_c)^2\,, \qquad \dot\gamma_0 > \Gamma_0\,.
\end{aligned}
$$

The detailed form of coefficients K, L, M is derived from the full CE, Eq. (14a), where a zero ISV was substituted. The energy E, Eq. (9), and the angular momentum H, Eq. (12a), contained in Eq. (14a), were included in the initial parameter values for the SPT.

The SC is regarded as the lower boundary of the spherical strip on the cavity surface within which a particular trajectory runs. The upper boundary is then the lower of the

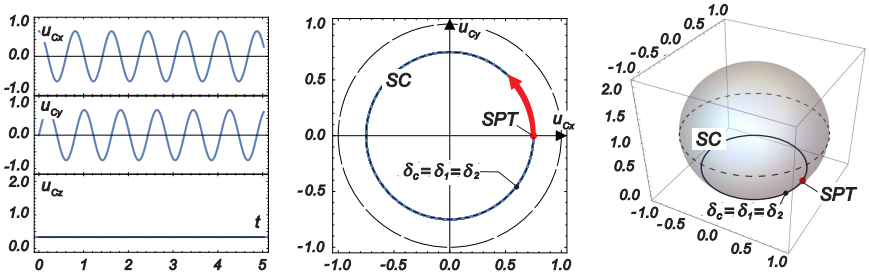

Fig. 6 Example of the trajectory of the SC type without influence of the ISV ($\omega_n = 0$): (a) time history, (b) top view, (c) axonometric demonstration.

remaining roots δ_2, δ_3. They can be calculated from the quadratic equation, which is outlined in Eq. (30):

$$\delta_{2,3} = \frac{1}{K}\left(-L \pm \sqrt{L^2 - K\cdot M}\right), \tag{31a}$$

$$D = L^2 - K\cdot M = \tag{31b}$$

$$= \left(2\omega_0^2 + \frac{1}{2}\dot\gamma_0^2\delta_c(2-\delta_c)\right)^2 - 2\omega_0^2\dot\gamma_0^2\delta_c(2-\delta_c)^2\,.$$

In order for both δ_2, δ_3 to always be real, it should hold that $D > 0$, regardless of the initial parameter settings. Therefore, the following must be valid for the slightly modified D:

$$D \;=\; \left(2\omega_0^2 - \frac{1}{2}\dot\gamma_0^2\delta_c(2-\delta_c)\right)^2 + 2\omega_0^2\dot\gamma_0^2\delta_c^2(2-\delta_c) \;>\; 0, \tag{32}$$

which is always true, and we can state once again that Eq. (14a) has three real roots. Furthermore, $0 < D < L^2$ and, consequently, all roots are positive and fulfill conditions $0 < \delta_c = \delta_1 < \delta_2 < 2$ and $\delta_3 > 2$. Of course, root δ_3 is geometrically out of scope, and it is no longer considered; see above, Sec. 2.2.

In order to outline the basic character of a trajectory occurring between boundaries $\delta_c = \delta_1, \delta_2$, we inspect the expression for the circumferential velocity $\dot\gamma$ following from Eq. (14b). In general, it can be assumed that the trajectory is periodical in the vertical direction, where the ratio of the period to the SC lengths is not a rational number. Therefore one round along the SC will not contain a whole number of periods. The angular momentum H is always positive, see Eq. (12a), and the second term of the numerator vanishes since $\omega_n = 0$. The denominator in this fraction is also positive, because $\delta(2-\delta) > 0$ for $\delta \in (0,2)$. Therefore, $\dot\gamma > 0$ regardless of the settings for the initial conditions at the SPT. Moreover, it can be supposed that the variability of $\dot\gamma$ during one period for given initial settings will not be dramatic. Indeed, it is obvious that the angular momentum H is constant during one period. Consequently, the horizontal angular velocity at the point where the trajectory touches the upper boundary of the strip, δ_2, follows from Eq. (12), where $\omega_n = 0$, and it holds that

$$\dot\gamma_2 \sin^2\alpha_2 \;=\; \dot\gamma_0 \sin^2\alpha_c, \tag{33}$$

where $\alpha_c, \dot\gamma_0$ or $\alpha_2, \dot\gamma_2$ are values of the respective parameters at the initial point ($\delta_c = \delta_1$) or at the touching point on the upper boundary (δ_2). Hence, it can be written:

$$\dot\gamma_{2T} = \dot\gamma_0 \left(\frac{\sin\alpha_c}{\sin\alpha_2}\right)^2 = \dot\gamma_0 \,\frac{(\delta_c-2)\,\delta_c}{(\delta_2-2)\,\delta_2} \tag{34a}$$

$$\dot\gamma_{2T} \approx \dot\gamma_0\,(1 - 2\Delta_\alpha \cot\alpha_c) \approx \dot\gamma_0\left(1 - \frac{2\,(\delta_c-1)\,\Delta_\delta}{(\delta_c-2)\,\delta_c}\right) \tag{34b}$$

where Eq. (34b) is valid for small values of the difference $\Delta_\alpha = \alpha_2 - \alpha_c$ or $\delta_\delta = \delta_2 - \delta_c$.

The horizontal velocity is slightly lower at the upper apex due to an increase in potential energy. At the same time, some qualitative confirmation of this fact follows from

the constant angular momentum H and δ, which changes more or less monotonously. This implies that no singular points emerge during one vertical period, and that the angular velocity along the trajectory is mildly variable. Thus, the trajectory has the shape of a simple periodic curve without any turnabout points reversing velocity $\dot{\gamma}$.

Here we assess the length and duration of one vertical period of the trajectory. Taking into account that the IHV leads to a trajectory which is symmetrical with respect to the initial point and with respect to the form of Eqs (11) and (12), we can assume that one period consists of two identical halves symmetrically distributed around a point on the upper boundary δ_2. Consequently, it is sufficient to examine the first half of the period within the interval $\delta \in (\delta_c = \delta_1, \delta_2)$. We revisit both relations in Eq. (14). Assuming $\omega_n = 0$, the following differential system can be written:

$$\dot{\delta}^2 = (E - 2\omega_0^2\delta)(2\delta - \delta^2) - H^2, \tag{35a}$$

$$\dot{\gamma} = \frac{H}{2\delta - \delta^2}. \tag{35b}$$

The first equation is $\dot{\gamma}$ independent, and, therefore, it can be solved as the first step. The pair $\pm\delta$ could be put into the second equation to obtain $\gamma(t)$ by means of integration between δ_c and δ_2. However, it comes to light that both points on the strip boundaries δ_c, δ_2 are singular and represent bifurcation points. In addition, the relevant Jacobi matrix is also singular and, consequently, does not enable us to predict the principal directions in the point neighborhood. Three solutions start from the SPT (including the constant δ_c), and all of them have the zero derivative. Therefore, neither an analytical nor a numerical stable solution can be deduced from these points. This difficulty can be overcome by differentiating Eq. (35a) with respect to time. After reducing by $\dot{\delta}$, the modified system reads

$$\ddot{\delta} = E(1 - \delta) - \omega_0^2\delta(4 - 3\delta)\,, \tag{36a}$$

$$\dot{\gamma} = \frac{H}{2\delta - \delta^2}\,, \tag{36b}$$

where $E = \dot{\gamma}_0^2\delta_c(2 - \delta_c) + 2\omega_0^2\delta_c$, $H = \dot{\gamma}_0\delta_c(2 - \delta_c)$, cf. Eq. (15).

The denominator in Eq. (36b) is always positive because $\delta \in (\delta_c, \delta_2)$. Then Eq. (36) can be solved for initial conditions $\delta(0) = \delta_c, \dot{\delta}(0) = 0$ sequentially putting partial results of Eq. (36a) into Eq. (36b). Finally, the time is eliminated, and one obtains δ

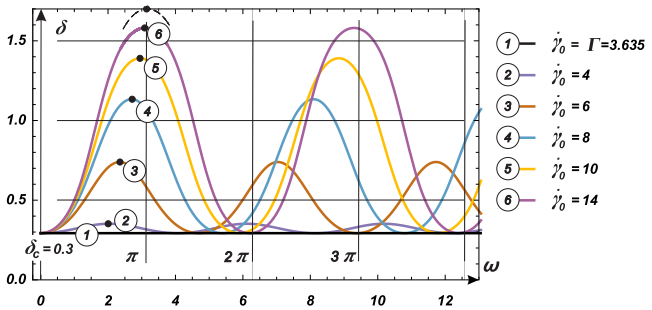

Fig. 7 Shape of the trajectory above the SC for various IHV.

as a function of γ. Some samples of the trajectory are plotted in Fig. 7, in which a set of five cases where $\dot{\gamma}_0 >> \Gamma_0$ for the selected $\delta_c = 0.3$ and the relevant $\Gamma_0 = 3.63494$ is demonstrated.

Notice the shape of the high curves in this figure. They correspond to the dominating first term in the right-hand side of Eq. (36a) when $\dot{\gamma}_0$ is large. Omitting the second term when $\dot{\gamma}_0 \gg\gg \Gamma_0$, we obtain a linear equation of harmonic oscillation with an adequate constant right-hand side. Consequently, we can see that for increasing $\dot{\gamma}_0$, the response curves approach a sinusoidal shape up to the dashed black curve segments which indicate infinite angular velocity $\dot{\gamma}_0$.

Some general attributes of the trajectories can be observed in Fig. 8; the blue curves above the SPT, $\dot{\gamma}_0 > \Gamma_0$ are regarded in this section. For a fixed Γ_0 and increasing IHV, the angular period γ_T slowly rises and approaches a planar trajectory length of diameter $2(R - r)$ for $\dot{\gamma}_0 \to \infty$. This corresponds to the horizontal asymptote at the $\gamma_T = 2\pi$ level; see picture (a). Picture (b) demonstrates the rising of the strip's upper level δ_2 with increasing IHV. The parameter δ_2 approaches the horizontal asymptote, symmetrically placed with respect to the EQC, in the particular case from 0.3 to 1.7. The limit case of $\dot{\gamma}_0 \to \infty$ will be discussed separately later in Sec. 4.2.

Using the above analytical results we can outline some detailed trajectory properties with respect to IHV and the height of the SPT above the SPC. A typical trajectory shape is plotted in Fig. 9. Comparing Figs 6 and 9, we can see that the trajectory time history is still a simple periodic curve synchronous in both horizontal coordinates with a slight additive modulation.

The frequency of vertical displacement u_{cz} in Fig. 9a is related to that of horizontal displacements via the angular period γ_T which depends on the $\delta_1 = \delta_c$ and δ_2 boundaries of the spherical strip. No visible influence of higher harmonics is observed, although a very light quasi-periodic character can be noticed, as it follows from the geometric character of the system. The shape in the top view is helical and resembles the form of a prolate type hypotrochoid close to a hypotrochoid form of prolate types. As no sharp apexes or loop multiple points are detected, we can conclude that no basic cycloid or curtate trochoid is approached.

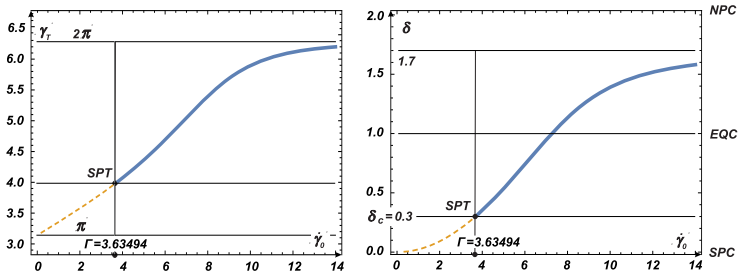

(a) (b)

Fig. 8 Trajectory above the SC (no spin applied), (a) spatial period dependent on the IHV ($\dot{\gamma}_0$); (b) upper boundary of the strip δ_2 as a function of $\dot{\gamma}_0$.

4.2 High initial horizontal velocity

Let us discuss the trajectories above the SC that emerge when the IHV distinctly exceeds the velocity Γ_0 or v_{qc} and simultaneously no ISV is applied, $\omega_n = 0$. The CF for an infinite IHV has a form corresponding to Fig. 3, which means that zero points δ_1, δ_2 are symmetrically distributed with respect to the point $\delta = 1$. A lower IHV shifts δ_2 to the left and the position of δ_1 remains the same.

The trajectories are again concentrated within the spherical strip delimited by roots $0 < \delta_1 = \delta_c < \delta_2 < 2$ of the characteristic equation Eq. (14a). We will inspect its evolution when $\dot{\gamma}_0 \gg \Gamma_0$. While it is always true that $\delta_1 < 1$, the upper boundary, being given by δ_2, can enter the upper hemisphere of the cavity reaching a value in the interval $1 < \delta_2 < 2$. The IHV corresponding to the transition case $\delta_2 = 1$ follows from equation Eq. (14a), where the two lowest roots δ_1, δ_2 are considered as known. After some manipulation, one can write

$$\dot{\gamma}_0^2 = \frac{8\omega_0^2 \cos\alpha_c}{\sin^2 2\alpha_c}\,, \qquad 1 - \cos\alpha_c = \delta_1 = \delta_c, \qquad 0 < \alpha_c < \pi/2\,, \tag{37}$$

where both the boundary values of α_c leading to an infinite IHV are obviously not admissible, as could be expected.

Increasing the IHV beyond all limits, the upper limit of the strip approaches a theoretical maximum:

$$\delta_2 = 2 - \delta_1. \tag{38}$$

It is an asymptotic position, which is monotonously approached as the initial velocity rises to infinity. In this theoretical state, the trajectory becomes planar, having a circular form with the diameter $2R$. This plane is inclined, being determined by the horizontal tangent at the SPT and by the cavity center; see Fig. 11a.

In the case when $\dot{\gamma}_0$ is high but finite, $0 < \Gamma_0 \ll |\dot{\gamma}_0| < \infty$, the root δ_2 is adequately lower:

$$\delta_2 = 2 - \delta_1 - \epsilon, \qquad 0 < \epsilon \ll 1. \tag{39}$$

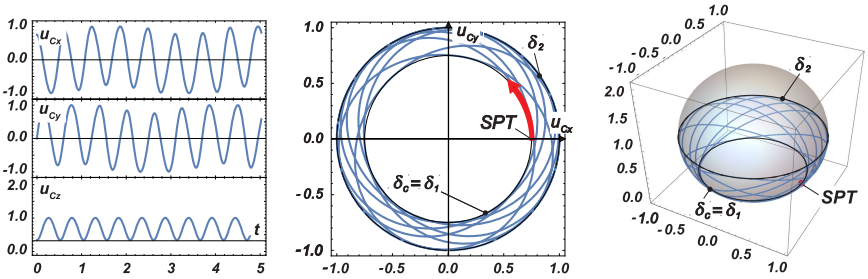

Fig. 9 Example of the trajectory above the SC with no ISV ($\omega_n = 0$): (a) time history, (b) top view, (c) axonometric demonstration.

Trajectories maintain their spatial character, but it is worthwhile to define an osculating plane at each point. The osculating plane makes sense from a physical perspective if it enables us to characterize the basic position of the trajectory using simpler elements than in the general case for lower IHV. In the case we are discussing, it can be assumed that the spiral does not differ much from a planar shape, and that its projection into the osculating plane at each point represents a good approximation. In other words, we can define an affine space which meets a sub-manifold at a point in such a way as to have a second order of contact at that point. The osculating plane passes the initial point δ_1 and a point in the upper hemisphere at the upper boundary of the strip $\delta_2 - \epsilon$, which is slightly below the level of the limit case Eq. (38). Therefore its inclination is slightly lower than that corresponding to the limit case for $\dot\gamma_0 \to |\infty|$. The osculating plane rotates around the vertical axis of the cavity with rotational speed Ω_v, which decreases as $\dot\gamma_0$ rises, and vanishes for an infinite IHV ($\dot\gamma_0$).

The velocity Ω_v can be estimated based on the position of the contact point of the trajectory and the upper boundary δ_2 evaluated at the conclusion of a single period. Although an explicit formula cannot be expressed, the process can be carried out observing the outline in Fig. 10. A sketch of the osculating plane behavior is graphically demonstrated in Fig. 11 for infinite IHV — picture (a), and finite IHV — pictures (b) and (c), showing position of this plane after the 1st and 3rd half-period, respectively (a negative movement sense has been selected for graphical reasons).

For a high but finite $\dot\gamma_0$, a ball starting at the SPT covers a distance of $2\pi - \eta$ along a nearly planar trajectory in the advancing osculating plane, where $\eta \to 0$ when $\dot\gamma_0 \to |\infty|$; see Fig. 10. Let us again consider Eq. (36), in particular equation (a) and the expression for E. Assuming that velocity $\dot\gamma_0$ is high, the second term of the right hand side in Eq. (36a) can be neglected and also enables E to be reduced. Then it can be approximately written:

$$\ddot\delta + E_\gamma \delta \;=\; E, \tag{40}$$

where $E_\gamma = E_{lim} = \dot\gamma_0^2 \delta_c(2-\delta_c)$ or $E_\gamma = E_\eta = (\dot\gamma_0 - \dot\eta)^2 \delta_c(2-\delta_c)$. For initial conditions $\delta(0) = \delta_c, \dot\delta(0) = 0$, the solution to equation Eq. (40) has the form

$$\delta = (\delta_c - 1)\cos t\sqrt{E_\gamma} + 1\,. \tag{41}$$

The length of the period in time is

$$T^t_{lim} = 2\pi E_{lim}^{-\frac{1}{2}} \quad \text{or} \quad T^t_\eta = 2\pi E_\eta^{\frac{1}{2}}\,, \tag{42}$$

and, therefore, for the rotational speed of the osculation plane around the z axis we can approximately write

$$\Omega_v \;\approx\; 1 - (\dot\gamma_0 - \eta)/\dot\gamma_0\,. \tag{43}$$

Since $\eta \to 0$ when $\dot\gamma_0 \to |\infty|$, $\lim_{\dot\gamma_0 \to |\infty|} \Omega_v = 0$ and $\delta_2 \to 2 - \delta_c$ as it corresponds with Eq. (38). These results can be confirmed intuitively by examining both of the graphs in Fig. 8. Indeed, the length of the period approaches the horizontal asymptote on the 2π level more or less exponentially. Because the tangential velocity along the trajectory is approximately constant, $\dot\gamma(t) \approx \dot\gamma_0 + \dot\eta$, the relation between $\gamma(t)$ and t can be expressed simply as $\gamma(t) \approx (\dot\gamma_0 + \dot\eta)t$. Then it holds approximately that

$$\Omega_v \;\approx\; -\frac{2T_{lim} - 2T_\eta}{2T_\eta}\cdot\dot\gamma_0 \;\approx\; \frac{-\exp\left(-\kappa\dot\gamma_0\right)}{2T_\eta}\cdot\dot\gamma_0, \tag{44}$$

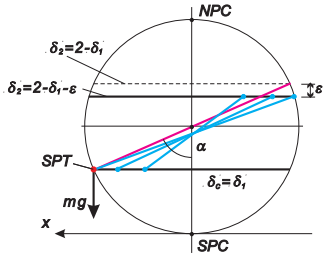

Fig. 10 Outline of the trajectory layer for high and infinite IHV.

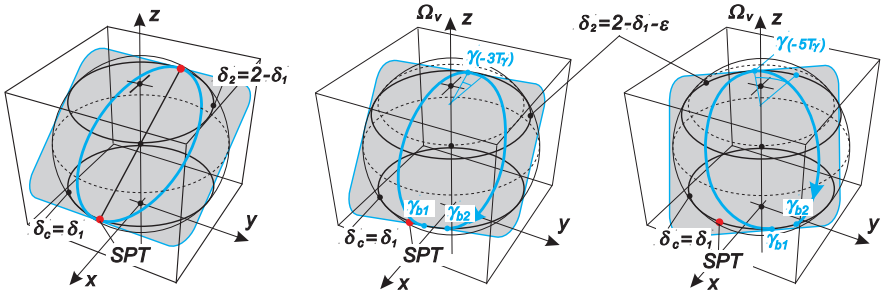

(a) (b) (c)

Fig. 11 Osculating plane (light grey) of a trajectory for high IHV (ISV is not applied): (a) infinite IHV; (b) finite IHV: - 3rd half-period; (c) finite IHV: - 5th half-period; γ_{b1}, γ_{b2}: starting or finishing points of one full period.

where $\kappa, [s]$ is a positive constant. Employing l'Hospital's rule, it is obvious that $\lim_{\dot{\gamma}_0 \to |\infty|} \Omega_v = 0$ holds as before.

Let us point out some properties of the trajectory discussed above, such as features of a curve passing through a layer of thickness ϵ; see Eq. (39) and Fig. 10. An analysis using the small parameter approach cannot be done directly because the solution for $\dot{\gamma}_0 \to |\infty|$, which serves as a zero approximation, does not exist in an explicit form for several reasons (infinite energy, infinite angular momentum, indefinite derivatives with respect to time, etc.). Despite this fact, we have seen that all trajectories are stable, whatever their parameter setting. Consequently, the existence of the zero approximation can be assumed in an implicit meaning of a certain limit. Therefore, analogously with Eq. (25), we are entitled to write

$$\dot{\gamma} \approx \dot{\gamma}_0 - \dot{\eta}, \qquad \alpha \approx \alpha_2 + \zeta, \tag{45}$$

where $\alpha_2, \dot{\gamma}_0$ are relevant to the planar trajectory incident with the inclined plane, see Fig. 11a, and $\dot{\eta}, \zeta$ are small unidirectional deviations. They enable us to define high values of $\dot{\gamma}, \alpha$ but still finite values of the initial approximations $\alpha_2, \dot{\gamma}_0$.

We recall Eq. (11). By the way, let us note that despite the fact that the ISV is not included in this section ($\omega_n = 0$), we can see that the proportion of the spin energy at high velocity $\dot{\gamma}$ is negligible anyway. Thus, putting approximations Eq. (45) into Eqs (11a,b), and comparing terms that involve the same powers of $\dot{\eta}, \zeta$, we can write

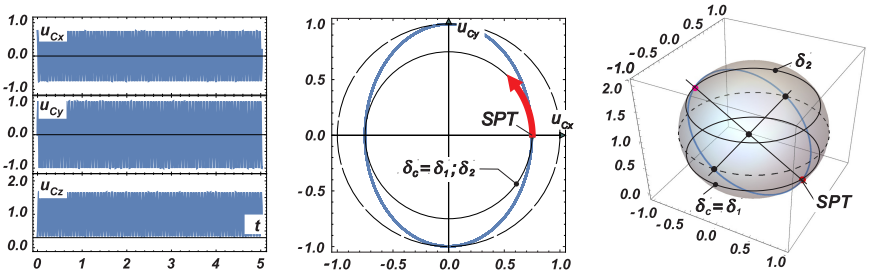

(a) (b) (c)

Fig. 12 Example of the trajectory above the SC with no ISV ($\omega_n = 0$) for a high IHV: (a) time history, (b) top view, (c) axonometric demonstration.

$$\dot{\eta}^0: \qquad \ddot{\alpha}_2 - \left(\dot{\gamma}_0^2 \cos\alpha_2 - \omega_0^2\right) \sin\alpha_2 = 0, \tag{46a}$$

$$\dot{\gamma}_0 \sin^2\alpha_2 = H, \tag{46b}$$

$$\dot{\eta}^1: \quad \ddot{\zeta} + \dot{\gamma}_0 \sin 2\alpha_2 \cdot \dot{\eta} - \left(\dot{\gamma}_0^2 \cos 2\alpha_2 - \omega_0^2 \cos\alpha_2\right) \cdot \zeta = 0, \tag{46c}$$

$$\sin^2\alpha_2 \cdot \dot{\eta} - \dot{\gamma}_0 \sin 2\alpha_2 \cdot \zeta = 0. \tag{46d}$$

Eqs (46a,b) are implicitly fulfilled and approximately represent a circular trajectory in the inclined osculating plane. Eqs (46c,d) represent a rough approximation of the trajectory behavior, provided a high IHV in the sense of Eq. (45) is applied. The system Eqs (46c,d) is linear because $\alpha_2, \dot{\gamma}_0$ are known parameters. Variable $\dot{\eta}$ can be eliminated, so it holds that

$$\ddot{\zeta} + \left(\dot{\gamma}_0^2 \left(2 + \cos 2\alpha_2\right) + \omega_0^2 \cos\alpha_2\right) \cdot \zeta = 0\,. \tag{47}$$

It is obvious that for high values of $\dot{\gamma}_0$, the term $\omega_0^2 \cos\alpha_2$ is negligible. The remaining coefficient is always positive. In a ratio to the length of the circular trajectory, it represents a parameter analogous with Eq. (29). It is proportional to the velocity Ω_v of the osculating plane rotation around the z axis, which approaches zero for $\dot{\gamma}_2 \to |\infty|$. This result is identical with the one obtained above in this section.

To demonstrate the character of the upper root δ_3 during the IHV limitation to $\pm\infty$, let us assess its value respecting Eq. (39), and the fact that the trajectory is running in a thin layer following the scheme in Fig. 10. The process is limited to within this domain, and, consequently, it can be linearized in the framework of this layer. Making use of these facts and a factored form of the polynomial, we can reformulate the CE, Eq. (14a) because two roots δ_c, δ_2 are known:

$$\begin{aligned} &(\delta - \delta_c)\,(\delta - (2 - \delta_c - \epsilon))\,(K\delta + L) = 0, \\ &K = 2\omega_0^2, \quad L = (\dot{\gamma}_0^2 \delta_c (2 - \delta_c) + 2\omega_0^2 (\delta_c + \epsilon)), \end{aligned} \tag{48}$$

which results in the third root:

$$\delta_3 \;=\; \frac{1}{2\omega_0^2}\left(\dot\gamma_0^2\delta_c(2-\delta_c)+2\omega_0^2(\delta_c-\epsilon)\right)\,. \tag{49}$$

This formula demonstrates that $2<\delta_3\to\infty$ for $\dot\gamma_0^2\to\pm\infty$.

For completeness, let us demonstrate an example of a trajectory based on a high IHV, Fig. 12. The time history, due to the high and nearly constant tangential velocity of the ball is homogeneous at all coordinates which interact rather on a geometrical basis. The circular character of the trajectory is obvious in pictures (b) and (c).

4.3 Trajectories below the SC

The CF has a form corresponding to curve (b) in Fig. 4. In general, δ_1 can descend to zero, as we can easily deduce from Eq. (50) or from the original characteristic equation, Eq. (14), with the vanishing absolute term. This case, together with the neighborhood of this value ($0\le\delta_1<\epsilon$), will be discussed in a separate section, Sec. 6. For these initial settings, the spin-free and the spin-considered cases of initial settings intermingle, and, hence, it is worthwhile to discuss the two of them together.

The spherical strip in which the trajectory for IHV $\dot\gamma_0<\mathit{\Gamma}_0$ emerges is below the SC. The strip is limited by the SC, which forms its upper boundary, $\delta_c=\delta_2$, and by the lower boundary δ_1, which is given by the quadratic term in Eq. (30). The basic analysis is similar to that which has been performed in the beginning of Sec. 4.1. The only difference is that the roots are ordered as follows: $0<\delta_1\le\delta_c=\delta_2<1<\delta_3$. The roots $\delta_{1,3}$ may be symbolically written as in Eq. (31):

$$\delta_{1,3}=\frac{1}{K}\left(-L\pm\sqrt{L^2-K\cdot M}\right)\,, \tag{50}$$

where the discriminant has the same form as in Eq. (31b) for $\delta_c=\delta_2$.

In order to determine velocity $\dot\gamma$ at the tangent point at the δ_1 boundary, we refer to Eq. (34), where α_1 is to be substituted instead of α_2:

$$\dot\gamma_{1T}=\dot\gamma_0\,\left(\frac{\sin\alpha_c}{\sin\alpha_1}\right)^2=\dot\gamma_0\,\frac{(\delta_c-2)\,\delta_c}{(\delta_1-2)\,\delta_1}\,. \tag{51}$$

It is obvious that $\dot\gamma_{1T}>\dot\gamma_0$ due to a lower potential energy at the δ_1 level. Inspecting Eq. (14), where $\omega_n=0$ is substituted, we can see that $\dot\gamma$ is a simple continuous function of δ, which is integrable on any interval $\delta\in(a,b)$ with $0<a,b<2$. This implies that no singular points emerge within one period, and the velocity along the trajectory is mildly variable. The trajectory has the shape of a simple curve without any multiple or turnabout points reversing its velocity.

As for the length of a single vertical period, a similar deduction can be made like in Sec. 4.1. However, care should be taken when the IHV approaches zero and the system Eqs (36) becomes unstable or discontinuous in the neighborhood of $\gamma=\pi/2$. For details, see Sec. 6. Nevertheless, in a common case, like in Sec. 4.1, we can assume once again that one period consists of two identical halves symmetrically distributed around the tangent point on the lower boundary δ_1, and, therefore, it is sufficient to examine only one half of the period.

Hence, the differential system Eq. (36) can also be used here, except that the zero initial conditions are formulated for the upper strip boundary, $\delta(0)=\delta_c,\dot\delta(0)=0$ and

the position of the lower boundary δ_1 should either be evaluated using Eq. (50e) or during solution of system Eq. (36).

Let us follow Fig. 13 demonstrating several trajectories comparable in their initial conditions for $\dot\gamma_0 < \Gamma_0$. Recalling Eq. (36a):

$$\ddot\delta = E(1-\delta) - \omega_0^2\delta(4-3\delta) \tag{36a}$$

for $E = \dot\gamma_0^2\delta_c(2-\delta_c)+2\omega_0^2\delta_c$, cf. Eq. (15), we can see that unlike cases with $\dot\gamma_0 > \Gamma_0$, the first term of the right hand side loses dominance, and a significant nonlinear character of the equation emerges. Retaining only the second term, we obtain an equation solvable using elliptic functions. This effect is obvious in Fig. 13, where the curves for decreasing IHV become more and more similar to an elliptic sinus. Returning to properties of the rational or irrational spiral form, see also Sec. 4.1, we can conclude that the vertical period length varies in the interval $2T_\gamma \in (\pi, 2\pi)$ throughout all $|\dot\gamma_0| \in (0,\infty)$, and, therefore, obviously no synchronization of the primary type can occur.

We shall point out some properties of the length and shift of periods that are specific for the trajectories below the SC. Characteristics of the vertical period length and the lower strip boundary position δ_1 as a function of the IHV and SPT level are demonstrated in Fig. 14; see the solid orange curves below $\Gamma_0 = 3.63494$. Both curves are smooth on the whole interval $\dot\gamma_0$ including the SPT. It is typical that the period $2\gamma_T$ shortens to π for $\dot\gamma_0 \to 0$, as it also corresponds to the character of an elliptical sinus that characterizes the shape of the trajectory; see [20] or [1]. The lower boundary of the strip δ_1 evidently tends to zero, i.e., towards the SPC.

With reference to Sec. 6, we can see that the period for $\dot\gamma_0 \to 0$ does not approach 2π, as could be intuitively expected. However, even cases discussed in this section evince some attributes which are distinctly visible for low IHV values . It is obvious, for instance, that the shape of the relevant curve depends on the SPT level. The phenomenon of period "shift" becomes more prominent as the height of the SPT or the boundary δ_1 level increase. This effect is discussed in more detail for both zero and non-zero ISV for low IHV in Sec. 6.

An example of a trajectory below the SC is plotted in Fig. 15. The time history in this domain appears as a simple periodic curve without any higher harmonics and with a weak multiplicative modulation. The SPC always lies inside individual loops. They run round the SPC and never pass it, whatever the SPT and IHV. The spatial character of the trajectory is obvious in plot (c) of Fig. 15. As in Sec. 4.1, no visible intervention of higher harmonics is observed, although a very light quasi-periodic character can be noticed. The shape in the top view is helical and close to a hypotrochoid form of a prolate type. As no sharp apexes or loop multiple points are detected, we can conclude that no basic cycloid or curtate hypotrochoid is approached.

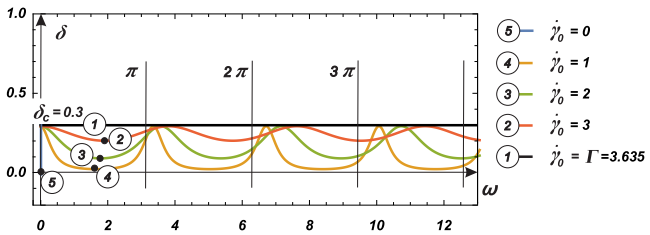

Fig. 13 Shape of the trajectory below the SC for various IHV.

5 TRAJECTORIES INFLUENCED BY AN INITIAL SPIN OF THE BALL

We again revisit Eq. (14). This time the ISV will be considered non-zero, $\omega_n \neq 0$. The characteristic function Eq. (14a) can be decomposed as in Eq. (30), however, the coefficients L, M will be different:

$$f(\delta) = (\delta - \delta_c)(K\delta^2 + 2L\delta + M) = 0, \tag{52a}$$

$$K = 2\omega_0^2, \quad M = \frac{1}{\delta_c}(H - \mu\omega_n)^2, \tag{52b}$$
$$L = \omega_0^2\delta_c - \frac{1}{2}(E + 4\omega_0^2 - \mu\omega_n^2(1-\mu)),$$

As in Sec. 4, either the lower or upper boundary of the strip is one of roots δ_i, $i = 1, 2$, which are determined by initial condition δ_c, i.e., $\delta_c = \delta_1$ or $\delta_c = \delta_2$ for the strip situated above or below the SC, respectively. The remaining two roots δ_1, δ_3 or δ_2, δ_3 can be calculated from the quadratic term in Eq. (52a) as in Eqs (31a) or (50):

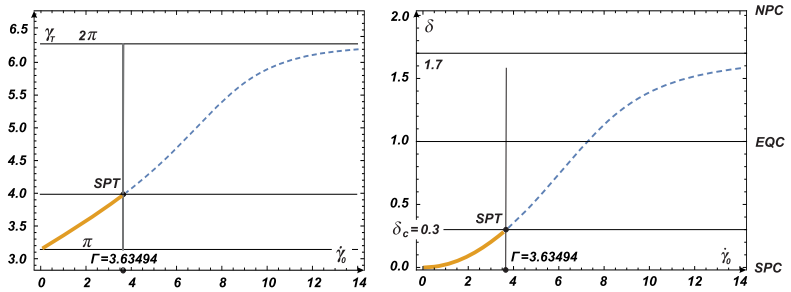

Fig. 14 A trajectory below the SC, (a) spatial period dependent on the IHV ($\dot{\gamma}_0$); (b) lower boundary of the strip δ_1 as a function of $\dot{\gamma}_0$.

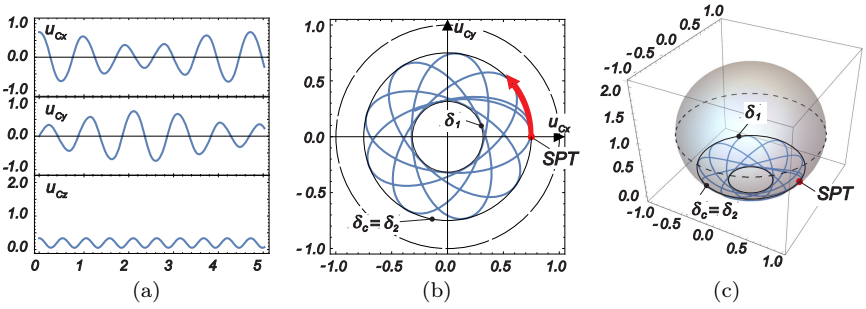

Fig. 15 Example of a trajectory below the SC with no ISV ($\omega_n = 0$): (a) time history, (b) top view, (c) axonometric demonstration.

$$\delta_{i,3} = \frac{1}{K}\left(-L \pm \sqrt{L^2 - K\cdot M}\right), \quad i = 1,2, \tag{31a,50}$$

$$\begin{aligned} D &= L^2 - K\cdot M \\ &= \left(\omega_0^2\delta_c - \frac{1}{2}\left(E + 4\omega_0^2 - \mu\omega_n^2(1-\mu)\right)\right)^2 \\ &\qquad - \frac{2\omega_0^2}{\delta_c}\left(H - \mu\omega_n\right)^2 . \end{aligned} \tag{53}$$

The expressions above can be reformulated with reference to Eqs (9,12a). Provided E, H are specified with respect to initial conditions, cf. Eq. (15), we obtain

$$\begin{aligned} K =& 2\omega_0^2,\ M = \delta_c\left(\dot\gamma_0(2-\delta_c) - \mu\omega_n\right)^2 , \\ L =& -\frac{1}{2}\left(\dot\gamma_0^2\delta_c(2-\delta_c) + 4\omega_0^2 + \mu^2\omega_n^2\right), \end{aligned} \tag{54a}$$

$$\begin{aligned} D =& \frac{1}{4}\left(\mu^2\omega_n^2 + \dot\gamma_0^2\delta_c(2-\delta_c) + 4\omega_0^2\right)^2 \\ &- 2\omega_0^2\delta_c\left(\mu\omega_n - \dot\gamma_0(2-\delta_c)\right)^2 . \end{aligned} \tag{54b}$$

Discriminant D is positive with the exception of two cases when $D = 0$:

$$\omega_n = 0, \dot\gamma_0 \to \infty \qquad \Longrightarrow \qquad \begin{cases} \delta_{1,2} = 0,\ \delta_3 = 2 \\ \delta_1 = 0,\ \delta_{2,3} = 2 \end{cases}$$

$$\omega_n = -\frac{\dot\gamma_0\delta_c}{\mu},\ \dot\gamma_0^2 = 2\frac{\omega_0^2}{\delta_c} \qquad \Longrightarrow \qquad \delta_1 = \delta_c,\ \delta_{2,3} = 2\,.$$

The first option represents two singular cases when $\omega_n = 0$ and $\delta_{1,2,3} \in \{0, 2\}$, while the latter one describes a particular trajectory which occurs for a given negative spin (assuming positive $\dot\gamma_0$) and passes through the NPC. This case, however, generally requires IHV $\dot\gamma_0 \neq \Gamma_0$; only for $\delta_c = 2/3$ does

$$\dot\gamma_0 = \Gamma_0 = \sqrt{3}\omega_0 \quad \text{and} \quad \omega_n = -2\frac{\omega_0}{\sqrt{3}\mu}\,. \tag{55}$$

The other particular case occurs when $M = 0$, i.e., for

$$\omega_n = \dot\gamma_0\frac{2-\delta_c}{\mu}\,. \tag{56}$$

Then $\delta_1 = 0$ and $\delta_3 = 2 + \dot\gamma_0(2-\delta_c)/\omega_0^2 > 2$.

In other cases $K > 0, M > 0$, and thus $0 < D < L^2$. Hence, both roots are real and positive and fulfill the relation: $0 \le \delta_1 \le \delta_2 < 2 < \delta_3$. Here δ_c is either δ_1 or δ_2, depending on what is considered given. For the rest of this section we consider the IHV to always be equal to positive velocity Γ_0, as it corresponds with the IHV of the SC.

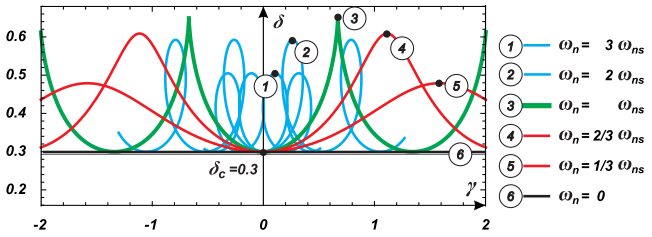

Fig. 16 Shape of the trajectory above the SC for various initial spin velocities; colors of curves: $\omega_n = 0$ - black, $\omega_{ns} < \omega_n < 0$ - red, ω_n - bold green ("kings crown" shape - separating case), $\omega_n < \omega_{ns}$ - blue.

5.1 Trajectories above the SC — negative spin

We can see that the trajectories influenced by a negative ISV, $\omega_n < 0$, lie within a spherical strip above the SC, with the bottom boundary $\delta_c = \delta_1$, and the upper boundary δ_2, which follows from Eq. (53). Note that the third first integral, Eqs (11c) or (12b), specifies that ω_n is constant throughout the whole investigated process.

First we briefly outline the basic character preliminarily inspecting Fig. 19 and taking into consideration also Figs 16, 17 and 18.

In general, observing the time history of the horizontal and vertical components of the response, it is noticeable that each trajectory consists of two basic components (except for some higher marginal harmonics). They are independent in their frequencies, as the first one is related to the basic spin-free movement and the second follows from the spinning rotation of the ball. The latter one proves to be more or less distinct in its amplitude according to the width of the strip where the particular trajectory is operating. In other words, it is determined by the active area $\delta \in (\delta_c, \delta_2)$. In general, the influence of the spin on the overall shape of the trajectory increases with the value of $|\omega_n|$ and acquires a significant dominance for ω_n above limit ω_{ns}, given by Eq. (60), and in particular for $0 > \omega_{ns} \gg \omega_n$ or $\omega_n \to -\infty$.

It follows from Eq. (14) that just three types of trajectories can be encountered when $\omega_n \neq 0$. Let us remember that the same equations, presented in Sec. 4.1, conclude that only one type of trajectory can exist within the strip if no spin of the ball is applied. The main reason for this alteration follows from the fact that the right hand side of Eq. (14b) can have both positive or negative values, when $\omega_n \neq 0$ is considered. The three types of trajectories can be classified with respect to the parameters and initial conditions of the system, namely the ISV. The shapes of the trajectory types differ significantly in the neighborhood of the contact point on the upper boundary of the strip; see Figs 16 and 17.

Let us now discuss some specific details of the individual trajectory types. The general form of the first type is obvious from Fig. 19 (i). The trajectories reflect the ISV in interval $\omega_n \in (0, \omega_{ns})$, where ω_{ns} is the ISV of the separating case, Eq. (60). Roughly observed, these trajectories are not too far from those discussed in Sec. 4, although some influence of the response component caused by the spin is discernible. However, the basic form again resembles an irrational spiral with slightly distorted detailed periods. The difference in the basic shape is rather quantitative, as the frequency of the spin is more or less related with that generated by the basic movement of the ball, and that is why it is hidden in the primary component influencing its amplitude. The trajectory

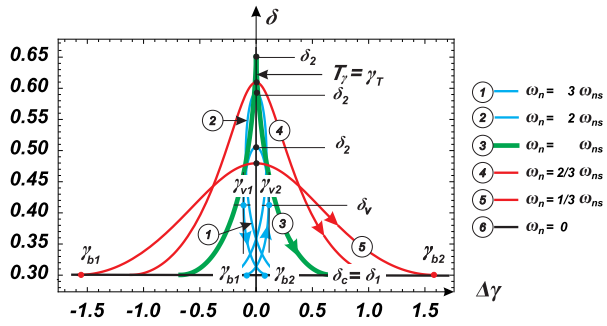

Fig. 17 Shapes of trajectories in the neighborhood of the contact point on the upper boundary of the strip (δ_2); $\omega_n = 0$ - black, $\omega_{ns} < \omega_n < 0$ - red, ω_n - bold green ("kings crown" shape - separating case), $\omega_n < \omega_{ns}$ - blue. The symbol $\Delta\gamma$ (horizontal axis) means a local coordinate within one period or an increase/decrease of γ with respect to $\gamma = \gamma_T$ (position of the tangential point on the δ_2 boundary).

shape is obvious from Fig. 16, where it is plotted as a function of angle γ (the two red curves relevant to $\omega_{ns} < \omega_n < 0$).

Details of the trajectory character near the contact point on the upper boundary are demonstrated in Fig. 17 (the two red curves). For the sake of a better visual comparison of individual trajectory behavior in the neighborhood of the contact point on the upper boundary δ_2, all trajectory graphs have been shifted and concentrated around this point, which serves as the origin of local coordinate $\Delta\gamma$. The starting and finishing points of one period on the lower boundary δ_c are denoted γ_{b1}, γ_{b2}. The width of the strip increases with descending ω_n from zero until a maximum width is reached for $\omega_n = \omega_{ns}$; see Figs 17 and 18(a,b). This corresponds to the total energy conservation principle.

The assessment of the length and duration of one period of the trajectory can be done analogously to Sec. 4.1. The reasoning which brought us to the differential system Eq. (36) is more or less the same, being based on the fact that contact points on the strip boundaries represent points with unavoidable singularity. Hence, with reference to Sec. 4.1, we can can deduce the following modified system:

$$\ddot{\delta} = E(1-\delta) - \omega_0^2\delta(4-3\delta) - \mu\omega_n\left(\omega_n(1-\mu)(1-\delta) + H\right), \tag{57a}$$

$$\dot{\gamma} = \frac{H - \mu\omega_n(1-\delta)}{\delta(2-\delta)}, \tag{57b}$$

where

$$E = \Gamma^2\delta_c(2-\delta_c) + 2\omega_0^2\delta_c + \mu\omega_n^2,$$
$$H = \Gamma\delta_c(2-\delta_c) + \mu\omega_n(1-\delta_c).$$

The denominator in Eq. (57b) is identical with that in Eq. (36b) and is positive in the considered interval. The system Eq. (57) is solved for initial conditions: $\delta(0) = \delta_c, \dot{\delta}(0) = 0$, and, eliminating the time, one obtains δ as the function of γ.

For the selected $\delta_c = 0.3$ and the relevant $\Gamma_0 = 3.63494$, two samples for $\omega_{ns} < \omega_n < 0$ are plotted in Figs 16 and 17. Together with the three diagrams in Fig. 18, we

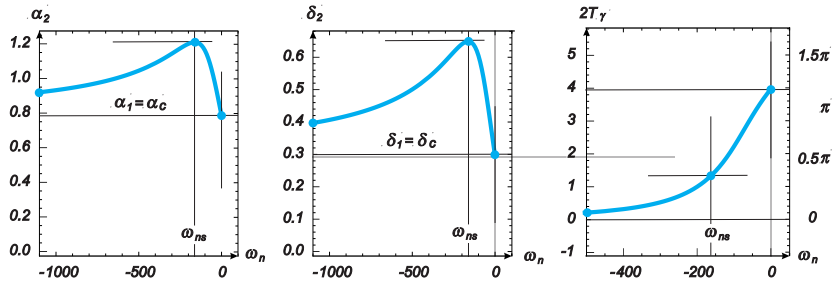

Fig. 18 Width of the strip above the SC for descending ISV or $\omega_n < 0$ passing throughout all three types of trajectories; (a) representation as $\alpha_2 - \alpha_c$ or (b) representation as $\delta_2 - \delta_c$; (c) width of the space period along the coordinate γ as a function of spin frequency $\omega_n < 0$.

can evaluate the character of a single period. Pictures (a) and (b) show the strip width as the difference between relevant angles α and parameters δ, respectively. Picture (c) presents the spatial width of a single period as a function of ω_n. It is obvious that a decrease in ISV ($\omega_n < 0$) leads to an increase in amplitude δ_2 or α_2 until a maximum is reached for $\omega_n = \omega_{ns}$. The length of the period simultaneously decreases. The trajectory for $\omega_n \in (\omega_{ns}, 0)$ could only have a periodic character if the ratio $2\pi\rho \sin\alpha_c / 2T_\gamma$ is a rational number, where T_γ denotes the half-period in the angular scale.

The second type of trajectory, see Fig. 19 (ii), occurs for the spin frequency $\omega_n = \omega_{ns}$, see the bold green curve in Figs 16 and 17. It represents a limit case separating groups below and above ω_{ns}. The trajectory shape in the axonometric view resembles a "kings crown". It contains a sharp apex in the midpoint of every period which touches the upper boundary δ_2. The derivative with respect to the circumferential coordinate γ is discontinuous in this singular point, jumping from ∞ to $-\infty$. All velocity components vanish, and both tangential acceleration components are discontinuous. A spin energy that is proportional to ω_n^2 is retained.

To determine the ISV needed to achieve this special type of trajectory, we take advantage of the fact that values of the first integrals for E and H, Eqs (9,12a), are constant throughout the entire time history. Indeed, at the SPT they can be expressed as follows:

$$\begin{aligned} E_{\delta_c} &= \Gamma^2 \delta_c (2 - \delta_c) + \mu\omega_n^2 + 2\omega_0^2 \delta_c \,, \\ H_{\delta_c} &= \Gamma \delta_c (2 - \delta_c) + \mu\omega_n (1 - \delta_c) \,, \end{aligned} \tag{58}$$

while in the sharp apex, at the δ_2 level, it holds that

$$E_{\delta_2} = \mu\omega_n^2 + 2\omega_0^2 \delta_2, \qquad H_{\delta_2} = \mu\omega_n (1 - \delta_2). \tag{59}$$

Evaluating the relevant equivalences $E_{\delta_c} = E_{\delta_2}$ and $H_{\delta_c} = H_{\delta_2}$, after some manipulations one obtains

$$\omega_{ns} = \omega_n = -\frac{2\omega_0^2}{\mu\Gamma}, \quad \delta_2 = \delta_c \left(1 + \frac{\Gamma^2}{2\omega_0^2} (2 - \delta_c) \right). \tag{60}$$

Substituting Γ from Eq. (23) only provides real results in an unrealistic situation when $\delta_c > 1$. However, when $\Gamma = \Gamma_0$, Eq. (24), Eq. (60) transforms to

$$\omega_{ns} = -\frac{2\omega_0^2}{\mu}\sqrt{1-\delta_c}, \qquad \delta_2 = \delta_c \frac{4-3\delta_c}{2(1-\delta_c)}\,. \tag{61}$$

Relations Eqs (59–61) are valid only when the apex occurs at δ_2. This is characterized by an infinite curvature of the trajectory, i.e., when $0 = (\dot\gamma^2 + \dot\delta^2)^{3/2}$. The necessary condition for $\dot\gamma = 0$, given by Eqs (9), (15), (24), is $0 < \delta_c \le 2/3$, cf. also Eq. (55).

It holds obviously that $\delta_2 > \delta_c$, and that the upper boundary of the trajectory can reach into the upper hemisphere of the cavity. This effect occurs when $\delta_c > 1 - 1/\sqrt{3}$. When δ_c is increased further, the apex may reach the NPC for $\delta_c = 2/3$; this case also nullifies the discriminant Eq. (54b). For even larger δ_c, the apex ceases to exist. These remarks are only theoretical, because in the upper hemisphere the contact force becomes negative particularly at the apex point, where all the components of the velocity vector $\mathbf{v}$ identically vanish.

The third type of trajectories, see Fig. 19 (iii), emerges provided $\omega_n < \omega_{sn}$ and possibly descending as $\omega_n \to -\infty$. The trajectory has a curly form making a loop

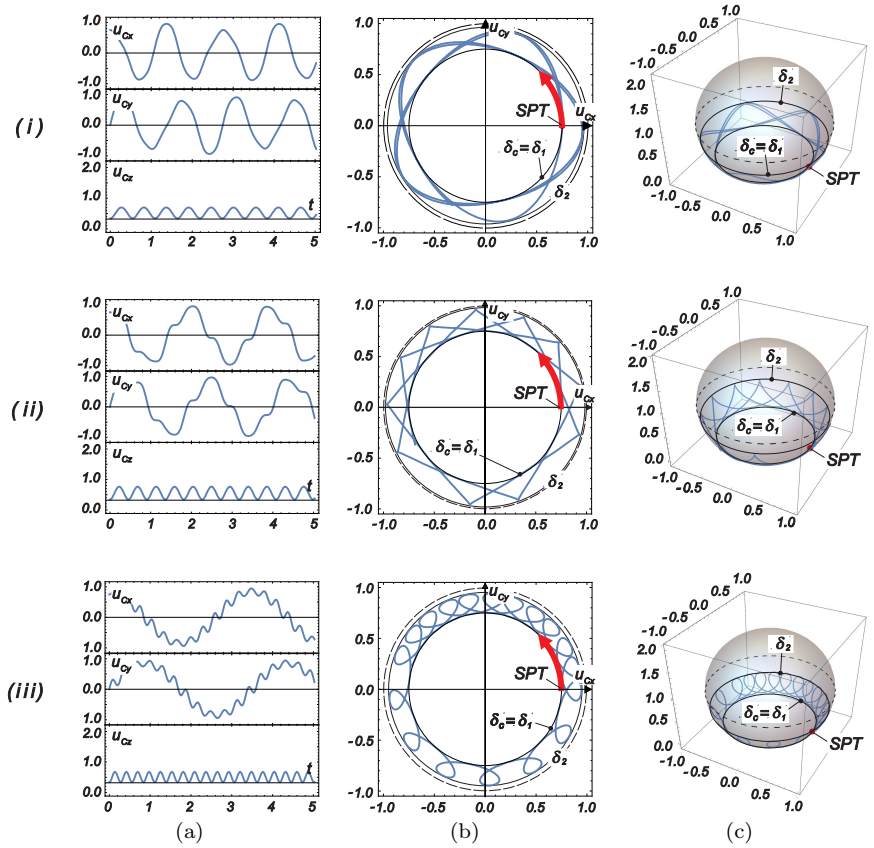

Fig. 19 Examples of trajectories with negative Initial Spin Velocity ISV ($\omega_n < 0$): 1st row: $\omega_{ns} < ISV < 0$; 2nd row: $ISV = \omega_{ns}$; 3rd row: $ISV < \omega_{ns}$. Column (a) time history, (b) top view, (c) axonometric demonstration.

every period; see Figs 16 and 17. As before, one period starts and finishes at the same vertical level, which is given by the root $\delta_c = \delta_1$. The highest point, reached in half a period, lies on the upper circle boundary. It is given by the root δ_2 according to Eqs (53,54). Let us turn our attention to the monotonously descending width of the strip, Fig. 18(a,b) for $\omega_n < \omega_{ns}$ depicted either with respect to angle α or to parameter δ.

The sharp apex—encountered in the previous type—delimiting the first and third types of trajectories prefigures a formation of two turnabout points γ_{v1}, γ_{v2} with tangents following their relevant meridians and with vanishing velocity $\dot{\gamma}$; see Figs 16, 17 (blue curves).

The vertical position of points γ_{v1}, γ_{v2} above δ_c can be found with respect to conservation of E and H values along the trajectory and due to the fact that $\dot{\gamma} = 0$ at turnabout points and $\dot{\alpha} = 0$ at the SPT. Indeed, using Eqs (9,12), we can write the following relations for unknown values $\dot{\alpha}_v, \delta_v$ at turnabout points:

$$\begin{aligned} \dot{\alpha}_v^2 + \mu\omega_n^2 + 2\omega_0^2\delta_v &= \Gamma^2\delta_c(2-\delta_c) + \mu\omega_n^2 + 2\omega_0^2\delta_c, \\ \mu\omega_n(1-\delta_v) &= \Gamma\delta_c(2-\delta_c) + \mu\omega_n(1-\delta_c). \end{aligned} \tag{62}$$

Simple manipulations result in

$$\begin{aligned} \dot{\alpha}_v =& \left(\Gamma\delta_c(2-\delta_c)(\Gamma + 2\frac{\omega_0^2}{\mu\omega_n})\right)^{1/2}, \\ & \text{where } \dot{\alpha}_{v1} = \dot{\alpha}_v,\ \dot{\alpha}_{v2} = -\dot{\alpha}_v\,, \\ \delta_v =& \delta_c\left(1 - \frac{\Gamma}{\mu\omega_n}(2-\delta_c)\right), \end{aligned} \tag{63}$$

which indicates that velocity $\dot{\alpha}$ is positive or negative in γ_{v1} or γ_{v2}, respectively, i.e., the trajectory is rising or descending. The level $\delta_v > \delta_c$, but the difference $\delta_v - \delta_c$ descends to zero as $\omega_n \to -\infty$; see Sec. 5.3. Both expressions remind us that ω_n should exceed a certain limit in order for the formulae to be meaningful, otherwise a curly form of the trajectory can exist.

The horizontal position of points γ_{v1}, γ_{v2} can be determined using the same system Eq. (57) as in the case of the first and second trajectory types, where $\gamma_{b1} = 0$ is taken as a reference point. The position of the remaining points γ_{v2}, γ_{b2} follows from the symmetry of the second half-period. Evaluation of the period length is already obvious and represents the difference $\gamma_{b2} - \gamma_{b1}$. Note that the point γ_{b1} always precedes the point γ_{b2} on the advancing coordinate γ like in the case of the first and second types of trajectories, and, consequently, the difference $\gamma_{b2} - \gamma_{b1}$ is always positive, but monotonously approaches zero for $\omega_n \to -\infty$; see Fig. 18(c).

Points γ_{v1}, γ_{v2} delimit the boundaries of the upper part of the loop, which is defined in the interval $\gamma \in (\gamma_{v1}, \gamma_{v2})$ in the framework of one trajectory period; see Fig. 18. The velocity $\dot{\gamma}$ in the upper part of the loop between the points γ_{v1}, γ_{v2} is of the opposite sign than that in the lower part of the loop. The width of interval $\gamma \in (\gamma_{v1}, \gamma_{v2})$ starts from zero for $\omega_n = \omega_{ns}$, where the curly form arises, and it increases for descending $\omega_n < \omega_{ns}$. This width reaches the period length and then becomes larger than the distance between the starting and finishing points $\gamma_{b2} - \gamma_{b1}$ of one period. Although both widths subsequently approach zero, the width of the loop becomes more and more dominant. In addition, the total (curvilinear) length of one loop significantly exceeds the simple distance $\gamma_{b2} - \gamma_{b1}$.

It is useful to define a certain average (or effective) velocity Ω_{av} of the ball advancement along the horizontal SC; it is given by the time and length of one period. This ratio drops as ω_n increases. Consequently, the average velocity Ω_{av} decreases accordingly. It approaches zero for high values ω_n; see Sec. 5.3. Due to the arrangement of points γ_{b1}, γ_{b2} on the γ axis, it holds that $\Omega_{av} > 0$. This positive sign is maintained throughout the whole interval $\omega_n < 0$.

5.2 Trajectories below the SC — positive spin

This section will be devoted to trajectories resulting from the same IHV Γ_0 and a positive ISV. The trajectories lie in a spherical strip below the SC, with the given upper boundary $\delta_c = \delta_2$ and lower boundary δ_1, which is determined by means of Eq. (53), $i = 1$. Similarly as before, we go through the main properties of these trajectories inspecting Figs 20, 21, 22 and 23 together with three examples of the trajectory with positive ω_n, which are presented in Fig. 24.

Trajectories below the SC can also be classified into three types or, in other words, into two groups separated by the special limit case corresponding to a fixed frequency $\omega_n = \omega_{ns}$ like in the previous section. In general, all trajectories apparently have a spiral form of the prolate hypotrochoid type, as we can see in the top view presented in Fig. 24 (pictures in column (b) for the three types). However, the shape of these spirals differs from those above the SC. The difference between particular types for $\omega_n > 0$ consists mainly in their relation to point A (SPC). Let us point out that the time history again has the distinct form of a two-component periodic process resulting from the movement of the ball and its rotation around the moving normal specified by the ISV (ω_n); see Fig. 24 column (a).

The shape of the trajectory in the neighborhood of the contact point on the lower boundary of the strip and the development of a curly trajectory is obvious in Figs 21 and 20. The width of the strip $\delta_c - \delta_1 \in (0, 1)$ changes from zero ($\omega_n = 0, \delta_1 = \delta_c$) until reaching δ_c (maximal width) when $\omega_n = \omega_{ns}$ and $\delta_1 = 0$. In this latter case, the trajectory passes through the SPC and represents the transition case. A further increase of $\omega_n > \omega_{ns}$ leads to rising of δ_1 backwards to the SC, which is reached for an infinite ISV; the width of the strip vanishes.

Let us point out some important features of particular trajectory types. The first type of trajectory, see Figs 20a, 22 (red curves) and Fig. 24 (i), is related to an ISV

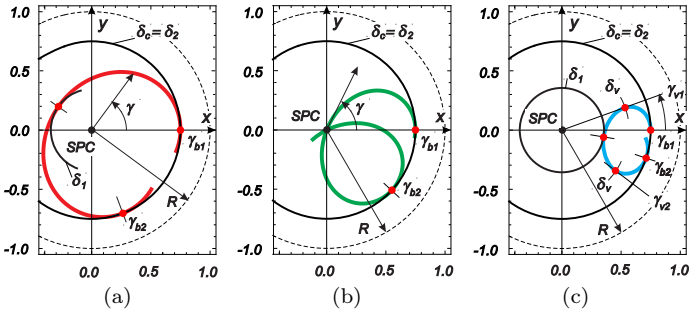

Fig. 20 Top view of one loop of the trajectory: (a) red: ISV $\omega_n < \omega_{ns}$, (b) green: $\omega_n = \omega_{ns}$ (passing the SPC — "separating case"), (c) blue: $\omega_n > \omega_{ns}$.

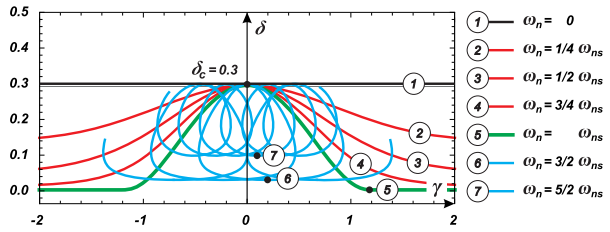

Fig. 21 Trajectory shapes below the SC for various initial spin velocities. colors of curves: $\omega_n = 0$ - black, $0 < \omega_n < \omega_{ns}$ - red, $\omega_n = \omega_{ns}$ - bold green (separating case), $\omega_{ns} < \omega_s$ - blue.

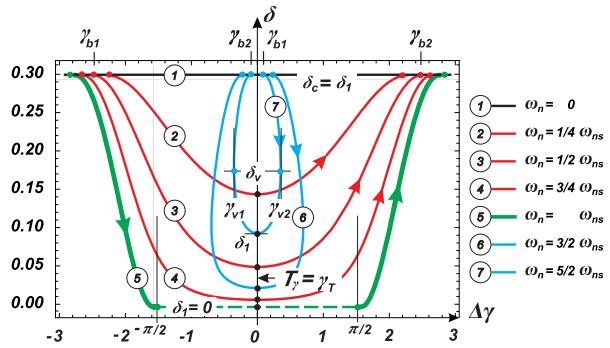

Fig. 22 Shapes of trajectories in the neighborhood of the contact point on the lower boundary of the strip (δ_1); $\omega_n = 0$ - black, $0 < \omega_n < \omega_{ns}$ - red, $\omega_n = \omega_{ns}$ - bold green (discontinuous - separating case), $\omega_{ns} < \omega_n$ - blue. The symbol $\Delta\gamma$ (horizontal axis) means a local coordinate within one period or an increase/decrease of γ with respect to $\gamma = \gamma_T$ (the position of the tangential point on the δ_1 boundary).

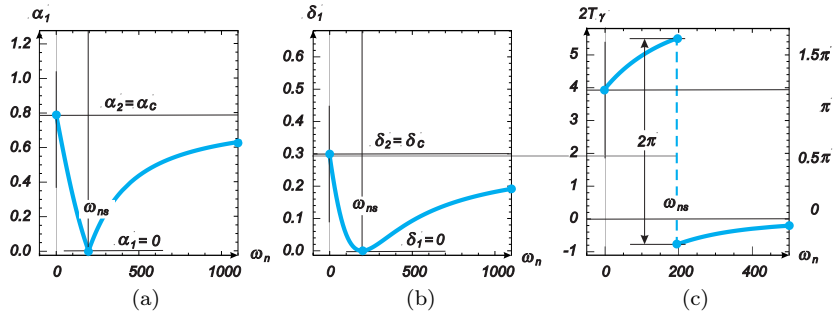

(a) (b) (c)

Fig. 23 Width of the strip below the SC for rising ISV or $\omega_n > 0$ covering all three types of trajectories; (a) representation as $\alpha_c - \alpha_1$ or (b) representation as $\delta_c - \delta_1$; (c) width of the spatial period along the coordinate γ as a function of spin frequency $\omega_n > 0$, note a jump in the point $\omega_n = \omega_{ns}$.

in the interval $0 < \omega_n < \omega_{ns}$. The trajectory has a spiral shape, where individual loops are prolate and running around the SPC. The influence of the second periodic component is small but still discernible; see Fig. 24(i). This phenomenon becomes more pronounced as the limit case ω_{ns} is approached.

Roughly observed (as in Sec. 5.1), the trajectories do not differ significantly from those discussed in Sec. 4.3. The basic form resembles again an irrational spiral with

807 slightly distorted detailed periods. The trajectory shape is obvious from Fig. 21, where
808 three red curves are plotted relevant to $\omega_{ns} < \omega_n < 0$ as functions of angle γ.
809 Details of the trajectory character near the contact point on the lower boundary δ_1
810 are demonstrated in Fig. 22 (three red curves) within a single period. This depiction
811 in Fig. 22 was used in order to facilitate a comparison of the trajectory behavior
812 throughout all ω_n considered in the neighborhood of the contact point on the lower
813 strip boundary δ_1. The width of the strip increases with ascending $0 < \omega_n < \omega_{ns}$ from
814 zero until a maximum is reached for $\omega_n = \omega_{ns}$ as it corresponds with the principle of
815 conservation of total energy.
816 The vertical position of the lower boundary δ_1 was determined using Eq. (53,54).
817 To assess the angular length and duration of one period of the trajectory and the
818 horizontal position of other important points, the same procedure as in Sec. 5.1 can
819 be applied. The system Eq. (57a) is solved for initial conditions: $\delta(0) = \delta_c, \dot{\delta}(0) = 0$,
820 and the results of Eq. (a) are put into Eq. (b). This way the time is eliminated and
821 one obtains δ as a function of γ.
822 For the selected $\delta_c = 0.3$ and the relevant $\Gamma_0 = 3.63494$, three samples for $0 <$
823 $\omega_n < \omega_{ns}0$ are plotted in Figs 21 and 22 (red curves) in γ and $\Delta\gamma$ coordinates. The
824 starting and finishing points of one period on the upper boundary δ_c are denoted
825 γ_{b1}, γ_{b2} in Figs 20, 22. Together with three diagrams in Fig. 23, we can evaluate the
826 character of one period. The graphs in Fig. 23a and b show the strip width expressed
827 in α or δ variables. Picture (c) presents the spatial width of one period as a function of
828 ω_n. It is obvious that increasing the ISV leads to increasing the amplitude δ_1 (or α_1)
829 up to a maximum reached for $\omega_n = \omega_{ns}$. At the same time, the length of the period
830 reaches its maximum for $\omega_n = \omega_{ns}$. The periodicity of the trajectory in the interval
831 $0 < \omega_n < \omega_{ns}$ is obvious. The half period is denoted T_γ (angular scale). Doubtlessly,
832 it can be expected that the spiral is irrational like in Sec. 4.1, except for some special
833 cases.
834 The second trajectory type represents the trajectory that separates the "lower and
835 upper" groups with respect to frequency ω_{ns}, see the bold-green curve in Figs 20b, 21,
836 22 and also case (ii) in Fig. 24. In this separating case, all loops pass through the SPC
837 (point A). This means that the cubic equation Eq. (14a) possesses one zero root, in
838 particular $\delta_1 = 0$. The absolute term in Eq. (14a) or (52) vanishes, a condition which
839 allows us to determine the corresponding ISV ω_{ns}:

$$H - \mu\omega_{ns} = 0, \;\Rightarrow\quad \Gamma \sin^2 \alpha_c + \mu\omega_{ns} \cos\alpha_c - \mu\omega_{ns} = 0. \tag{64}$$

840 This means that for the fixed elevation δ_c of the SPT, and the implicitly defined velocity
841 Γ_0, the following ISV should be applied:

$$\mu\omega_{ns} \;=\; \Gamma_0(2 - \delta_c), \qquad 0 < \delta_c < 1, \tag{65}$$

842 in order to produce a trajectory the loops of which go through the SPC; see also
843 Eq. (56).
844 Coordinate γ becomes discontinuous when approaching the SPC; see the discon-
845 tinuity in the green curve and the jump of length π in Fig. 22. For the same reason
846 the derivative of the curve describing the width of the strip in ω_{ns} is non-continuous,
847 Fig. 23a. However, the one-sided derivatives with respect to ω_n at point ω_{ns} are fi-
848 nite and equal in absolute value. Therefore, the non-smooth character of the curve is
849 merely a result of maintaining the polar angle α as positive. Similar reasoning regards

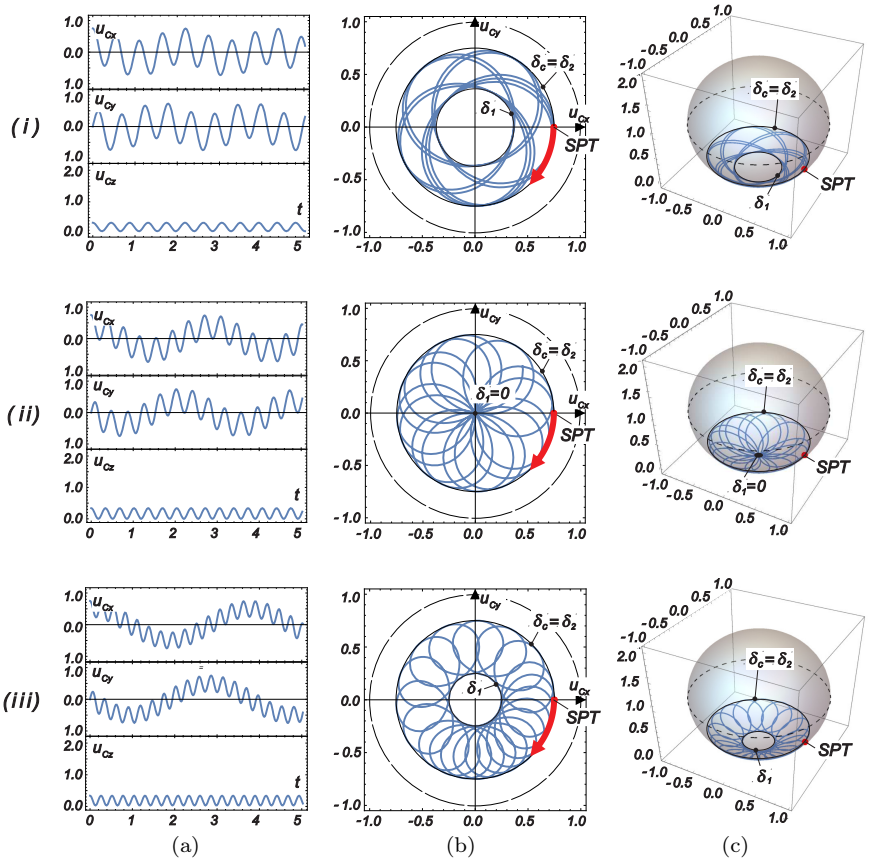

Fig. 24 Examples of trajectories with a positive "Initial Spin Velocity ISV" ($\omega_n > 0$): 1st row: $0 < \omega_n < \omega_{ns}$; 2nd row: $\omega_n = \omega_{ns}$; 3rd row: $\omega_n > \omega_{ns}$. Column (a) time history, (b) top view, (c) axonometric demonstration.

the discontinuity in the length of the spatial period in Fig. 23c. The 2π jump originates also from the fact that the relevant radius-vector length is always positive.

The third type of trajectory can be observed when $\omega_n > \omega_{ns}$ and possibly $\omega_n \to \infty$ as the blue curves in Figs 20c, 21, 22 and also in case (iii) of Fig. 24. These initial conditions result in trajectories that pass by the SPC, which remains outside each loop; see Fig. 20c. The position of the lower boundary δ_1 can be obtained from Eq. (53). It rises monotonously towards δ_c for an increasing ω_n. Accordingly, as $\omega_n \to \infty$ we can observe that the width of the spherical strip diminishes; see Fig. 22a,b.

The angular length of one half of the period and the position of the turnabout points can be evaluated in a similar way as in the case of the third type trajectories for the $\omega_n < 0$, i.e., to employ system Eq. (57). The analogous deduction from the previous section concerning limitations, singular points and numerical stability remains in force. The results are included in Figs 21 and 22 (two blue curves).

Two turnabout points γ_{v1}, γ_{v2} in Figs 21 and 22 can be recognized. Their attributes are similar to those encountered in the previous section, although their geometrical

interpretation is slightly different. Also here we can define a bottom part of the loop within points γ_{v1}, γ_{v2} where velocity $\dot{\gamma}$ is of the opposite sign. In contrast to Sec. 5.1 (negative ISV), the loops do not include any twofold point, and the period length $\gamma_{b2} - \gamma_{b1}$ becomes negative for $\omega_{ns} < \omega_n$; see the two blue curves with an indication of the movement direction in Fig. 22. Both properties of the loops follow from the ordering of starting and finishing points of the period and are typical for trajectories with a positive ISV. It is obvious that as $\omega_n \to \infty$ the particular loops approach a zero amplitude; see also Sec. 5.3. The same also applies to the length of period T_γ.

With reference to points γ_{v1}, γ_{v2} and the starting and finishing points of the period γ_{b1}, γ_{b2}, we can define the average (or effective) angular velocity $\Omega_{av} < 0$ of the ball movement forward along the SC for $\omega_{ns} \ll \omega_n$. It is obvious that the clockwise movement of points $\gamma_{b1}, \gamma_{b2}, \gamma_{v1}, \gamma_{v2}$ between consecutive loops gets slower for increasing ω_n, i.e., as $\Omega_{av} \to 0$. The limit case of $\omega_n \to \infty$ is discussed in detail in Sec. 5.3; see also Fig. 26.

5.3 High initial spin values

In this section, we will investigate trajectories starting from the SC, when an extremely high ISV is applied in either the positive or negative sense. We have seen in Secs 5.1 and 5.2 that the shape of individual trajectories differs significantly if a positive or negative velocity of initial spin is introduced, even though some analogy can be noticed.

Significantly increasing the ISV, the trajectory properties for $\omega_n \ll 0$ and $\omega_n \gg 0$ become more and more related, and finally produce a symmetric image with respect to the SC. Both of them are far from the transition case, in which the curly-form trajectories start. For $\omega_n \ll 0$, the curly trajectory is located on the upper side of the SC. The upper boundary δ_2 descends from a level above the SC to root $\delta_c = \delta_1$ as $\omega_n \to -\infty$. Provided $\omega_n \gg 0$, the lower boundary (root δ_1) moves upwards to the SC, represented by $\delta_c = \delta_2$, when $\omega_n \to \infty$.

Let us outline approximately this process. Either roots δ_2, δ_3 or δ_1, δ_3 (depending on which trajectory group is being analyzed) can be determined using the quadratic equation Eq. (52) or its symbolic solution Eq. (53), respectively. For a high $|\omega_n|$, the term L becomes dominant due to the higher power of $|\omega_n|$, so it holds: $L^2 \gg K \cdot M$, and, consequently, it can be approximately written for $i = 1, 2$:

$$\delta_{i,3} \approx \frac{1}{K}\left(-L \pm \left(L - \frac{1}{2}\frac{KM}{L} - \frac{1}{8}\frac{(KM)^2}{L^3} - \dots\right)\right). \tag{66}$$

It is obvious that $\delta_3 \to \infty$ and is therefore of no interest. The other root can be approximated:

$$\delta_i = -\frac{1}{2}\frac{M}{L} - \frac{1}{8}\frac{K \cdot M^2}{L^3} - \dots \tag{67}$$

The second and higher terms can be neglected, as they vanish for $|\omega_n| \to \infty$. Substituting now for K, M from Eq. (54b), and neglecting terms with the zero degree of ω_n, we obtain

$$\delta_i \;=\; \delta_c\Big(1 - 2\frac{\Gamma(2-\delta_c)}{\mu\omega_n}\Big), \qquad i = 1, 2. \tag{68}$$

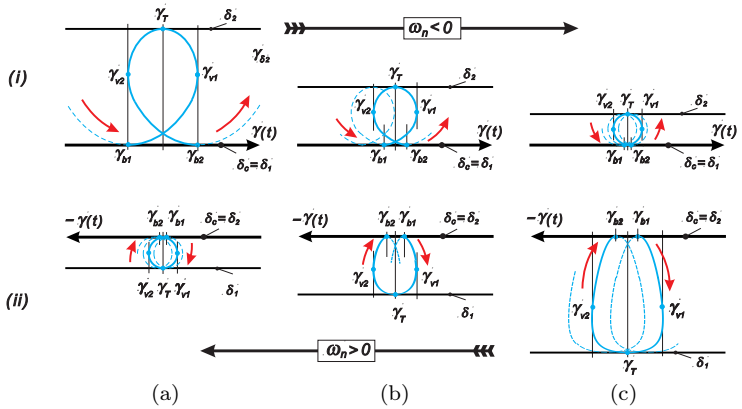

Fig. 25 Shape of the trajectory in the neighborhood of the contact point γ_T; (i) upper boundary δ_2 of the spherical strip for very low ISV: columns (a-c) - descending $\omega_n \ll \omega_{ns}$; (ii) lower boundary δ_1: columns (a-c) - rising $\omega_n \gg \omega_{ns}$.

Formula Eq. (68) shows that δ_i converges to δ_c from above or below depending on the sign of the ISV. The width of the spherical strip decreases for increasing $|\omega_n|$ and so does the width of the curly trajectory period, as it has been defined in Secs 5.1 and 5.2; see the plots in Fig. 25. Graph (i) represents the case $\omega_n \ll 0$ advancing from left to right, whereas (ii) regards $\omega_n \gg 0$ from right to left. The shape of the individual loops for $|\omega_n| \gg 0$ approaches a circle, which is followed in a negative or positive angular sense (with respect to the normal n), when $\omega_n \ll 0$ or $\omega_n \gg 0$, respectively. This approximative circle decreases in diameter and moves slowly along the upper or lower part of the SC.

The increment of the distance which the circle performs during one loop decreases rapidly with growing $|\omega_n|$ because the distance between the starting and finishing points γ_{b1}, γ_{b2} of one period (positive or negative) decreases faster than the circle diameter. In general, the effective distance passed along the SC within one period of a curly trajectory is mostly exploited by the approximating circle. Therefore, the effective velocity Ω_{av} of the ball advancement along the SC decreases. Let us remind the reader, referring to Secs 5.1 and 5.2, that the sense of this slow rotation around the z axis is either positive ($\Omega_{av} > 0, \omega_n \ll 0$) — above the SC, or negative ($\Omega_{av} < 0, \omega_n \gg 0$), but at any time it holds that $\Omega_a v \to 0$, when $|\omega_n| \to \infty$.

This deduction concludes with a phenomenon which seems paradoxical at first glance. As we have seen, as $\omega_n \to \pm\infty$, both the diameter and effective horizontal velocity of the approximating circle degenerate to zero. Therefore, the ball does not evince any movement along the SC, the loops reduce to a single point, and the ball is apparently at rest, only spinning around its normal at the SPT with an infinite spin velocity. Its position, which seems to be out of static equilibrium, is fixed by an infinitely strong gyroscopic effect, whatever the IHV. This type of trajectory is illustrated as a numerical simulation in Fig. 26: (a) displacement time history, (b) top view, (c) axonometric demonstration. The results correspond to negative $\omega \ll 0$; compare with Fig. 25(i).

6 Vertical plane related trajectories

6.1 Transformation of the governing system

We examine trajectories which emerge for a very small initial horizontal velocity ($0 \leq |\dot{\gamma}_0| \ll \Gamma$) and a zero or small initial spin. If both IHV and ISV are zero, the trajectory of the ball defines a vertical plane passing through the initial point, ball center and point A of the cavity (SPC). With an injection of a small IHV or ISP, the trajectory mildly declines from this vertical plane. However, the distance from the vertical plane remains small. To describe the character of this spatial curve, it is worthwhile to consider the difference from the vertical plane as a small parameter. This simplification enables us to get into some special properties of this trajectory family.

With reference to Fig. 3, root δ_1 will either coincide with the origin, i.e. $\delta_1 = 0$, or get a small positive value. The position of root $\delta_2 = \delta_c$ depends on the initial position of the ball.

To conveniently describe the movement of the ball in a narrow strip adjacent to plane yz, where the azimuthal angle γ exhibits a jump of 2π when α passes the zero value, it is advisable to rotate the coordinate system around the y axis.

The polar angle of the new coordinate system is denoted by ξ, and it represents an almost constant value perturbed by a small parameter, $\xi = \pi/2 \pm \varepsilon$, Fig. 27. The azimuthal angle ζ then describes movement in the vertical plane parallel to axis y. This way the formula for kinetic energy T, Eq. (7a), remains identical when we formally substitute $\alpha = \xi$ and $\gamma = \zeta$, and the potential energy V, Eq. (7b), is modified as follows:

$$V_{mod} \;=\; mg\varrho(1 - \sin\xi\cos\zeta). \tag{69}$$

The constant term $mg\varrho \cdot 1$ does not influence the dynamic equilibria, and, therefore, the total energy Eq. (9) can be rewritten in the form

$$\dot{\xi}^2 + \dot{\zeta}^2 \sin^2\xi + \mu\omega_n^2 - 2\omega_0^2 \sin\xi\cos\zeta \;=\; E. \tag{70}$$

Revisiting Eq. (1), one can write Lagrangian equations for coordinates ξ and ζ:

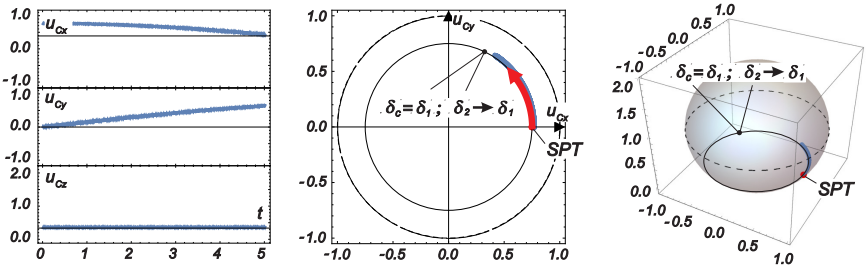

(a) (b) (c)

Fig. 26 Example of a trajectory with negative ISV ($\omega_n \ll 0$): (a) time history, (b) top view, (c) axonometric demonstration.

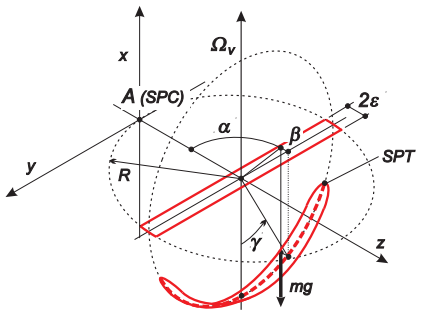

Fig. 27 Arrangement of coordinates for investigation of cases with low IHV.

$$\xi: \quad \ddot{\xi} - \left(\dot{\zeta}^2 \cos\xi - \mu\omega_n\dot{\zeta}\right)\sin\xi - \omega_0^2 \cos\xi\cos\zeta = 0\,, \tag{71a}$$

$$\zeta: \quad \ddot{\zeta}\sin\xi + 2\dot{\xi}\dot{\zeta}\cos\xi - \mu\omega_n\dot{\xi} + \omega_0^2\sin\zeta = 0\,. \tag{71b}$$

6.2 Approximated governing system and relevant trajectories

The small parameter can be introduced as follows: $\xi \approx \pi/2 - \varepsilon$; see Fig. 27. Hence, Eq. (71) get a modified form:

$$\xi: \quad \ddot{\varepsilon} + \dot{\zeta}^2\varepsilon - \mu\omega_n\dot{\zeta} + \omega_0^2\cos\zeta\cdot\varepsilon = 0, \tag{72a}$$

$$\zeta: \quad \ddot{\zeta} - 2\dot{\varepsilon}\varepsilon\dot{\zeta} + \mu\omega_n\dot{\varepsilon} + \omega_0^2\sin\zeta = 0. \tag{72b}$$

Provided no IHV or ISV is applied, ε vanishes. Eq. (72a) is fulfilled identically and Eq. (72b) degenerates into a non-linear pendulum equation. This equation can be solved in elliptic functions. Depending on the initial velocity $\dot{\zeta}(0)$, the solution is either periodic—for small $\dot{\zeta}(0)$— or continuously increasing in time with periodically variable velocity. Detailed discussion can be found in a number of papers and monographs; see for instance [28,33]. On the other hand, cases for $\zeta_0 \geq \pi/2$ are physically meaningless due to a negative contact force. Note that the case considering $\zeta = 0$ and $\varepsilon \neq 0$ represents only a perturbation, which can be treated using linearized expressions.

Under the assumption that the amplitudes of ζ are small, the nonlinear terms in Eq. (72) may be approximated as

$$\sin\zeta \approx \frac{y}{\rho},\ \cos\zeta \approx 1 \ \text{ and } \ \dot{\zeta}^2\varepsilon \approx 0,\ \dot{\varepsilon}\varepsilon\dot{\zeta} \approx 0,$$

and the system can be linearized. The following reduced system can be formulated:

$$\xi: \quad \ddot{z} - \mu\omega_n\dot{y} + \omega_0^2\cdot z = 0, \tag{73a}$$

$$\zeta: \quad \ddot{y} + \mu\omega_n\dot{z} + \omega_0^2\cdot y = 0. \tag{73b}$$

For a non-zero ISV, equations Eq. (73) are coupled by a pair of gyroscopic forces which cause the spatial character of the trajectory even if the IHV vanishes. For a zero

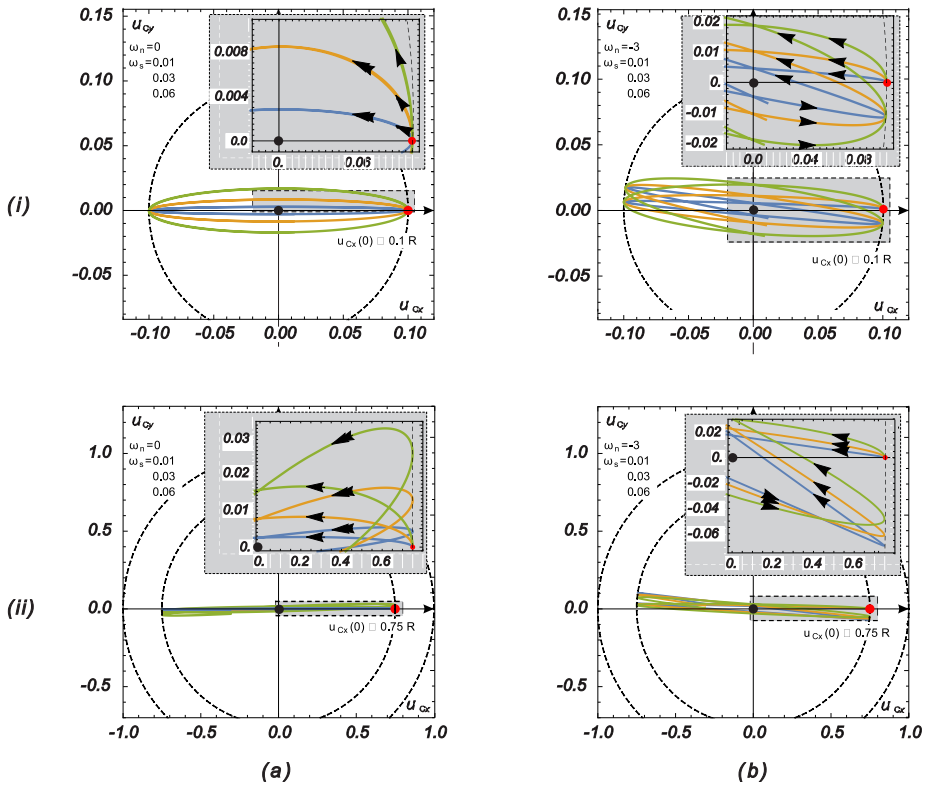

Fig. 28 Trajectory at a low IHV: line (i) linear approach - low level SPT, line (ii) nonlinear approach; column (a) no initial spin, column (b) initial spin included.

ISV the system is characterized by two independent linear oscillators with identical eigen frequencies. Consequently, no rosette form trajectory can occur for a non-trivial IHV, and a simple ellipse-like curve is observed. Indeed, considering initial conditions: IHV: $\dot{z}(0) = z_0^*$, and an initial deviation along the meridian in the plane xy : $y(0) = y_0$, a solution to linear system Eq. (73) can be expressed as follows:

$$\begin{aligned} w &= \frac{1}{2d}\left((y_0(d-\Omega_v)+z_0^*)\exp(\mathrm{i}(d+\Omega_v)t)\right. \\ &\qquad \left.+(y_0(d+\Omega_v)-z_0^*)\exp(-\mathrm{i}(d-\Omega_v)t)\right), \\ w &= y+\mathrm{i}z, \quad \mathrm{d}^2=\Omega_v^2+\omega_0^2, \quad \Omega_v = -\frac{\mu\omega_n}{2}, \end{aligned} \tag{74}$$

which produces a pair of independent components: $w = y_0\cos\omega_0 t + \mathrm{i}z_0^*/\omega_0 \sin\omega t$, if the ISV $\omega_n = 0$. Provided $\omega_n \neq 0$, but is rather small, the top view of the trajectory obviously has the form of a strongly prolate hypotrochoid. Therefore, it is worthwhile to define an affine space which meets a sub-manifold at a point in such a way as to have a second order of contact at this point. From a geometrical point of view, this case is similar to the one we discussed in Sec. 4.2. Indeed, we can assume that the shape of the spiral does not deviate much from the vertical plane during one cycle. The osculating plane rotates slowly around the vertical axis with an angular velocity $\Omega_v = -\mu\omega_n/2$.

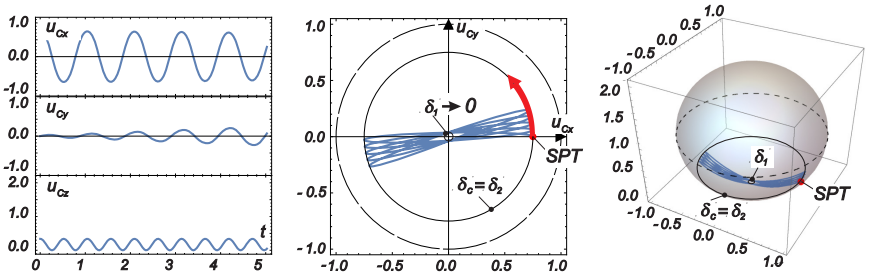

(a) (b) (c)

Fig. 29 Example of the trajectory below the SC without ISV ($\omega_n = 0$) for low IHV: (a) time history, (b) top view, (c) axonometric demonstration.

Several plots of trajectories following this linear approach are demonstrated in Fig. 28, row (i), without or with an ISV, pictures (a) or (b), respectively.

When the ζ amplitude is large and the nonlinear character of the system must be respected, the second terms in Eq. (72) remain in force. In a certain sense, they also have the character of gyroscopic forces and lead to a rosette character of the trajectory when a small IHV is applied, see Fig. 28, row (ii), including details near the upper boundary of the strip. Observing picture (b) (a nonlinear approach) we can see that $\Omega_v > 0$ when only IHV is considered and no ISV is applied (counter-clockwise). If $\omega_n > 0$ then $\Omega_v < 0$ (clockwise).

As a demonstration, we show a trajectory resulting from a numerical simulation; see Fig. 29. The scheme of this figure is the same as that in Fig. 6. Although an ISV was introduced in this initial setting, we can see in the top view that a slightly counterclockwise rotating spiral emerges. Subsequent simulations for the descending SPT level showed a decreasing value of this rotation velocity and vice versa, just as we have seen above for small initial amplitudes (the level of the SPT), Eq. (74), and higher amplitudes, Eq. (72), where the nonlinear character was respected. Hence, the top view of the trajectory is similar to that of the Foucault pendulum even if no ISV is applied. Note that the individual loops go around point A (SPC) regardless of the initial setting if no ISV is applied, i.e., for $\omega_n = 0$.

7 CONCLUSIONS

The dynamic behavior of a non-holonomic system represented by a ball moving inside a spherical cavity has been investigated. The rolling of the ball is considered to be slipping-less and free of damping at the contact of the ball and cavity. The cavity is assumed to be fixed. Energy is introduced into the system by means of appropriate settings of initial conditions at the SPT of each particular case. The reason for this system layout consists in the possibility to differentiate individual groups of trajectory types and to investigate each one separately. Simultaneously, this setting enables the involvement of analytical means of investigation. This strategy provides much more general insight into the problem than one only focused on simulation procedures. The analytical approach allows us to define and separately characterize individual trajectory types and to make sure that all groups were examined. Another advantage is the

ability to compare at least selected results obtained using principally different methods. Moreover, the comparison that was performed worked with numerically obtained results following from the Appell-Gibbs approach, whereas the analytical results followed from the Lagrangian governing system.

In general, it can be concluded that the results obtained using these two fundamentally different approaches coincide perfectly. The two sets of results complement one another well with regard to their strengths and weaknesses. The positions of limit cases match with respect to their relevant parameter settings. The analytical method of investigation indicated a set of trajectory types and limit cases that either separate them or demonstrate a process of limitation of some parameters to certain special values (infinity, zero, etc.). Transition zones were also qualitatively and quantitatively examined and interpreted, which was impossible using solely numerical simulations.

For the investigation of particular properties of the system, two types of basic relations were used: (i) a Lagrangian governing system with incorporated Pfaff type non-holonomic constraints and (ii) three first integrals corresponding to the total energy of the ball, its constant angular momentum with respect to fixed vertical axis, and its constant angular momentum with respect to the common normal at the contact point of the ball and cavity. The last one showed that spin velocity is constant throughout the whole period the ball is moving along its trajectory.

A cubic algebraic equation makes up the backbone, characterizing the energy flow within the system. This equation always possesses three real roots, where the two lower roots are physically meaningful (the highest root has no physical interpretation and is therefore of no interest). The two lower roots depict the lower and upper horizontal boundaries on the spherical surface of the cavity. They delimit a spherical strip inside of which the relevant trajectory emerges. The properties of these roots enabled us to define individual trajectory types, indicate transition, limit and other cases, as well as perform parametric analyses within each group of trajectories.

It should be stressed that all trajectories, whatever their initial conditions setting, are deterministic. They do not approach any chaotic state. No cascade bifurcations emerge, which would have indicated the onset of a chaotic state; this is not the case, however, with ball movement due to kinematic excitation of a cavity. This conclusion was also indirectly confirmed by means of Lyapunov exponent testing.

The "Separation Circle" (SC), a horizontal circular trajectory at a certain level above the SPC and below the EQC of the cavity, was revealed to be the main classification element. The selected level on a meridian of the cavity determines the particular IHV value necessary to maintain the ball moving along the SC at a constant horizontal level. In general, to establish the SC, zero spin initial velocity is assumed, but compensation using non-zero spin velocity is also possible if the IHV is not exactly equal to the critical velocity. Trajectories within the close neighborhood of the SC were examined, confirming the stability of the SC trajectory with respect to perturbation in initial conditions and to a small cross impulse imparted to the ball.

Trajectory types above the SC were classified with respect to "Initial Spin Velocity" (ISV), which should be non-negative, and IHV, which is higher than the critical velocity. As a rule, spin-free trajectories have a form of irrational spirals within the spherical strip. Their form is similar to a prolate hypotrochoid. The horizontal velocity of the ball is always positive (more exactly, corresponding to the sign of the IHV). Increasing IHV beyond all limits, one approaches the limit state, which is represented by a planar trajectory that is symmetrically distributed with respect to the cavity center. Adjacent

cases of high but not infinite initial velocities are discussed as well, along with the rotating osculating plane.

Settings with a positive ISV can be classified into two sub-groups separated by the case that is represented by a "kings-crown" shaped trajectory. Every loop contains a singular point (apex) which lies on the upper boundary of the spherical strip. A closed loop expands from this point for higher spin velocities, imparting a curly form to the trajectory. In this case, one twofold (intersection) point is observed in every loop, and the horizontal velocity of the ball becomes negative in its upper part, which is delimited by two turnabout points. Lower spin velocities produce spirals without loops analogously to cases without spin, despite the fact that the shape of the spiral itself is different.

Trajectories below the SC have a significantly different character from those occurring above the SC. Nevertheless, they still have a hypo-trochoidal character. The lower limit of spin-free trajectories successively descends due to the lowest root of the cubic equation. This limit approaches the SPC, where it degenerates into a point. Regarding cases with negative spin, they can also be classified into two sub-groups. The separating case between sub-groups is represented by a curly trajectory, where every loop passes through the SPC. Higher spin velocities result in trajectories the individual loops of which go round the SPC, while lower spin velocities produce loops that miss this point. Thus, the lower boundary of the strip again rises toward the SC.

An interesting process is encountered when the ISV velocity tends to $\pm\infty$. The width of the spherical strip where the trajectory is being traced decreases to zero from above or from below respectively with regard to the sign of the spin velocity. In both variants, the trajectory has a shape approaching a small circle slowly moving along the SC. For infinite spin velocity (positive or negative), the ball is seemingly fixed at the initial point of the trajectory; moving neither along the SC nor along a meridian of the cavity. Its position is fixed due to infinite energy concentrated in the spin of the ball producing an infinite gyroscopic effect.

The last group includes associated cases regarding initial settings, which produce either vertical plane related trajectories or correspond to zero IHV and higher ISV. Basically, these settings are characterized by low initial energy of the ball, i.e., the horizontal initial velocity and spin velocity of the ball are small or vanishing when the trajectory starts on a certain level along a cavity meridian. For zero ISV and low-level initial position above the SPC, the problem can be linearized. In the top view, a simple ellipse emerges, degenerating into a line segment for zero IHV. If nonlinear terms are respected, then this ellipse-like curve slowly rotates counter-clockwise and remotely resembles the Foucault pendulum trajectory. Introducing a slight ISV, the elliptical trajectory shape changes into a significantly prolate hypotrochoid. The slow rotation of the one-loop trajectory accelerates or decelerates according to the spin velocity sign.

As regards future investigation in this area, non-conservative systems should be paid attention on the basis of analytical processes. Specific difficulties should be expected related to first integrals, which will need to be generalized significantly in order to overcome variable total energy, angular momentum and spin velocity. The mutual penetration of groups and sub-groups when moving along one particular trajectory will have to be taken into account. Chaotic response processes will doubtlessly emerge, as has already been shown when doing numerical simulations. It will be necessary to reconcile with the fact that some steps used in this paper will become inapplicable. Nevertheless, some alternative methods of analysis are emerging and seem promising.

List of abbreviations

SC — Separation Circle,
CF — Characteristic Function,
CE — Characteristic Equation,
SPC — Southern Pole of the Cavity (the lowest point of the cavity, A),
EQC — Equator of the Cavity,
NPC — Northern Pole of the Cavity (the highest point of the cavity),
IHV — Initial Horizontal Velocity $\dot{\gamma}_0$,
ISV — Initial Spin Velocity ω_n,
SPT — Starting Point of the Trajectory,

Declarations

Acknowledgement The kind support of the Czech Scientific Foundation No. 19-21817S and RVO 68378297 institutional support are gratefully acknowledged.

Conflicts of interest The authors declare that they have no conflict of interest.

Availability of data and material Not applicable

Code availability Not applicable

References

1. Akhiezer, N.I.: Elements of the theory of elliptic functions. Nauka, Moscow (1970). (in Russian)
2. Arnold, V.I.: Mathematical methods of classical mechanics. Springer, New York (1978)
3. Baruh, H.: Analytical dynamics. McGraw-Hill, New York (1998)
4. Bloch, A.M., Marsden, J.E., Zenkov, D.V.: Nonholonomic dynamics. Notices of the American Mathematical Society **52**, 324–333 (2005)
5. Borisov, A.V., Fedorov, Y.N., Mamaev, I.S.: Chaplygin ball over a fixed sphere: an explicit integration. Regular and Chaotic Dynamics **13**(6), 557–571 (2008). DOI 10.1134/s1560354708060063
6. Borisov, A.V., Kilin, A.A., Mamaev, I.S.: Rolling of a homogeneous ball over a dynamically asymmetric sphere. Regular and Chaotic Dynamics **16**(5), 465 (2011). DOI 10.1134/S1560354711050042. URL https://doi.org/10.1134/S1560354711050042
7. Borisov, A.V., Mamaev, I.S., Kilin, A.A.: Rolling of a ball on a surface. New integrals and hierarchy of dynamics. Regular and Chaotic Dynamics **7**(2), 201–219 (2002). DOI 10.1070/rd2002v007n02abeh000205
8. Chen, J., Georgakis, C.T.: Tuned rolling-ball dampers for vibration control in wind turbines. Journal of Sound and Vibration **332**(21), 5271–5282 (2013). DOI 10.1016/j.jsv.2013.05.019
9. Chetayev, N.G.: Stability of motion. AN SSSR, Moscow (1962). (in Russian)
10. Cui, W., Ma, T., Caracoglia, L.: Time-cost "trade-off" analysis for wind-induced inhabitability of tall buildings equipped with tuned mass dampers. Journal of Wind Engineering and Industrial Aerodynamics **207**, 104394 (2020). DOI 10.1016/j.jweia.2020.104394
11. Desloge, E.: The Gibbs-Appell equation of motion. American Journal of Physics **56**(9), 841–846 (1988)
12. Eiserman, M.A.: Classical mechanics. Nauka, Moscow (1980). (in Russian)
13. Emami, M., Zohoor, H., Sohrabpour, S.: Solving high order nonholonomic systems using Gibbs-Appell method. In: V. Balan (ed.) Proceedings of The International Conference Differential Geometry and Dynamical Systems, pp. 70–79. Geometry Balkan Press, Mangalia, Romania (2009)

14. Hamel, G.: Theoretische Mechanik. Springer, Berlin, Heidelberg (1949). DOI 10.1007/978-3-642-88463-4
15. Haxton, R.S., Barr, A.D.S.: The autoparametric vibration absorber. Journal of Engineering for Industry **94**(1), 119–125 (1972). DOI 10.1115/1.3428100
16. Hedrih, K.: Vibro-impact dynamics of two rolling balls along curvilinear trace. Procedia Engineering **199**, 663–668 (2017). DOI 10.1016/j.proeng.2017.09.120
17. Hedrih, K.: Rolling heavy ball over the sphere in real Rn3 space. Nonlinear Dynamics **97**(1), 63–82 (2019). DOI 10.1007/s11071-019-04947-1
18. Hermans, J.: A symmetric sphere rolling on a surface. Nonlinearity **8**(4), 493–515 (1995). DOI 10.1088/0951-7715/8/4/003
19. Jurdjevic, V., Zimmerman, J.: Rolling sphere problems on spaces of constant curvature. Mathematical Proceedings of the Cambridge Philosophical Society **144**(3), 729–747 (2008). DOI 10.1017/s0305004108001084
20. Kamke, E.: Differentialgleichungen Lösungsmethoden und Lösungen. Teubner Verlag, Leipzig (1977)
21. Koiller, J., Ehlers, K.: Rubber rolling over a sphere. Regular and Chaotic Dynamics **12**(2), 127–152 (2007). DOI 10.1134/S1560354707020025. URL https://doi.org/10.1134/S1560354707020025
22. Lee, W., Hsu, C.: A global analysis of an harmonically excited spring-pendulum system with internal resonance. Journal of Sound and Vibration **171**(3), 335–359 (1994)
23. Legeza, V., Dychka, I., Hadyniak, R., Oleshchenko, L.: Mathematical model of the dynamics in a one nonholonomic vibration protection system. International Journal of Intelligent Systems and Applications **10**(10), 20–26 (2018). DOI 10.5815/ijisa.2018.10.03
24. Legeza, V.P.: Numerical analysis of the motion of a ball in an ellipsoidal cavity with a moving upper bearing. Soviet Applied Mechanics **23**(2), 191–195 (1987). DOI 10.1007/bf00889017
25. Lewis, A.: The geometry of the Gibbs-Appell equations and Gauss's principle of least constraints. Reports on Mathematical Physics **38**(1), 11–28 (1996)
26. Matta, E.: A novel bidirectional pendulum tuned mass damper using variable homogeneous friction to achieve amplitude-independent control. Earthquake Engineering & Structural Dynamics **48**(6), 653–677 (2019). DOI 10.1002/eqe.3153
27. Matta, E., De Stefano, A., Spencer Jr., B.F.: A new passive rolling-pendulum vibration absorber using a non-axial guide to achieve bidirectional tuning. Earthquake Engineering and Structural Dynamics **38**, 1729–1750 (2009)
28. Minorski, M.: Nonlinear oscillations. Van Nostrand, Princeton, NJ (1962)
29. Nabergoj, R., Tondl, A.: A simulation of parametric ship rolling: Effects of hull bending and torsional elasticity. Non-linear Dynamics **6**, 265–284 (1994)
30. Nabergoj, R., Tondl, A., Virag, Z.: Autoparametric resonance in an externally excited system. Chaos, Solitons & Fractals **4**(2), 263–273 (1994). DOI 10.1016/0960-0779(94)90149-x
31. Neimark, J.I., Fufaev, N.A.: Dynamics of nonholonomic systems, *Translations of Mathematical Monographs*, vol. 33. AMS, Providence, Rhode Island (1972)
32. Nekomoto, Y., Matsuki, K.: Self-tuning type vibration damping apparatus (1997). EU Patent EP0838556A1
33. Neto, J.P.J.: Solving the nonlinear pendulum equation with nonhomogeneous initial conditions. International Journal of Apllied Mathematics **30**(3) (2017). DOI 10.12732/ijam.v30i3.5
34. Náprstek, J.: Stochastic exponential and asymptotic stability of simple non-linear systems. International Journal of Non-Linear Mechanics **31**(5), 693–705 (1996). DOI 10.1016/0020-7462(96)00031-5
35. Náprstek, J.: Non-linear self-excited random vibrations and stability of an SDOF system with parametric noises. Meccanica **33**(3), 267–277 (1998). DOI 10.1023/A:1004399114582. URL https://doi.org/10.1023/A:1004399114582
36. Náprstek, J.: Construction of Lyapunov function in stochastic domain using first integrals of deterministic system. In: M. di Paola (ed.) EUROMECH 413 - Stochastic Dynamics of Nonlinear Mechanical Systems, pp. EM413–5. University of Palermo, Palermo (2000)
37. Náprstek, J., Fischer, C.: Auto-parametric semi-trivial and post-critical response of a spherical pendulum damper. Computers and Structures **87**(19–20), 1204–1215 (2009)
38. Náprstek, J., Fischer, C.: Dynamic response of a heavy ball rolling inside a spherical dish under external excitation. In: I. Zolotarev (ed.) Proc. Engineering Mechanics 2013, pp. 96–106. IT AS CR, Prague (2013). Paper #46

39. Náprstek, J., Fischer, C.: Dynamic behavior and stability of a ball rolling inside a spherical surface under external excitation. In: A. Zingoni (ed.) Insights and innovations in structural engineering, mechanics and computation, pp. 214–219. Taylor & Francis, London (2016)
40. Náprstek, J., Fischer, C.: Limit trajectories in a non-holonomic system of a ball moving inside a spherical cavity. Journal of Vibration Engineering & Technologies **8**(2), 269–284 (2020). DOI 10.1007/s42417-019-00132-1
41. Náprstek, J., Fischer, C.: Stable and unstable solutions in auto-parametric resonance zone of a non-holonomic system. Nonlinear Dynamics **99**(1), 299–312 (2020). DOI 10.1007/s11071-019-04948-0
42. Náprstek, J., Fischer, C., Pirner, M., Fischer, O.: Non-linear model of a ball vibration absorber. In: M. Papadrakakis, M. Fragiadakis, V. Plevris (eds.) Computational Methods in Applied Sciences, vol. 2, pp. 381–396. Springer Netherlands, Dordrecht (2013). DOI 10.1007/978-94-007-6573-3_18
43. Náprstek, J., Pirner, M.: Non-linear behaviour and dynamic stability of a vibration spherical absorber. In: A.W. Smyth (ed.) Proc. 15th ASCE Engineering Mechanics Division Conference. Columbia Univ., New York (2002). CD ROM, paper 150
44. Pars, L.: A Treatise on Analytical Dynamics, 2 edn. Ox Bow Press, Connecticut, USA (1972)
45. Pirner, M.: Dissipation of kinetic energy of large-span bridges. Acta Technica, CSAV **39**, 407–418 (1994)
46. Pirner, M., Fischer, O.: The development of a ball vibration absorber for the use on towers. Journal of the International Association for Shell and Spatial Structures **41**(2), 91–99 (2000)
47. Routh, E.: Dynamics of a system of rigid bodies. Dover Publications, New York (1905)
48. Soltakhanov, S.K., Yushkov, M., Zegzhda, S.: Mechanics of non-holonomic systems. Springer-Verlag GmbH, Berlin - Heidelberg (2009)
49. Tondl, A.: To the analysis of autoparametric systems. Z. Angew. Math. Mech. **77**(6), 407–418 (1997)
50. Udwadia, F., Kalaba, R.: The explicit Gibbs-Appell equation and generalized inverse forms. Quarterly of applied mathematics **56**(2), 277–288 (1998)
51. Wolfram, S.: Mathematica: A system for doing mathematics by computer, first edn. Addison-Wesley Publishing Company, Redwood City (1988)
52. Yong-fen, Q.: Gibbs-Appell's equations of variable mass nonlinear nonholonomic mechanical systems. Applied Mathematics and Mechanics **11**(10), 973–983 (1990). DOI 10.1007/BF02115681

Figures

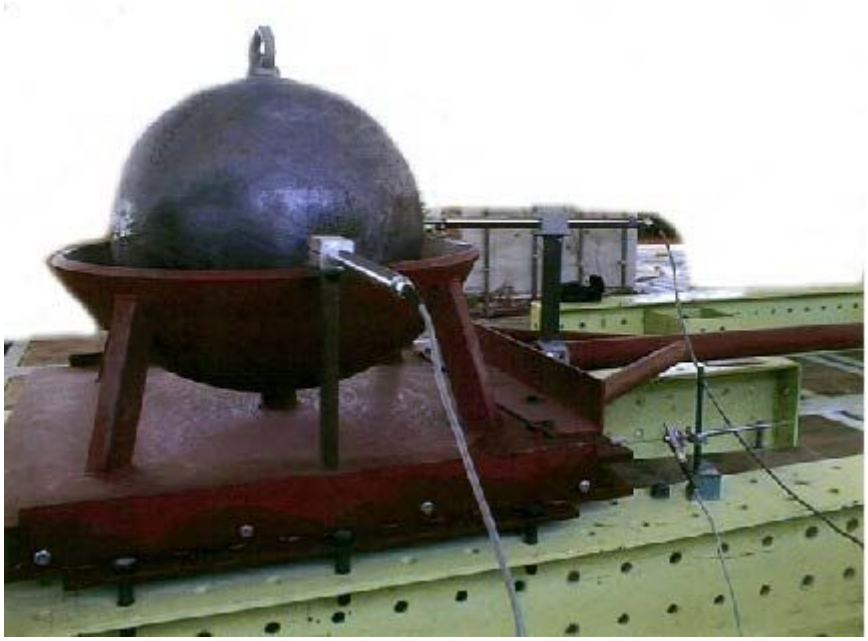

Figure 1

Ball vibration absorber in a dynamic testing laboratory

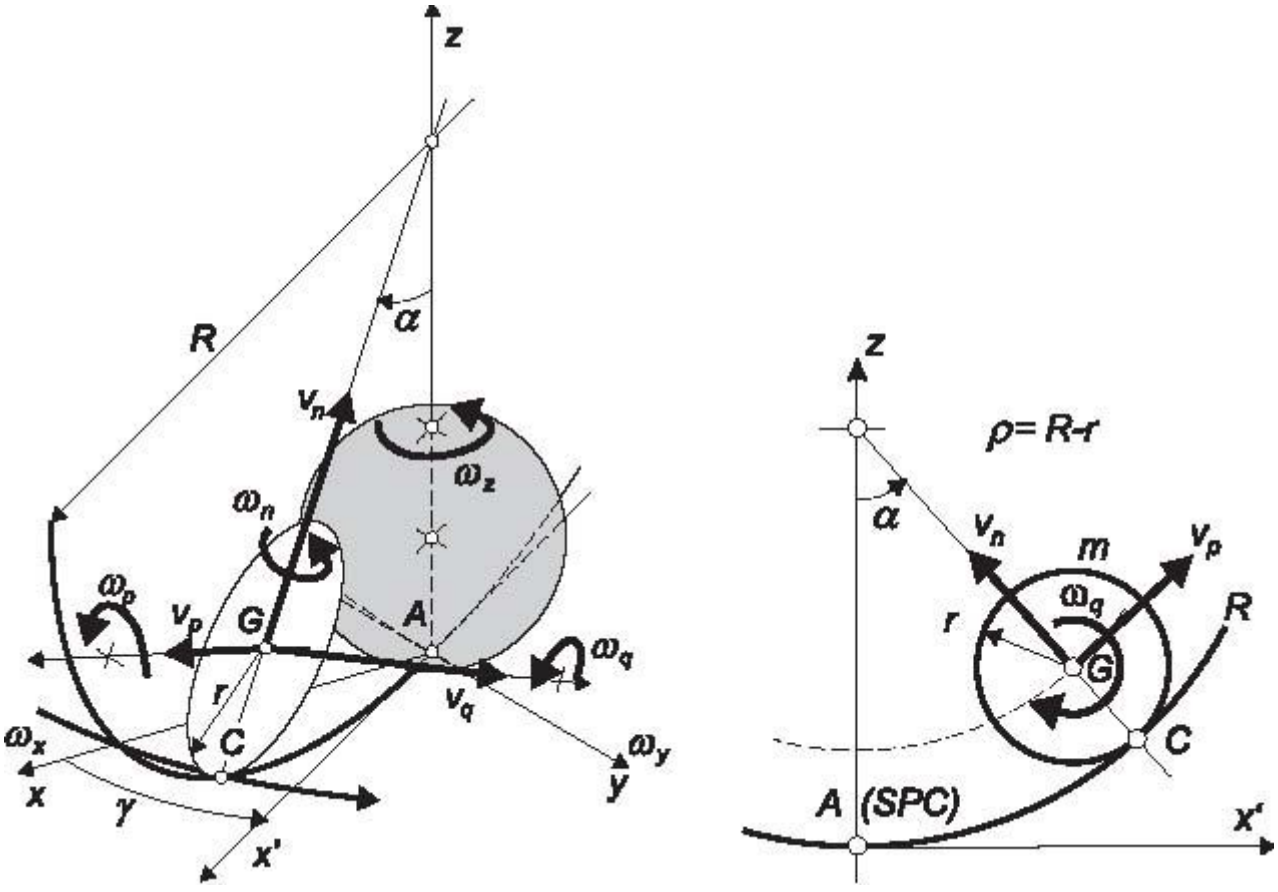

Figure 2

Outline of coordinate systems; left: axonometric view; right: plane ξz view — along γ orientation.

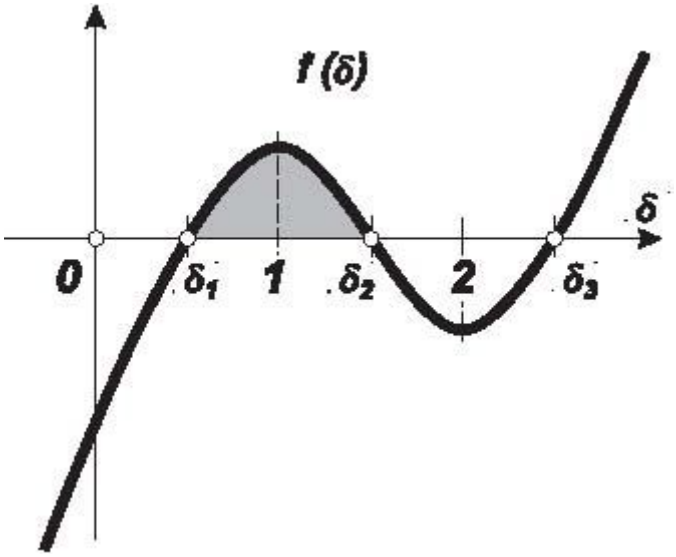

Figure 3

General shape of Characteristic Function f(δ) and of the area delimiting the active spherical strip in the interval δ ∈ (δ1, δ2)

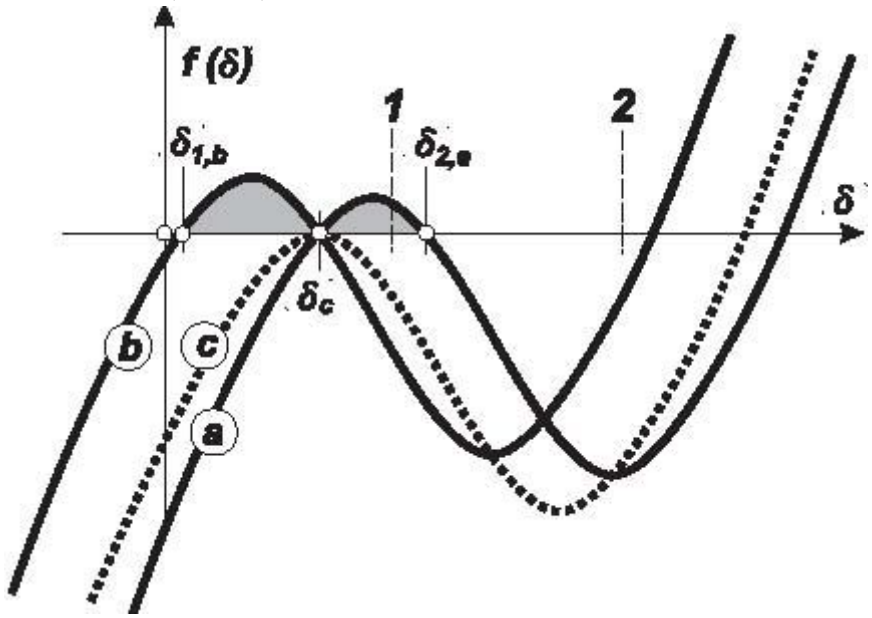

Figure 4

Active area: solid curve (b) - trajectory below the SC: δ ∈ (δ1,b, δ2,b = δc); solid curve (a) - trajectory above the SC: δ ∈ (δ1,a = δc, δ2,b); dashed curve (c) - transition case representing the SC - no active area due to coincidence δc = δ1 = δ2.

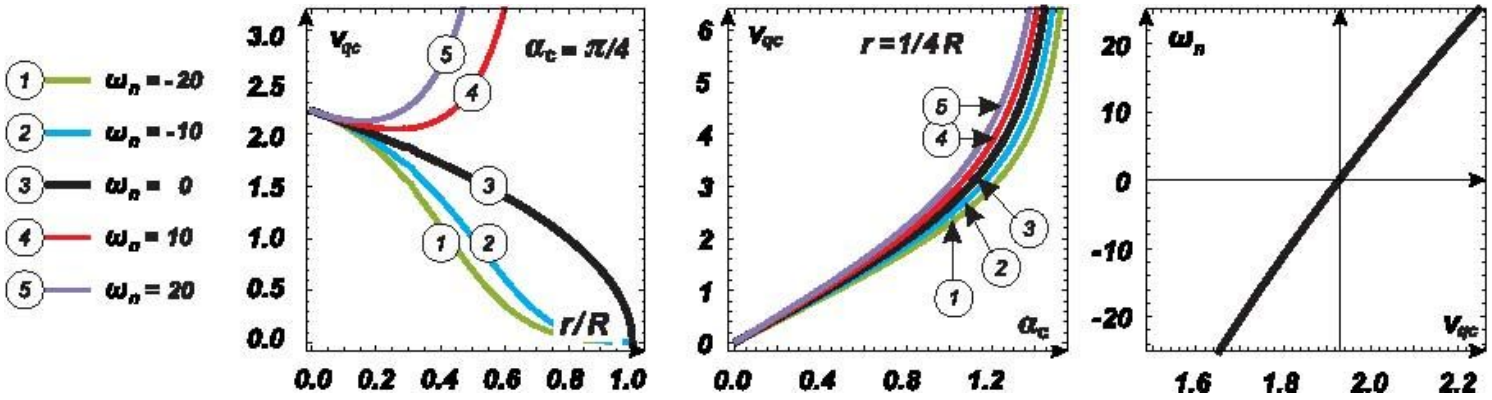

Figure 5

Initial Horizontal Velocity producing the trajectory of the SC: (a) fixed initial height αc = π/4, varying ratios r/R, (b) fixed ratio r/R, various heights αc; color curves in (a) and (b) correspond to various spin values, (c) compensation spin.

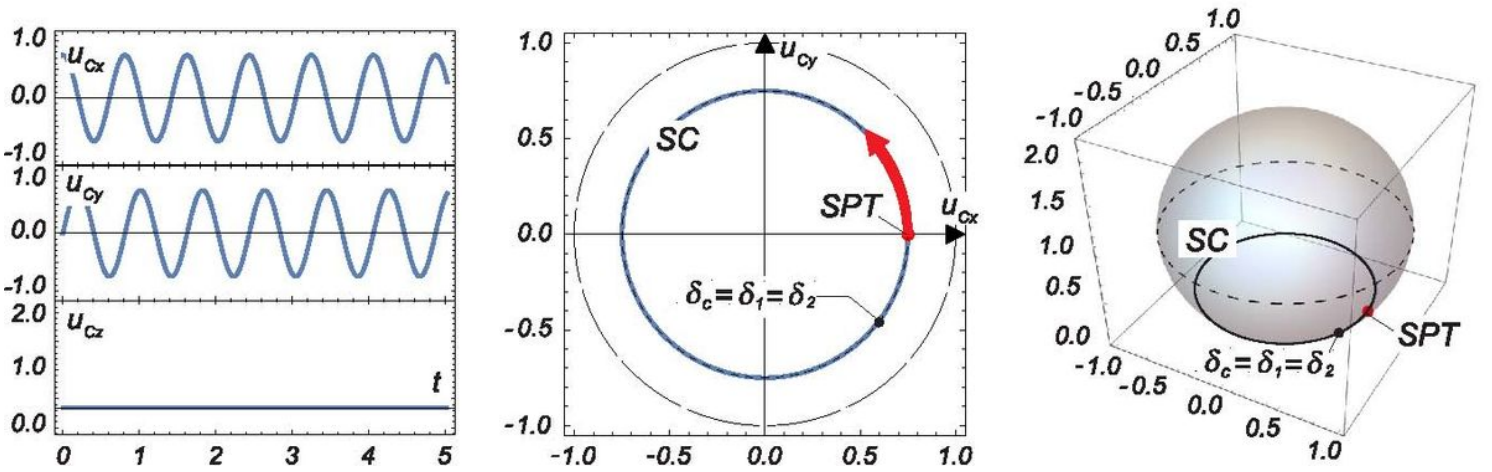

Figure 6

Example of the trajectory of the SC type without influence of the ISV (ωn = 0): (a) time history, (b) top view, (c) axonometric demonstration.

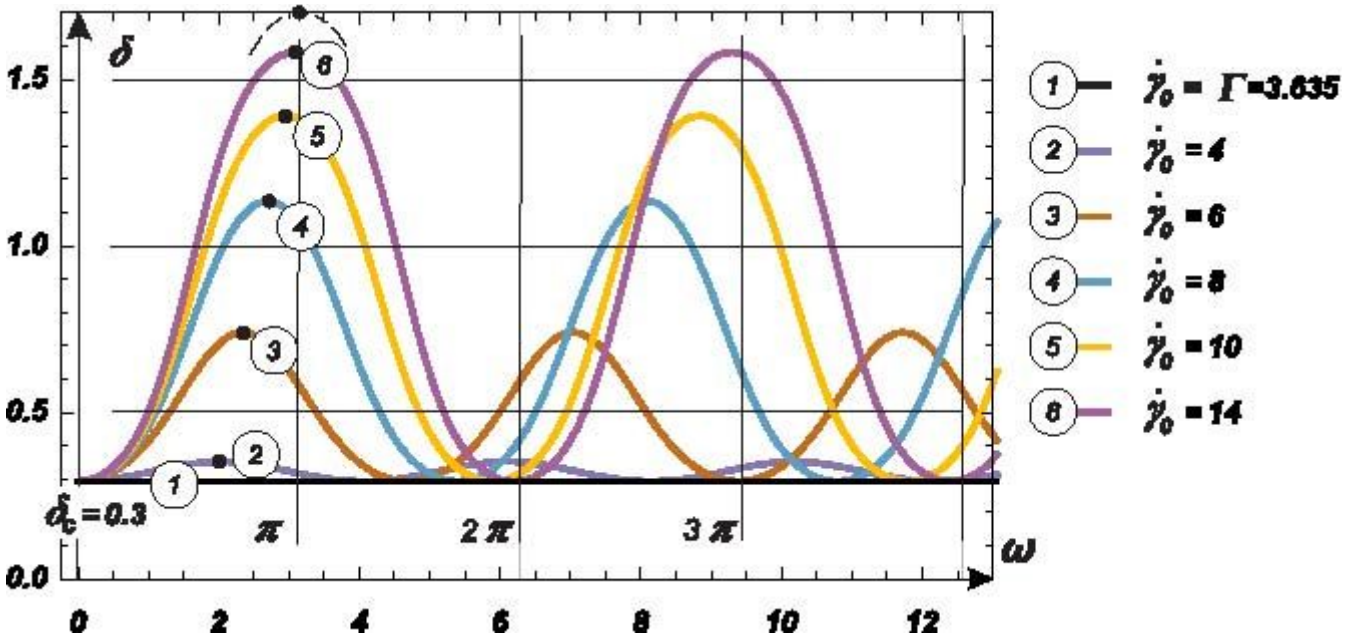

Figure 7

Shape of the trajectory above the SC for various IHV.

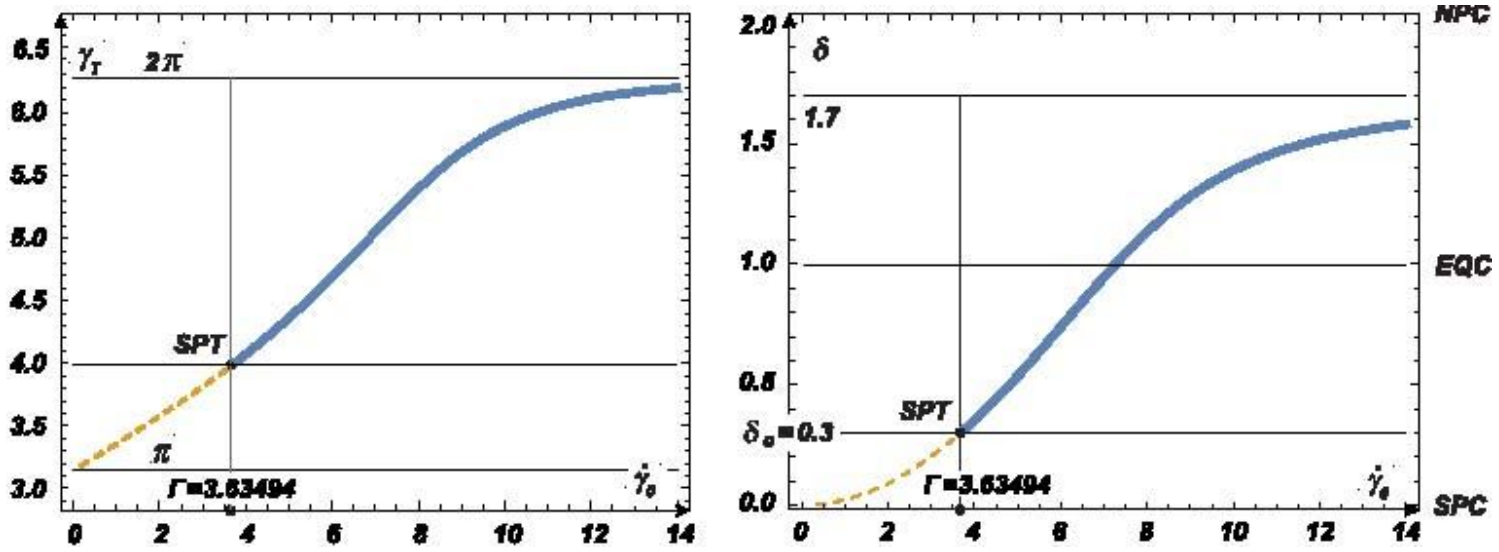

Figure 8

Trajectory above the SC (no spin applied), (a) spatial period dependent on the IHV (γ˙0); (b) upper boundary of the strip δ2 as a function of γ˙0.

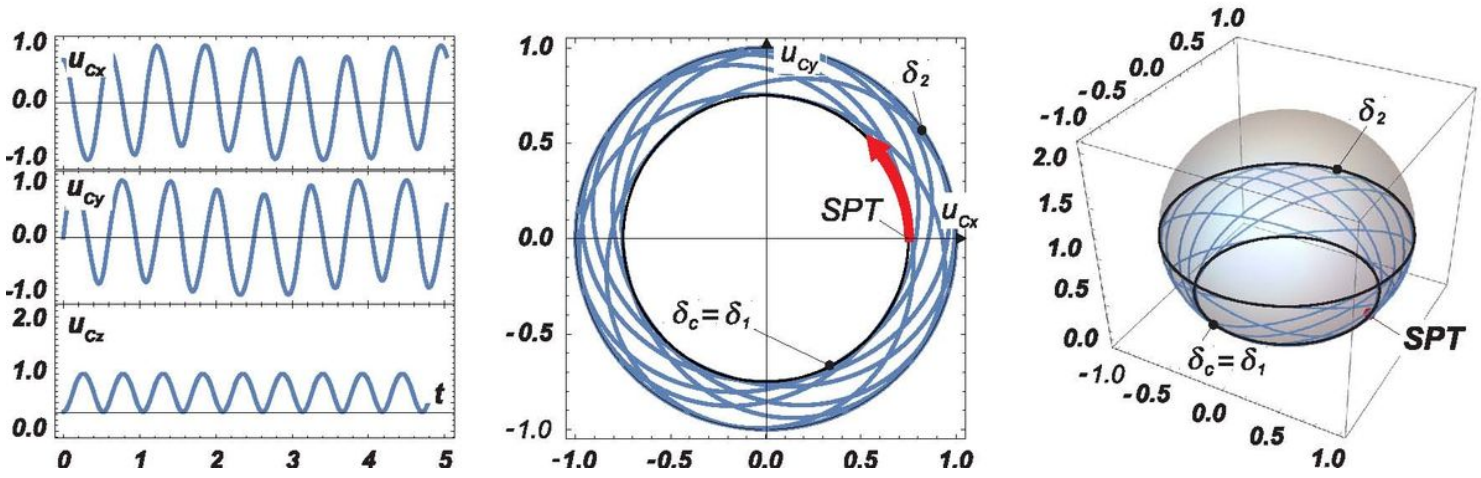

Figure 9

Example of the trajectory above the SC with no ISV (ωn = 0): (a) time history, (b) top view, (c) axonometric demonstration.

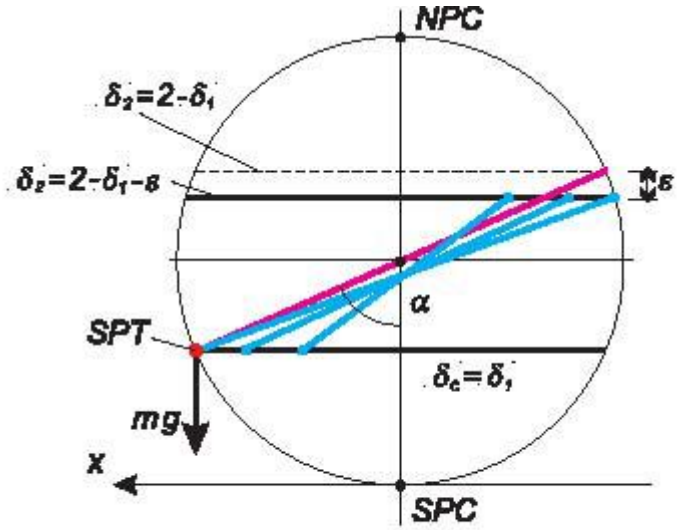

Figure 10

Outline of the trajectory layer for high and infinite IHV.

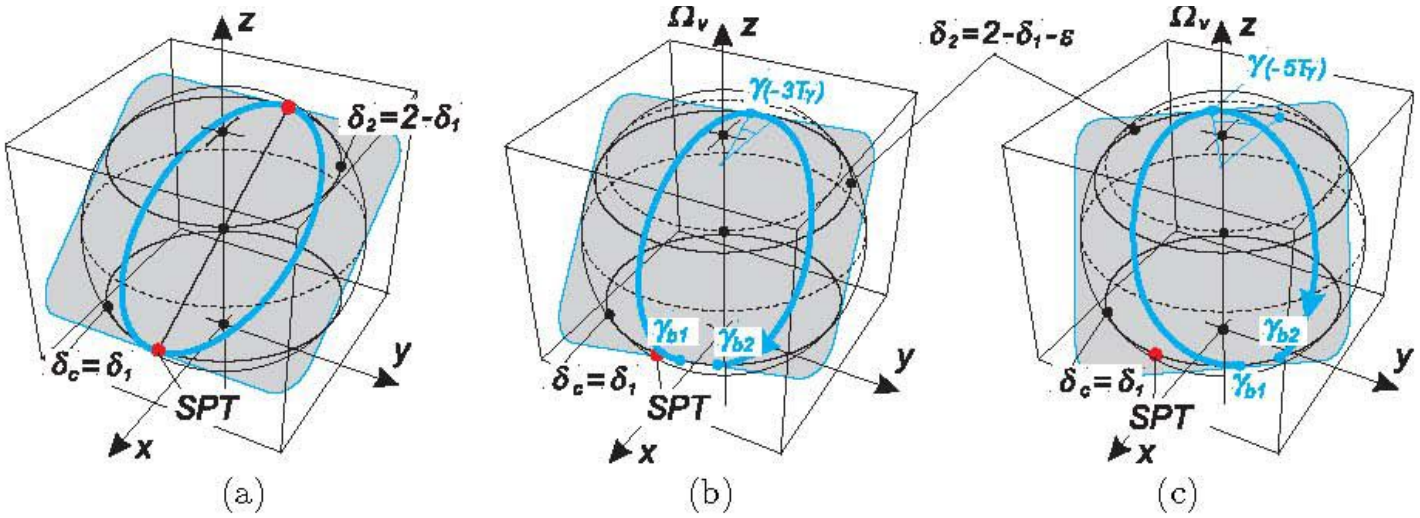

Figure 11

Osculating plane (light grey) of a trajectory for high IHV (ISV is not applied): (a) infinite IHV; (b) finite IHV: - 3rd half-period; (c) finite IHV: - 5th half-period; γb1, γb2: starting or finishing points of one full period.

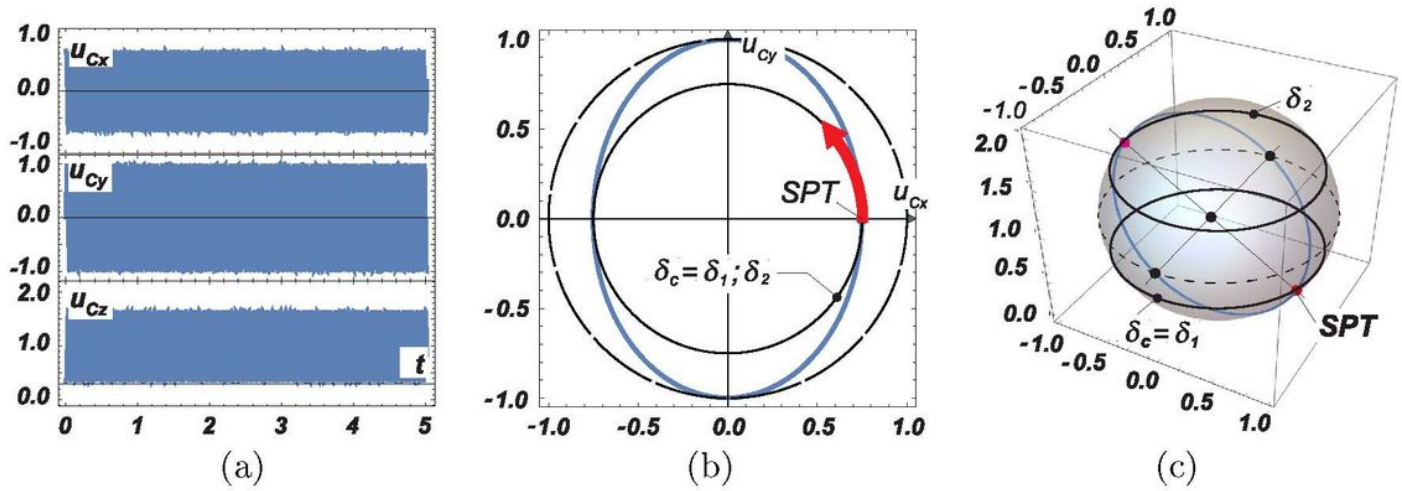

Figure 12

Example of the trajectory above the SC with no ISV (ωn = 0) for a high IHV: (a) time history, (b) top view, (c) axonometric demonstration.

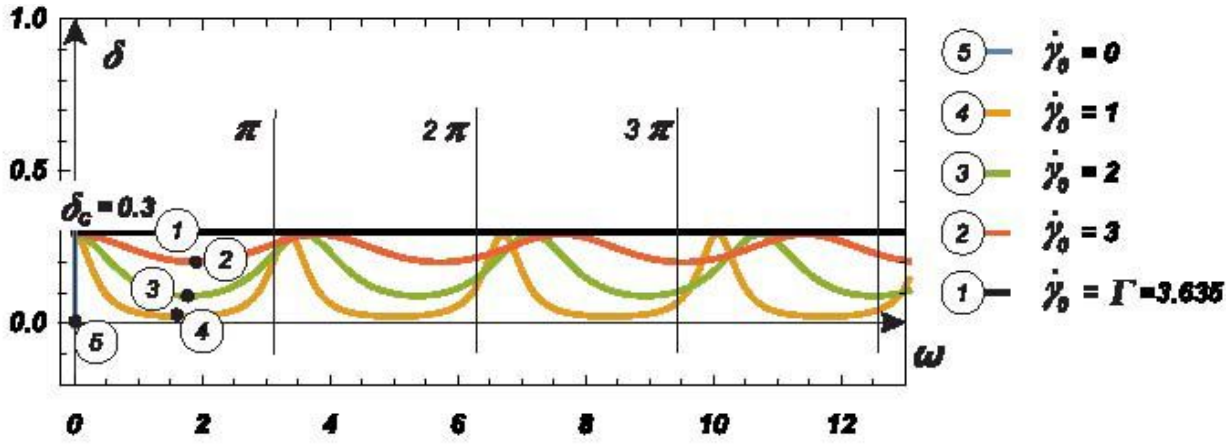

Figure 13

Shape of the trajectory below the SC for various IHV.

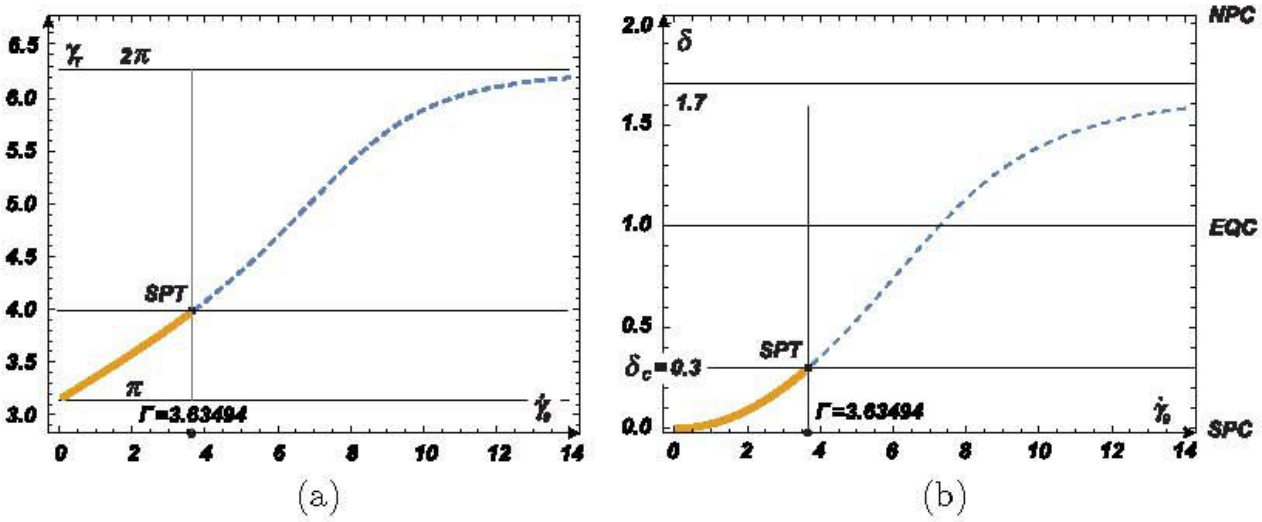

Figure 14

A trajectory below the SC, (a) spatial period dependent on the IHV (γ˙0); (b) lower boundary of the strip δ1 as a function of γ˙0.

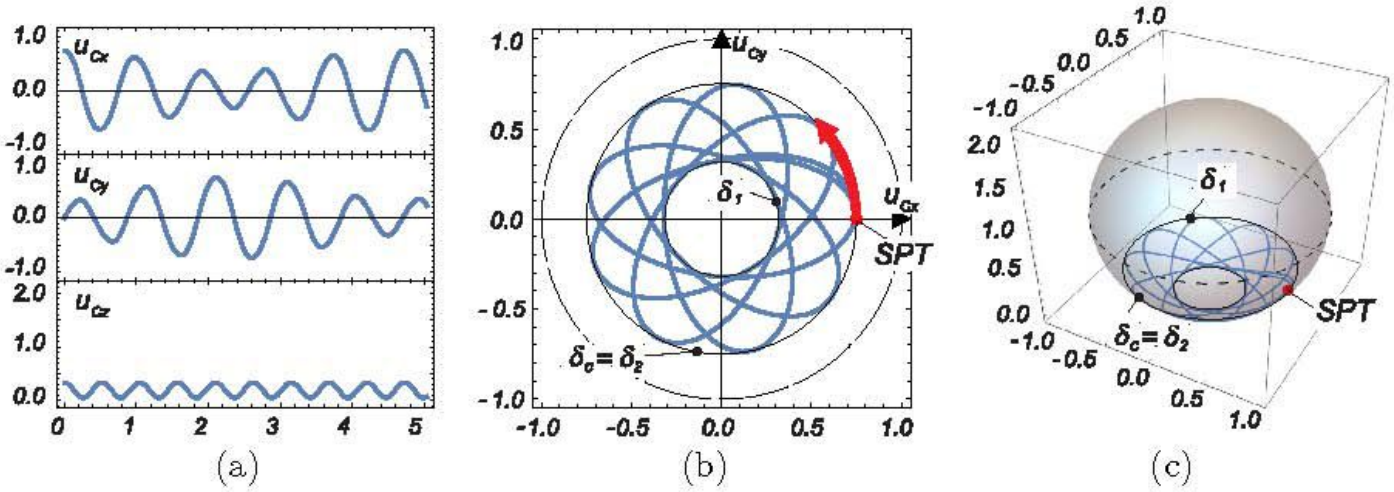

Figure 15

Example of a trajectory below the SC with no ISV (ωn = 0): (a) time history, (b) top view, (c) axonometric demonstration.

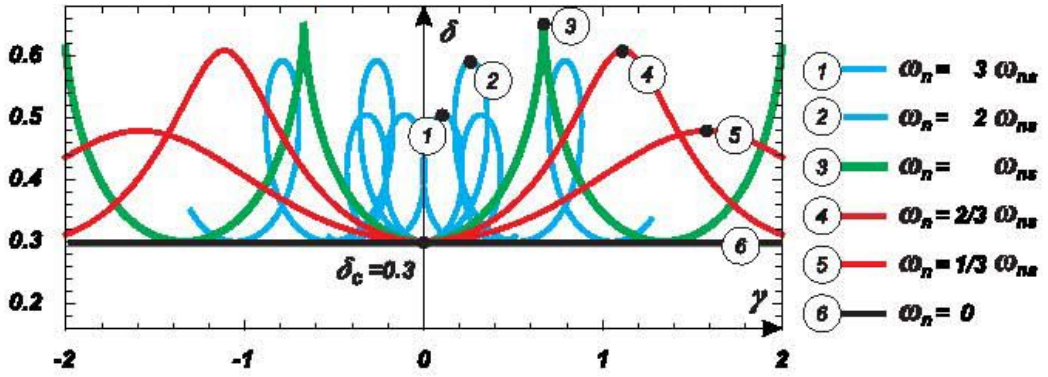

Figure 16

Shape of the trajectory above the SC for various initial spin velocities; colors of curves: ωn = 0 - black, ωns < ωn < 0 - red, ωn - bold green (“kings crown” shape - separating case), ωn < ωns - blue.

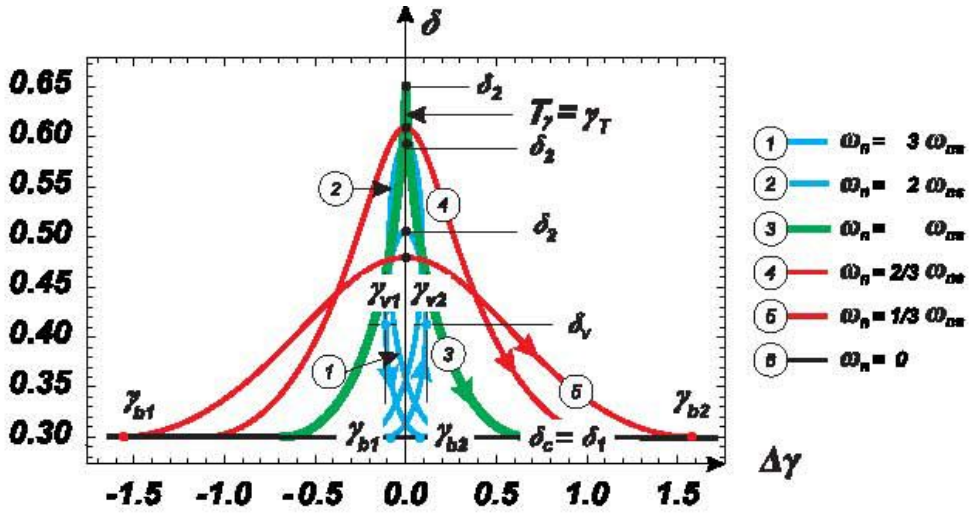

Figure 17

Shapes of trajectories in the neighborhood of the contact point on the upper boundary of the strip (δ2); ωn = 0 - black, ωns < ωn < 0 - red, ωn - bold green (“kings crown” shape - separating case), ωn < ωns - blue. The symbol Δγ (horizontal axis) means a local coordinate within one period or an increase/decrease of γ with respect to γ = γT (position of the tangential point on the δ2 boundary).

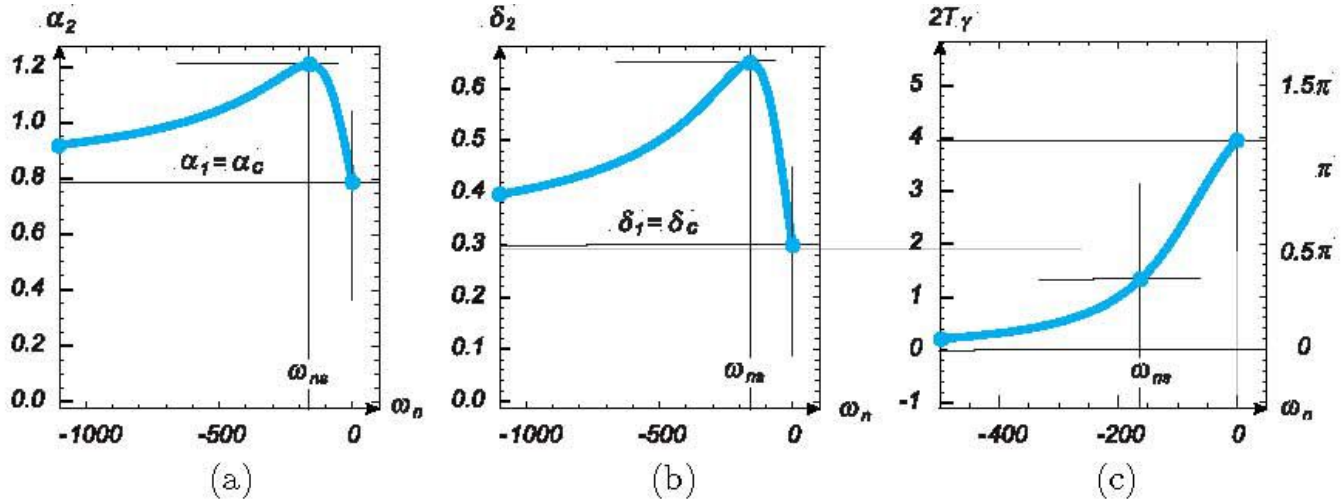

Figure 18

Width of the strip above the SC for descending ISV or ωn < 0 passing throughout all three types of trajectories; (a) representation as α2 − αc or (b) representation as δ2 − δc; (c) width of the space period

along the coordinate γ as a function of spin frequency ωn < 0.

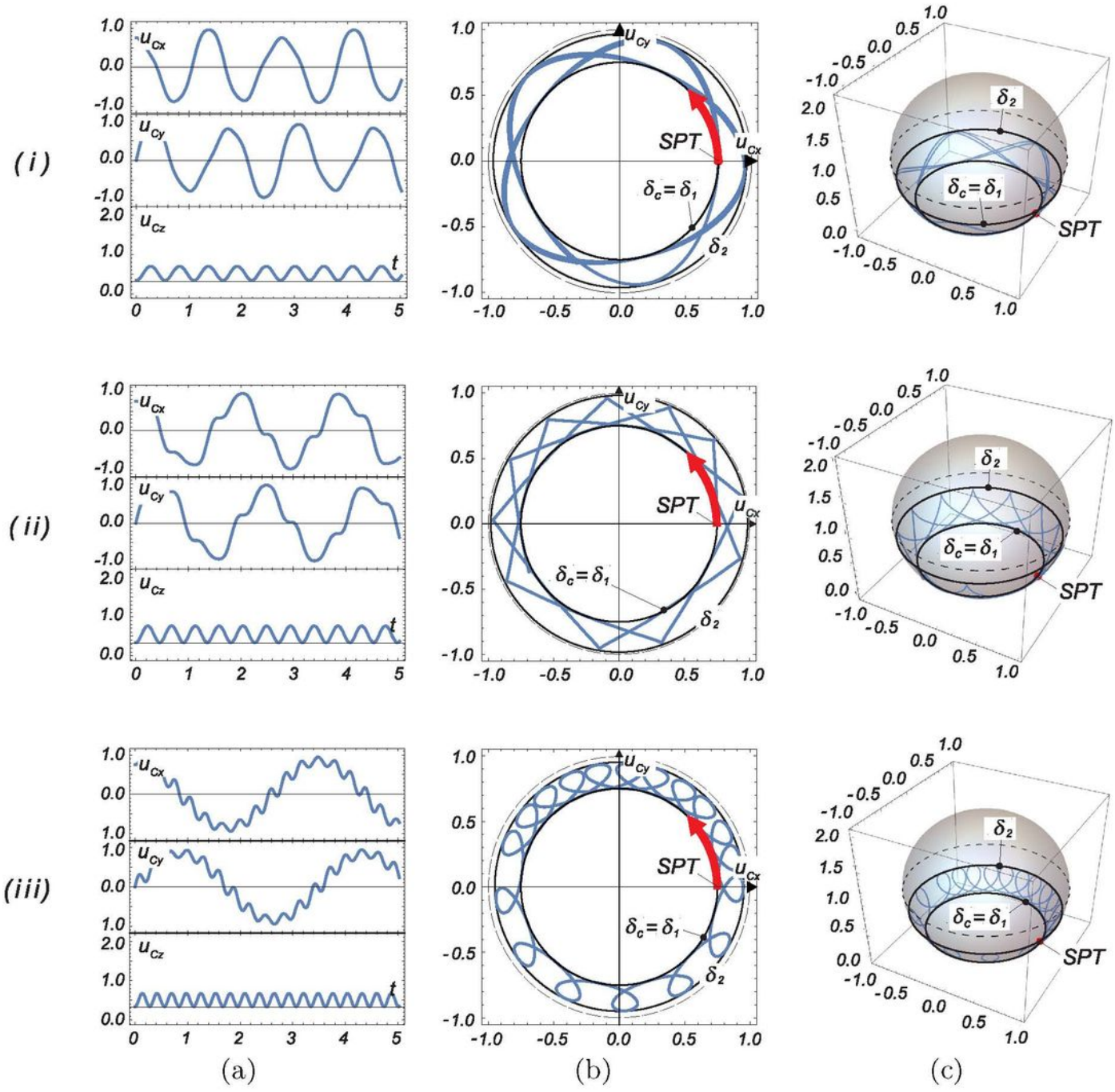

Figure 19

Examples of trajectories with negative Initial Spin Velocity ISV (ωn < 0): 1st row: ωns < ISV < 0; 2nd row: ISV = ωns; 3rd row: ISV < ωns. Column (a) time history, (b) top view, (c) axonometric demonstration.

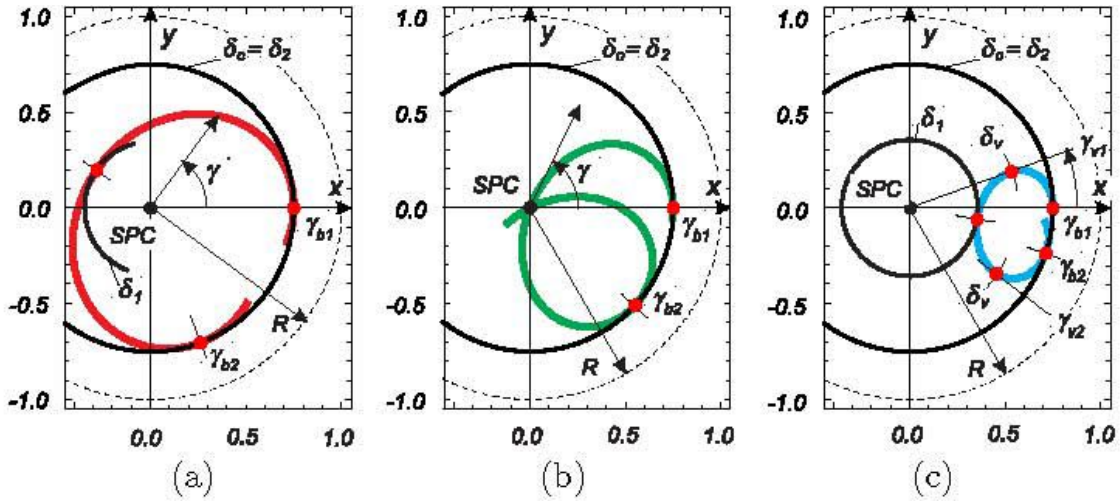

Figure 20

Top view of one loop of the trajectory: (a) red: ISV ωn < ωns, (b) green: ωn = ωns (passing the SPC — “separating case”), (c) blue: ωn > ωns.

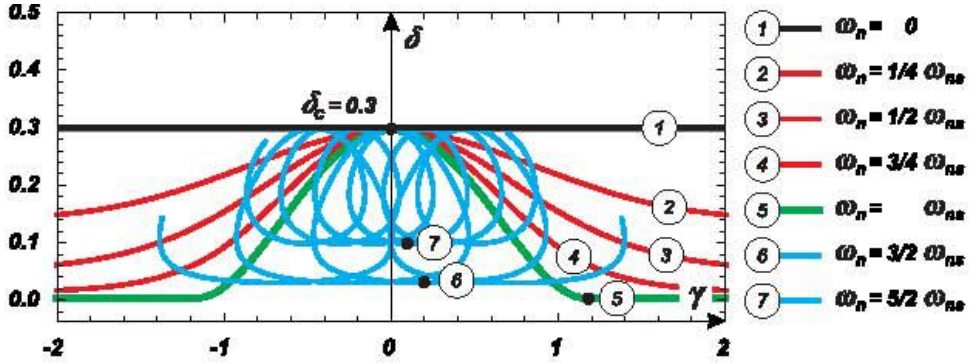

Figure 21

Trajectory shapes below the SC for various initial spin velocities. colors of curves: ωn = 0 - black, 0 < ωn < ωns - red, ωn = ωns - bold green (separating case), ωns < ωs - blue.

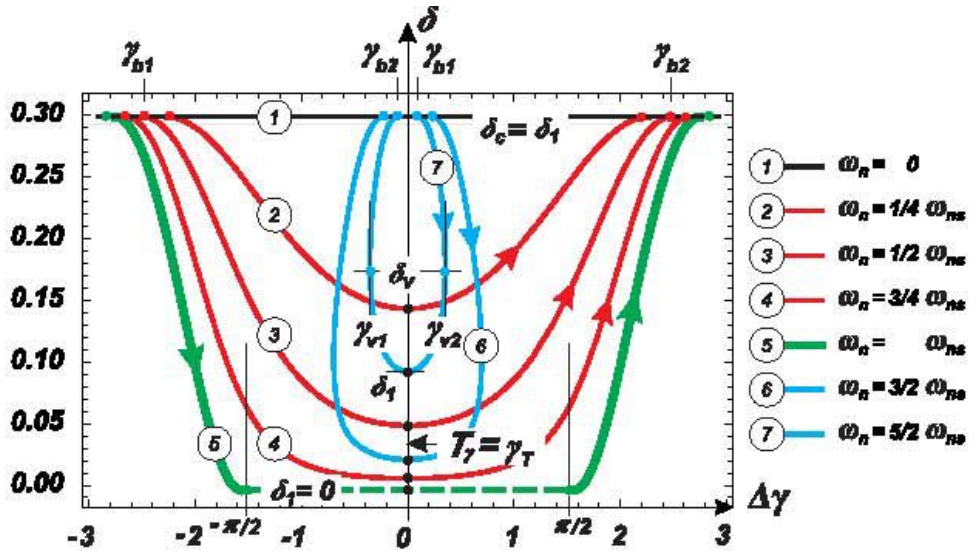

Figure 22

Shapes of trajectories in the neighborhood of the contact point on the lower boundary of the strip (δ1); ωn = 0 - black, 0 < ωn < ωns - red, ωn = ωns - bold green (discontinuous - separating case), ωns < ωn - blue. The symbol Δγ (horizontal axis) means a local coordinate within one period or an increase/decrease of γ with respect to γ = γT (the position of the tangential point on the δ1 boundary).

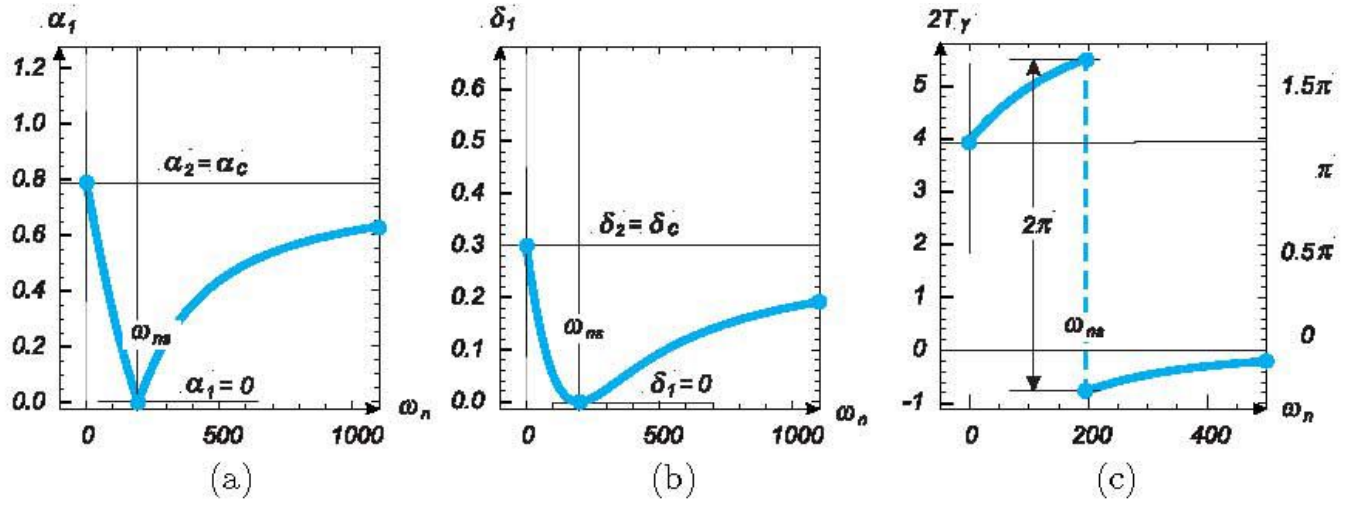

Figure 23

Width of the strip below the SC for rising ISV or ωn > 0 covering all three types of trajectories; (a) representation as αc − α1 or (b) representation as δc − δ1; (c) width of the spatial period along the coordinate γ as a function of spin frequency ωn > 0, note a jump in the point ωn = ωns.

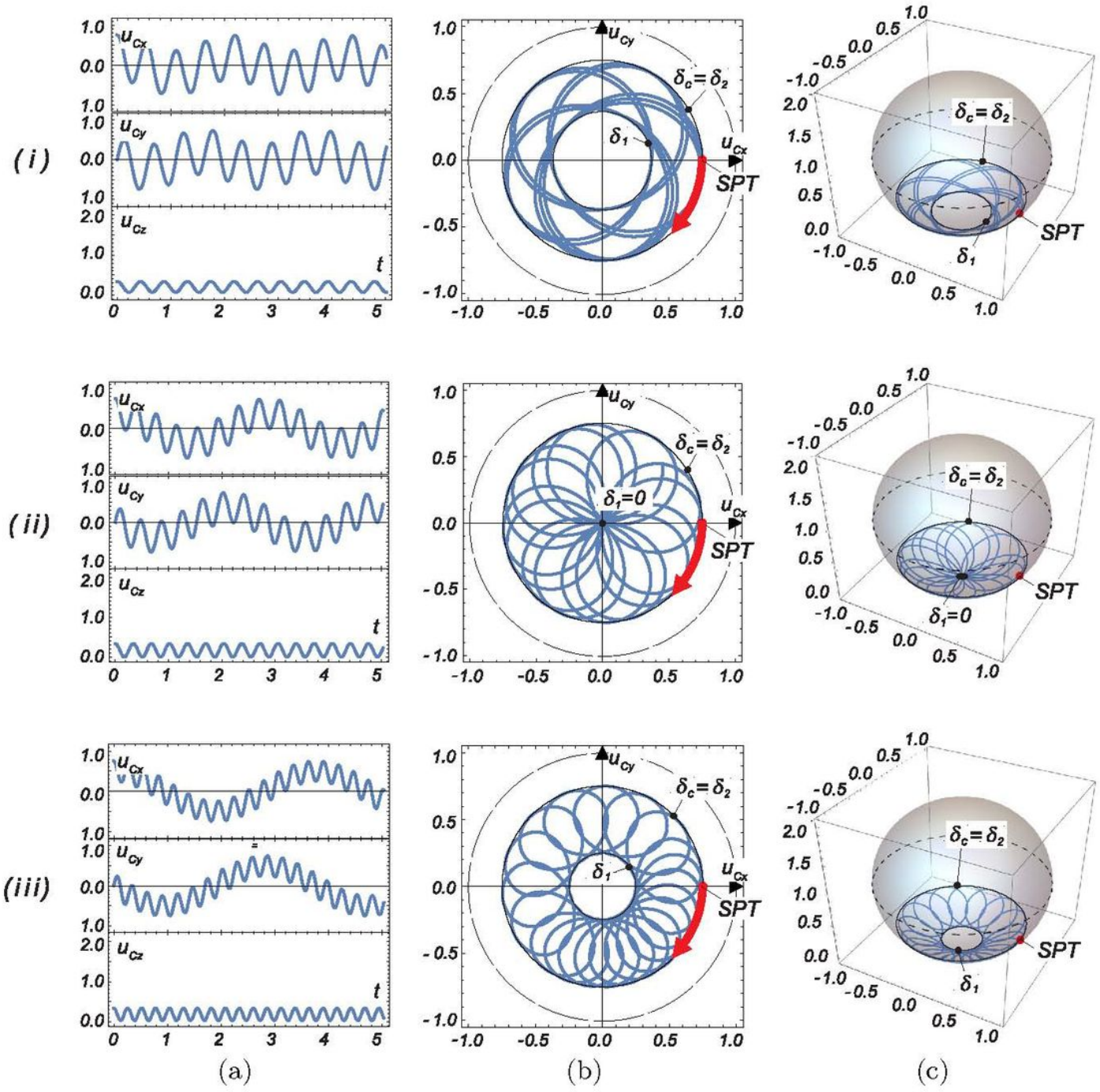

Figure 24

Examples of trajectories with a positive “Initial Spin Velocity ISV” (ωn > 0): 1st row: 0 < ωn < ωns; 2nd row: ωn = ωns; 3rd row: ωn > ωns. Column (a) time history, (b) top view, (c) axonometric demonstration.

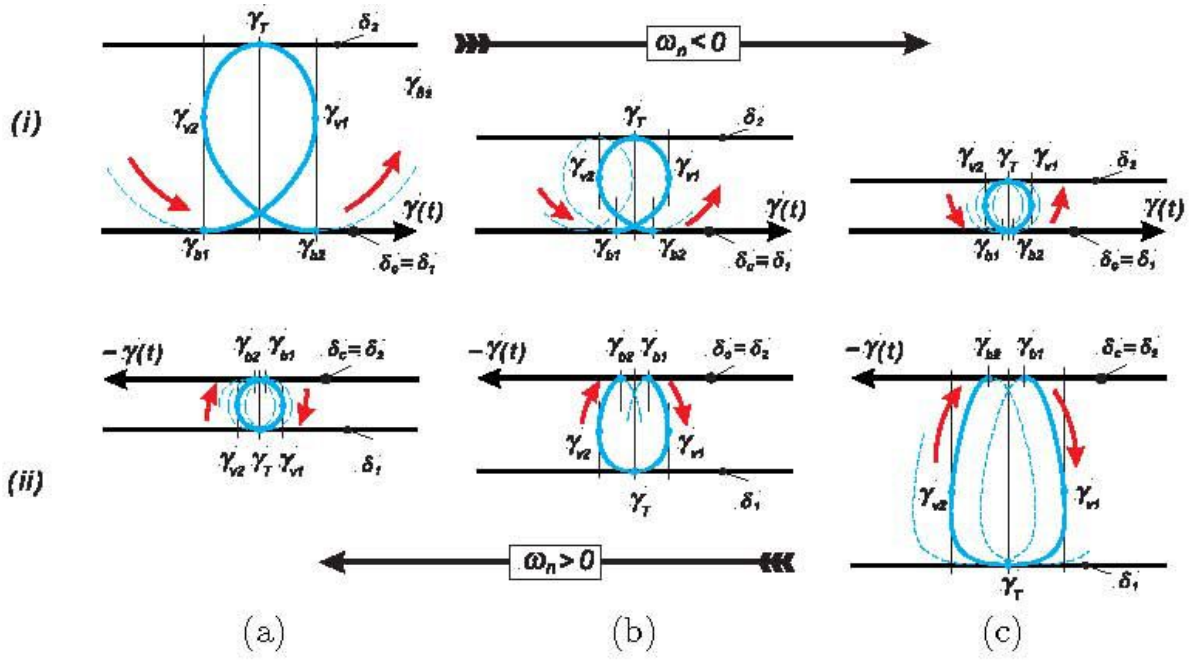

Figure 25

Shape of the trajectory in the neighborhood of the contact point γT ; (i) upper boundary δ2 of the spherical strip for very low ISV: columns (a-c) - descending ωn « ωns; (ii) lower boundary δ1: columns (a-c) - rising ωn » ωns.

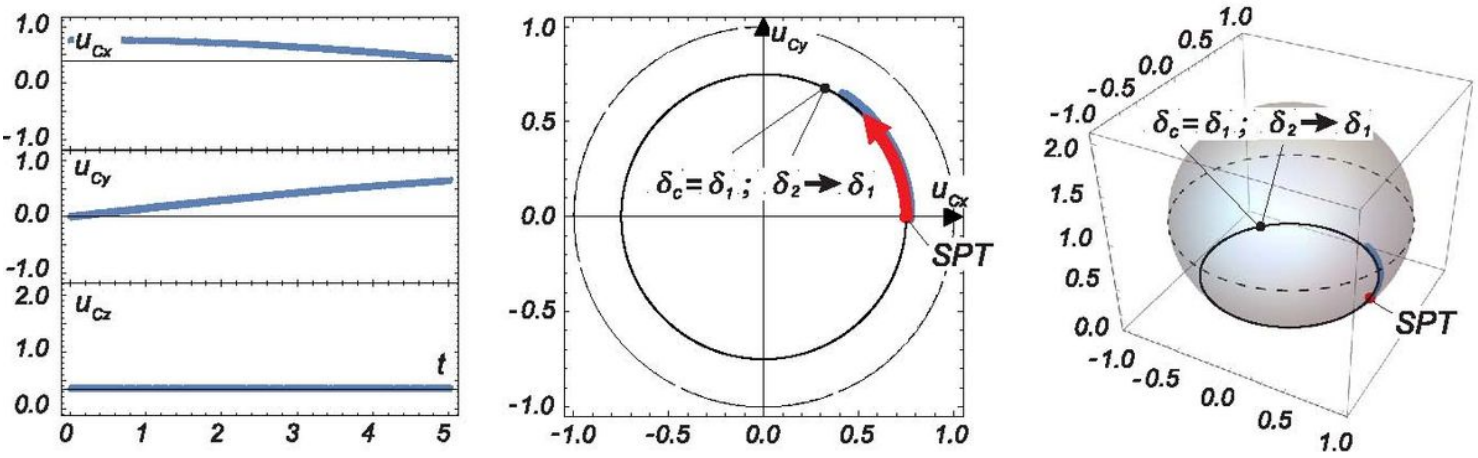

Figure 26

Example of a trajectory with negative ISV (ωn « 0): (a) time history, (b) top view, (c) axonometric demonstration.

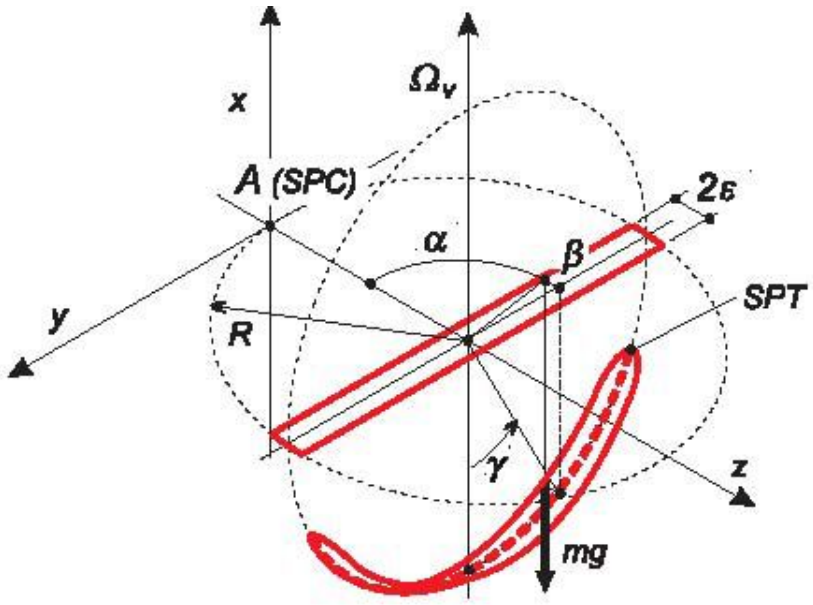

Figure 27

Arrangement of coordinates for investigation of cases with low IHV.

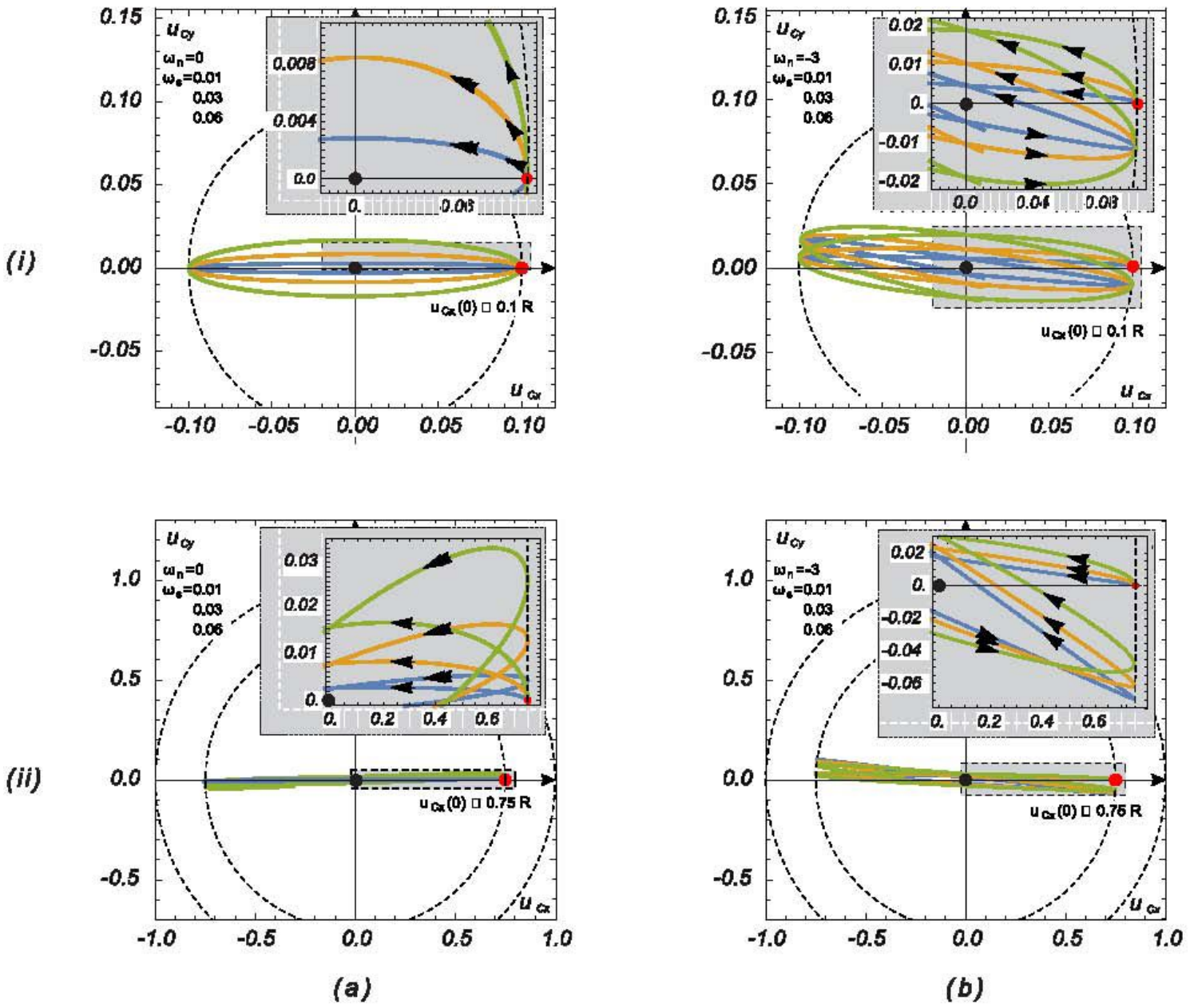

Figure 28

Trajectory at a low IHV: line (i) linear approach - low level SPT, line (ii) nonlinear approach; column (a) no initial spin, column (b) initial spin included.

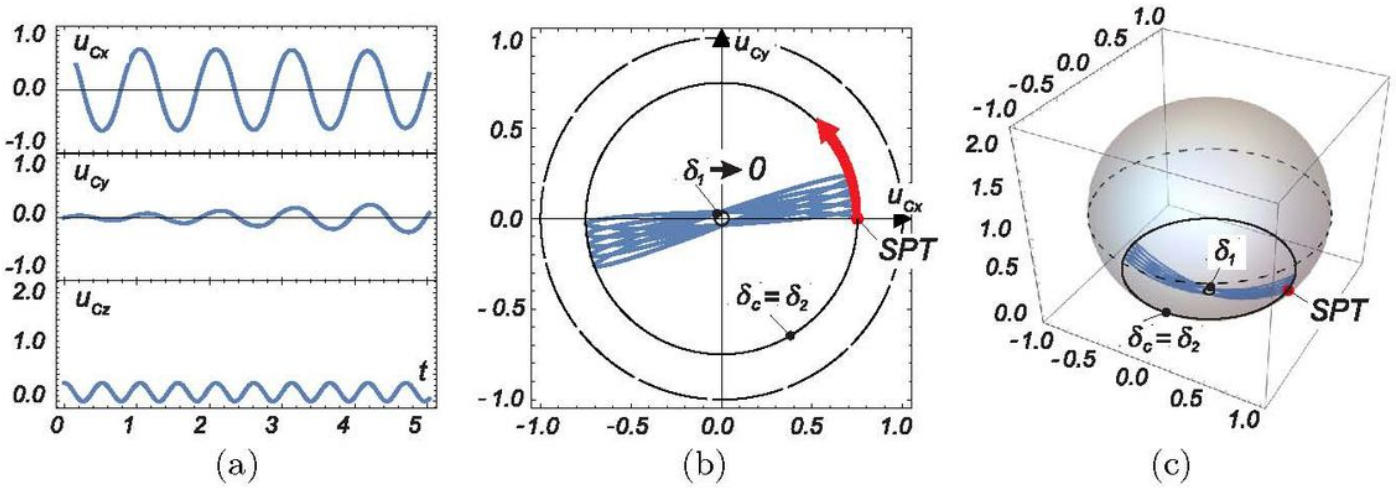

Figure 29

Example of the trajectory below the SC without ISV (ωn = 0) for low IHV: (a) time history, (b) top view, (c) axonometric demonstration.